# Atomic scale in situ observation of solid-liquid interface - the additive effect on hydration structure and growth rate of calcite-

# Doctoral thesis

Atomic Scale in situ observation of solid-liquid interface

-The additive effect on hydration structure and growth rate of calcite-

（固液界面の原子レベル″その場″観察 −カルサイトの水和構造と成長速度に対する添加物効果−）

Yuki Araki

2013

## Abstract

Calcium carbonate is one of common minerals on the earth. Calcium carbonate crystals are utilized industrially in various fields, so that the control of crystal growth is required. It has been known that organisms control the morphology and polymorph of calcium carbonate crystals by utilizing inorganic and organic additives in biomineralization. Understanding the additive effects on growth of calcium carbonate crystal is necessary to control the crystal growth.

The effect of additives on growth of calcite which is a stable polymorph of calcium carbonate has been investigated. The additive effect on calcite surface, such as incorporation of magnesium ions into calcite and pinning of step propagation by organic molecules has been confirmed. On the other hand, the additive effect on hydration of calcite has remained unclear even if that effect has been suggested by the measurement of growth rate of calcite in the presence of additives. Hydration affects adsorption and surface diffusion of ions on calcite surface. Also, the dehydration has been considered as rate-determining process in solution growth by the estimation of energy barriers of solution growth processes. Therefore, hydration is a key to control the kinetics of calcite growth.

Hydration at the vicinity of calcite surface has been estimated by molecular dynamics (MD) simulation and observed by surface X-ray diffraction. Although these techniques made the description of hydration structure clear, they do not show the local difference of hydration structure between on the terrace and the step front which is capture site of ions. Hence, we employed the newly frequency modulation atomic force microscopy (FM-AFM) for in situ observation of local hydration structure in atomic scale. This technique is expected to provide insight into the atomic scale distribution of hydrated water molecules in growth solution even at step front. This study describes the first in situ examination of the additive effect of organic molecules and magnesium ions on local hydration structure of calcite surface in atomic scale utilizing FM-AFM. The hydration images were compared with the growth rate of calcite measured using phase shift interferometry so as to validate the influence of hydration of the growth rate of calcite.

Previous studies of influences of inorganic and organic additives on calcite growth were reviewed in Chapter 1. We described the additive effect of magnesium ion and the synthetic polypeptide on hydration structure by the result of in situ observation of hydration structure in atomic scale at the interface between calcite surface and solution in Chapter 2. In Chapter 3, we showed the result of measurement of calcite growth rate

by the phase shift interferometry. The additive effects on nucleation and adsorption of ion on calcite surface were discussed. In Chapter 4, the influence of hydration on growth rate of calcite was validated based on the results of visualization of hydration structure and measurement of growth rate.

The findings are summarized as follows:

(1) The synthetic polypeptide, even that with high hydrophilicity, does not affect hydration at the surface of calcite.
(2) Combination of magnesium ions and the synthetic polypeptides provides a rigid hydration on calcite surface.
(3) Magnesium ions and the synthetic polypeptides influence hydration and the surface pattern of calcite, respectively.
(4) Structured water distribution eases the energy gap between the calcite surface and solution. As a result, the interfacial tension between the calcite surface and the solution is decreased.
(5) Magnesium ions and the synthetic polypeptide act in unison to accelerate nucleation via changes in hydration structure.
(6) Hydration contributes to interfacial energy between the calcite and the solution, but not for the adsorption of ions on the calcite steps.

This study demonstrated that additives affect the interfacial tension via altering hydration structure by application of FM-AFM for crystal growth experiment for the first time. Our results also showed that there is hardly any change in the adsorption of ions on calcite surface due to the hydration structure. That suggests that dehydration is not a rate-determining process, an observation that is contrary to the currently prevailing theory. The further observation of hydration of step front will be carried out by FM-AFM to demonstrate the effect of hydration on adsorption of ions. These findings indicate that the control of interfacial tension is possible utilizing the additive effect on hydration. That provides a new knowledge to regulate the polymorphism of calcium carbonate.

**Acknowledgement**

First of all, I am deeply grateful to Prof. Katsuo Tsukamoto to instruct me the pleasure to study crystal growth. I acknowledge Prof. Hirofumi Yamada, Drs. Kei Kobayashi, Noriaki Oyabu, and Masushige laboratory, Kyoto University, for valuable advices and technical supports for FM-AFM observation. The use of FM-AFM was enabled by the Kyoto-advanced Nanotechnology Network. I also appreciate the acceptance to use the synthetic polypeptide for Profs. Tomoyuki Miyashita and Ryosuke Takagi, KinkiUniversity. I feel gratitude for constructive discussions and persistent help from Profs. Hitoshi Miura and Yuki Kimura. I thank to Dr. Hisao Sato for his support of PSI measurements. I received helpful advices for FM-AFM imaging from Profs. Hiroshi Onishi, Angelika Kühnle, Dr. Ken Nagashima. I would like to express my gratitude to Profs. Tomoki Nakamura, Takeshi Kakegawa, Michihiko Nakamura, Hiroki Nada, Jun Kawano, Drs. Yoshihiro Furukawa, and Mihoko Hirao for their incisive comments, constructive suggestions, and warm encouragements. I also would like to thank clerical staffs in department of Earth science and my colleagues of Tsukamoto laboratory and Nakamura laboratory. Ms. Takako Otomo and Ms. Ayumi Ishii gave me clerical and moral supports. Finally, I would like to express my deepest appreciation to my family for their moral support and warm encouragements.

Financial support was provided by Grants-in Aid for the Research Fellow of the Japan Society for the Promotion of Science for Y. A. This work was also supported by Tohoku University International Advanced Research and Education Organization.

# *Contents*

# *Chapter 1. Background*

## 1.1 Calcium carbonate crystal

Calcium carbonate is a common mineral found on the earth in limestone, stalactite, neritic sediments, and molluscan shell, among others. Calcite is the most stable polymorph of calcium carbonate at ambient temperature and pressure. There are two other types of calcium carbonate polymorphs: aragonite and vaterite (table.1). Aragonite is metastable under ambient conditions; however, when subjected to high pressure and low temperature, it becomes stable (Fig.1-1). On the other hand, vaterite is metastable under any condition. These crystals are formed under hydrothermal environments and occur in solutions, such as sea water.

Calcium carbonate crystals find applications in various industries that use them for optical devices, filler of paper and rubber, pharmaceutical (as antacids), $CO_2$ gas storage, and adsorption substrate for radionuclides, among others (Meece and Benninger, 1993; Aizenberg *et al.*, 2003; Hu *et al*., 2009; Sorai and Sasaki, 2013). Using processed imitating natural biomineralization, several researchers have focused their efforts toward controlling the growth of calcium carbonate crystals using inorganic and organic additives (Cölfen, 2003; Hosoda *et al*., 2003; Kuang *et al.*, 2005; Nishimura *et al.*, 2007; Oaki *et al.*, 2011). In biomineralization, inorganic and organic materials are combined by organisms to form biominerals. Through biomineralization, organisms control the polymorphism and morphology of calcium carbonate crystals, thereby hardering existing tissues to provide them with featuring such as sea shells, egg shells, and eye lenses of trilobites (Mann, 2001). In this study, the effects of inorganic and organic additives on the solution and the surface properties of calcium carbonate crystals were investigated.

## 1.2 Typical additive effect on calcite growth

The surface pattern of calcite in the presence and absence of additives has been widely investigated. Calcite surfaces are composed of terraces, steps, and kink sites. The calcite grows by lateral movement of monomolecular steps across the calcite surface. The steps consist of two obtuse and two acute edges (Gratz and Hillner, 1993). Inorganic and organic additives adsorbed at the step fronts disturb the forward step motion of the growing layer (Walters *et al.*, 1997; Davis *et al.*, 2000; Astilleros *et al.*, 2003; Davis *et al.*, 2004; Kim *et al.*, 2006). The effect of the additive on the step velocity is anisotropic and depends on the size, molecular structure, and functional group of the additive. This is because additives are adsorbed on the step fronts in

accordance with the anisotropic structure of calcite steps (Orme *et al*., 2001) (Fig. 1-2). For example, magnesium ions are largely adsorbed on the acute steps, with only a few being adsorbed on the obtuse steps of calcite (Davis *et al.*, 2000). The extent of adsorption of additives on the step front is estimated from the observed roughing and rounding of the step edges in calcite (Fig.1-3). It has been suggested that the kink sites are the most reactive toward magnesium ions (Paquette *et al.*, 1995). In this incorporation model, the solubility of calcite increases with the concentration of magnesium ions (Fig.1-4).

With organic additives, the phenomenon of step pinning is often observed (Cabrera and Vermileya, 1958) (Fig.1-5). Organic molecules hamper the propagation of the layer, thereby pinning the step motion and presenting a tough step front. It has been suggested that the organic additives are not retained at the step front for a long time (Maruyama, PhD thesis 2008). However, the adsorption of organic molecules even for a short period of time affects the step velocity of calcite (Elhadj *et al.*, 2006a, b).

## 1.3 Interrelation of hydration and calcite growth

In addition to the effects of organic and inorganic additives as mentioned in 1-2, additive effect on hydration of calcite has also been suggested (Elhadj *et al.*, 2006a, b). In the solution growth of calcite, among several processes, such as volume diffusion, dehydration of ions and crystal surface, surface diffusion, and capture at kink sites (Fig.1-6), dehydration has been concluded to be the rate-determining process. This is because the estimated energy barrier for dehydration is the highest (Bennema, 1967a, b).

Elhadj *et al.* have shown that the step velocity of calcite on cleavage plane increased in supersaturated $CaCO_3$ solutions containing low peptide concentrations ($10^{-6}$ - $10^{-4}$ M) (Elhadj *et al.*, 2006a, b). In addition, this acceleration in step velocity increases with the hydrophilicity of the additive peptide. Therefore, to explain the observed phenomenon, it was proposed that at low concentrations, hydrophilic peptides capture water molecules and alter the hydration structure at the step front of calcite. This was the first report to suggest that organic additives influence the hydration of calcite surface. In addition, recent interferometry measurements of calcite growth rate reveal that the characteristic surface diffusion length of calcite terraces increased in the presence of L-Aspartic acid (Maruyama *et al.*, 2009). This observation is the likely result of the capture of water molecules by L-Aspartic acid on the terraces.

Magnesium ions have been proposed to influence the hydration of calcite surface.

These ions are hydrated more easily than calcium ions due to their higher charge density (Noyes, 1962; Mucci and Morse, 1983). Therefore, it has been suggested that the incorporation of magnesium ions into calcite surfaces makes calcite surfaces harder to hydrate (De Groot and Duyvis, 1966; Berner, 1966; Möller and Parekh, 1975).

Although these studies have predicted the effects of additives on the hydration and growth rate of calcite; direct experimental evidence for these effects has not been demonstrated.

## 1.4 Objective

In this study, we evaluate the influence of additives on the hydration of calcite surface and growth rate by frequency modulation atomic force microscopy (Chapter 2) and phase shift interferometry (Chapter 3), respectively. The evaluation of the effect of additives on hydration and growth rate of calcite allows us to gain an understanding into the effect of hydration on the growth rate of calcite.

| | calcite | aragonite | Vaterite |
|---|---|---|---|
| Crystal system | Trigonal | orthorhombic | Hexagonal |
| Space group | R3c | Pmcn | $P6_3/mmc$ |
| cleavage | (1014) perfect | (010) imperfect | - |
| Hardness | 3 | 3.5 - 4 | 3 |
| Unit cell (Å) | a = 4.990<br>c= 17.061 | a = 4.96<br>b = 7.97<br>c = 5.74 | a = 4.120<br>c = 8.556 |

Table.1-1 Properties of polymorphs of calcium carbonate crystal (Deer, Howie, and Zussman: *An Intriduction to the Rock Forming Minerals*).

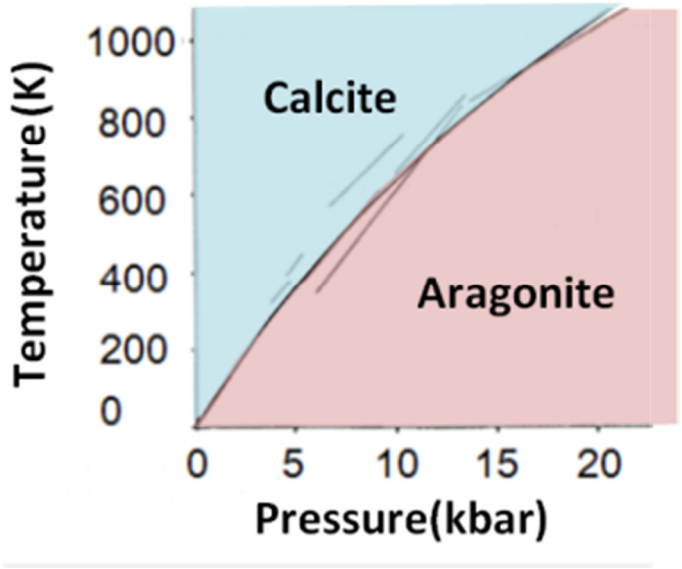


Fig.1-1 Phase diagram of calcium carbonate crystal (according to Redfern *et al*., 1989).

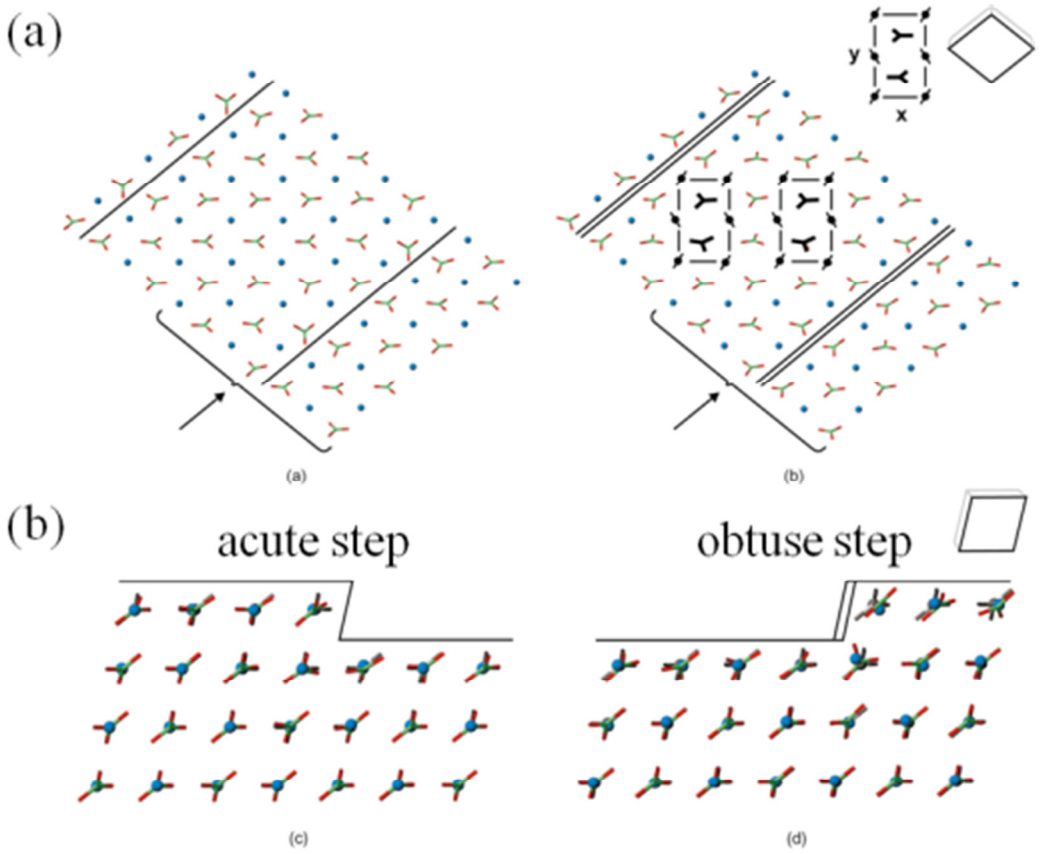


Fig.1-2

Schematic representation of anisotropic structure of calcite steps (according to Kristensen *et al.*, 2004). (a) Top view of the $(10\bar{1}4)$ face of calcite. Single and double lines represent the acute and obtuse step fronts, respectively. (b) Side view illustrating the angular relationship between acute and obtuse step edges with terraces.

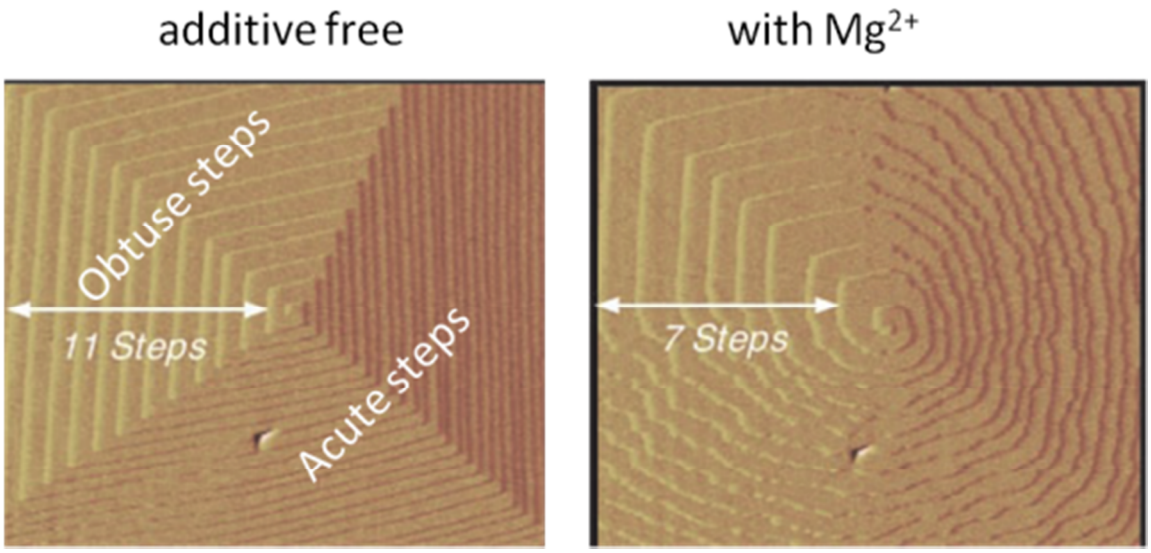


Fig.1-3 Kink blocking by magnesium ions on the acute steps of calcite (according to Davis *et al.*, 2000).

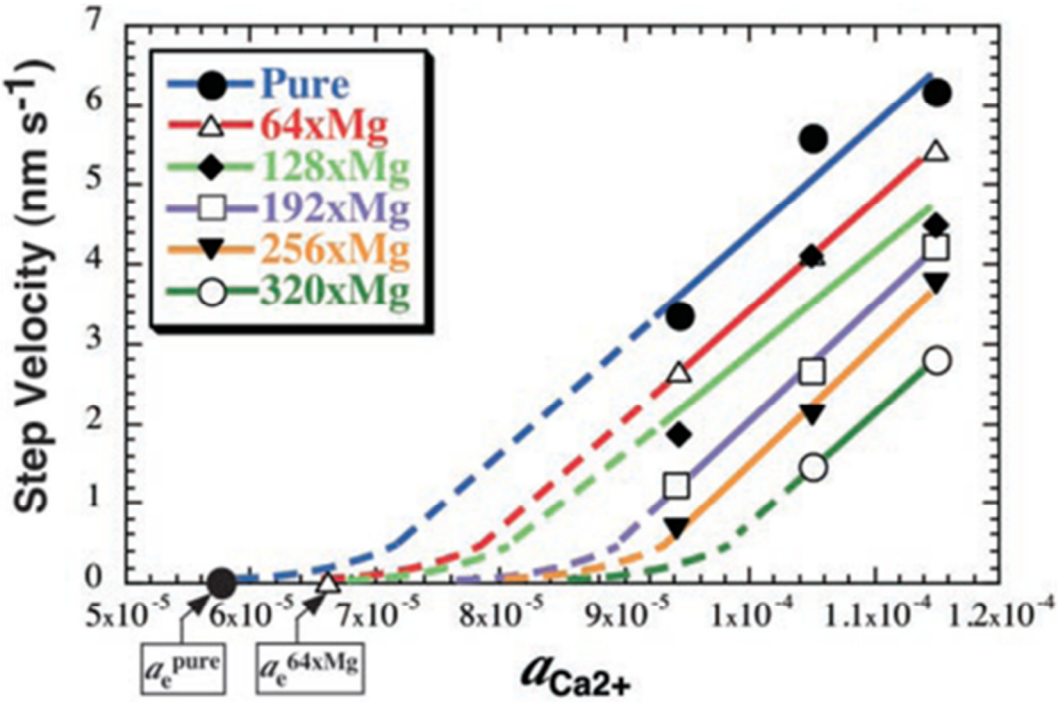


Fig.1-4

Shifts in calcite solubility with the incorporation of magnesium ions (Davis *et al.*, 2000). The concentration of magnesium ions for the curves of step velocity versus activity of calcium ion is shown in the inset.

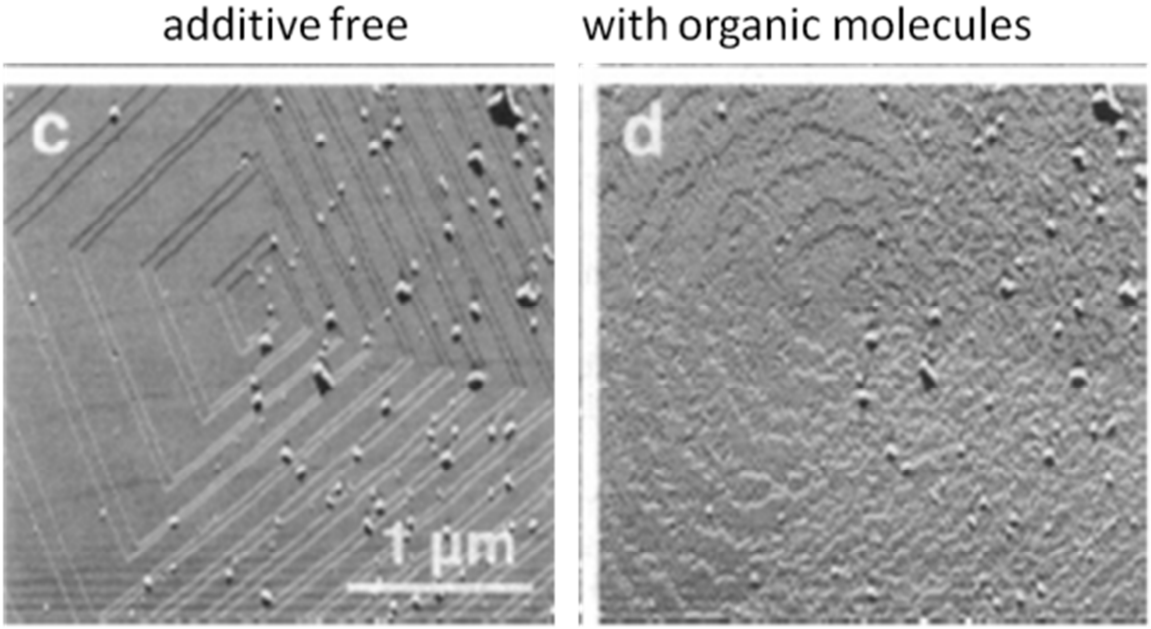


Fig.1-5 Pinning of organic molecules on calcite steps (according to Walters *et al*., 1997).

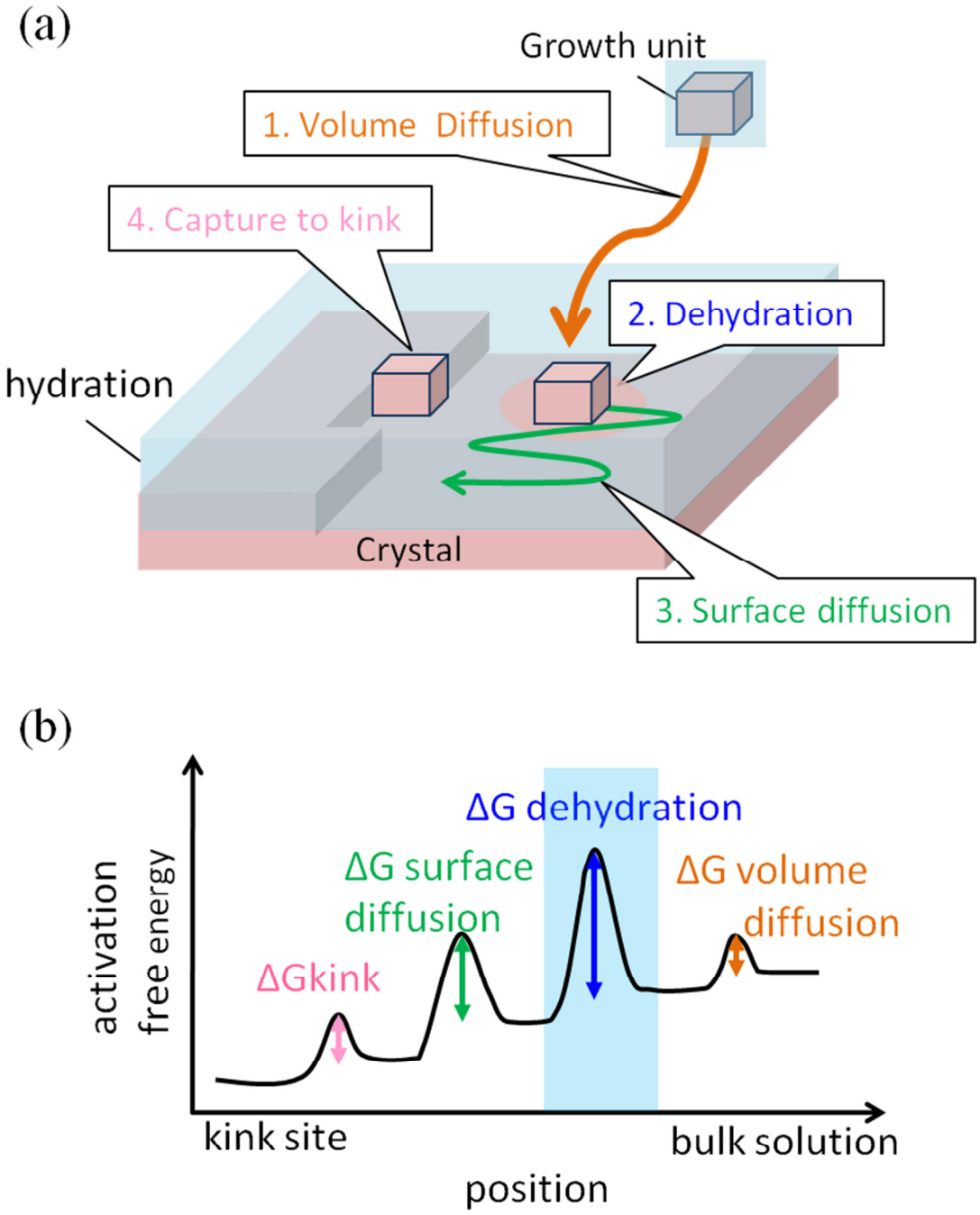


Fig.1-6

(a) Schematic image of the pathways of a growth unit in solution growth. (b) Schematic representation of energy barriers in solution growth processes (according to Bennema, 1967).

## *References in Chapter 1*


[1] Aizenberg, J., Muller, D. A., Grazul, J. L., Hamann, D. R. *Science* **2003**, 299, 1205-1208.

[2] Astilleros, J. M., Pina, C. M., Fernández-Díaz, L., Putnis, A. *Surf. Sci*. **2003**, 545, 767-773.

[3] Bennema, P., *J. Cryst. Growth* **1967**, 1, 278-286.

[4] Bennema, P., *J. Cryst. Growth* **1967**, 1, 287-292.

[5] Berner, R. A. *Science* **1966**, 153, 188-191.

[6] Cabrera, N. and Vermileya, D. A. In *Growth and Perfection of Crystals*; Doremus, R. H., Roberts, B. W., Turnbul, D., Eds.; Wiley: New York, **1958**.

[7] Cölfen, H. *Curr. Opin. Colloid Interface Sci.* **2003**, 8, 23-31.

[8] Davis, K. J.; Dove, P. M.; De Yoreo, J. J. *Science* **2000**, 290, 1134-1137.

[9] Davis, K. J., Dove, P. M., Wasylenki, L. E., De Yoreo, J. J. *Amer. Mineral.* **2004**, 89, 714-720.

[10] De Groot, K. and Duyvis, E. M. *Nature* **1966**, 212, 183-184.

[11] Elhadj, S.; De Yoreo, J. J.; Hoyer, J. R.; Dove, P. M. *Proc. Natl. Acad. Sci. U.S.A.* **2006**, 103, 19237-19242.

[12] Elhadj, S.; Salter, E. A.; Wierzbicki, A.; De Yoreo, J. J.; Han, N.; Dove, P. M. *Cryst. Growth Des*. **2006**, 6, 197-201.

[13] Gratz, A. J., Hillner, P. E., Hansma, P. K. *Geochim. Cosmochim. Acta*, **1993**, 57, 491-495.

[14] Hosoda, N., Sugawara, A. and Kato, T. *Macromolecules*, **2003**, 36, 6449 - 6452.

[15] Hu, Z., Shao, M., Cai, Q., Ding, S., Zhong, C., Wei, X., Deng, Y. *J. Mater. Process Tech.* **2009**, 1607-1611.

[16] Kim, W., Darragh, M. R., Orme, C., Evans, J. S. *Cryst. Growth and Des.* **2006**, 6, 5-10.

[17] Kristensen, R. K., Stipp, S. L. S., Refson, K. J. Chem. Phys. 2004, 121, 8511-8523.

[18] Kuang, M., Wang, D., Gao, M., Hartmann, J., Möhwald, H. *Chem. Mater* **2005**, 17, 656-660.

[19] Mann, S. *Biomineralization* (Oxford University Press, Oxford, U.K., **2001**)

[20] Maruyama, M., *doctoral thesis, Tohoku University*, **2008**.

[21] Maruyama, M.; Tsukamoto, K.; Sazaki, G.; Nishimura, Y.; Vekilov, P. G. *Cryst. Growth Des*. **2009**, 9, 127-135.

[22] Meece, D. E., and Benninger, L. K. *Geochim. Cosmochim. Acta*, **1993**, 57, 1447-1458.

[23] Möller, P. and Parekh, P. P. *Mar. Chem.* **1975**, 3, 63-77.
[24] Mucci, A., and Morse, J. W. *Geochim. Cosmochim. Acta*, **1983**, 47, 217-233.
[25] Nishimura, T., Ito, T., Yamamoto, Y., Yoshino, M., and Kato, T. *Angew. Chem*. **2008**, 47, 2800 - 2803.
[26] Noyes, R. M. J. Am. Chem. Soc. **1962**, 84(4), 513-522.
[27] Oaki, Y., Kijima, M., Imai, H. *J. Am. Chem. Soc.* **2011**, 133, 8594-8599.
[28] Orme, C. A., Noy, A., Wierzbicki, A., McBride, M. T., Grantham, M., Teng, H. H., Dove, P. M., De Yoreo, J. J., *Nature* **2001**, 411, 775-779.
[29] Paquette, J., Reeder, R. J., *Geochim. Cosmochim. Acta*, **1995**, 59, 735-749.
[30] Sorai , M., and Sasaki, M. *Energy Procedia* **2013**, 37, 5539-5544.
[31] Walters, D.A., Smith, B.L., Belcher, A.L., Paloczi, G.T., Stucky, G.D., Morse, D.E, and Hansma, P.K. *Biophysical Journal*, **1997**, 72, 1425 - 1433.

# *Chapter 2. Clarification of additive effects on hydration of calcite surface by FM-AFM*

## 2.1 Introduction

The clarification of the additive-induced changes in the calcite surface hydration hinges on the observation of the interface between calcite surface and additive solution at the atomic level. Hydration structure on calcite surface in water has been estimated by molecular dynamics (MD) simulations. It was predicted that there are three hydration layers and the distribution of hydrated water molecules are consistent with the atomic pattern of calcite surface by MD simulations (Fig.2-1) (Raiteri *et al*., 2010; Reischl *et al.*, 2012; Ricci *et al.* 2013). However, it is difficult to simulate the hydration structure in complicated system in the presence of organic molecules by MD simulations. Recently, the hydration at the vicinity of calcite surface has been measured by surface X-ray diffraction (s-XRD) (Geissbühler *et al.*, 2004; Fenter and Sturchip, 2012; Fenter *et al*., 2013) As a result, three hydration layers of calcite surface has been visualized in water by s-XRD (Fig.2-2). However, this method was not localized enough to give a direct experimental evidence for the additive effects. Calcite crystals grow through a lateral step movement, allowing molecules to attach to the step fronts. Therefore, an approach that gives distinct and detailed structural information on the hydration of the step front and the terrace is needed to identify the additive-induced changes in hydration structure and analyze hydration effects on the crystal growth mechanism.

The newly developed frequency modulation atomic force microscopy (FM-AFM) technique is expected to meet these requirements. FM-AFM has been used to examine the local hydration of mica surfaces in KCl solution with atomic resolution. (Fukuma *et al.*, 2007; Kimura *et al.*, 2010; Kobayashi *et al.*, 2013) *In situ* imaging of the hydration structure at the atomic scale using this technique should therefore provide insight into the local distribution of hydrated water molecules in growth solution and the effect of hydrophilic organic molecules and magnesium ions on local hydration.

## 2.2 Experimental section

### 2.2.1 Frequency modulation atomic force microscopy (FM-AFM)

The FM-AFM instrument working in liquid was developed by modifying the optical beam displacement sensor of the commercial SPM-9600 microscope (Shimadzu Corp., Japan) (Fukuma *et al.*, 2005) (Fig.2-3). The instrument was equipped with gold-coated highly doped n-type Si cantilevers (Nanosensors, PPP-NCHAuD) which displayed a

typical eigenfrequency of 160 kHz in liquids and self-oscillated with a peak-to-peak amplitude of 1 nm at their resonance frequency in the constant amplitude mode. Samples were placed in a 6-mm-deep open fluid cell with a diameter of 15 mm for imaging. The instrument was kept in an incubator (Mitsubishi Electric Engineering CN-40A) which was maintained at 295 ± 0.15 K during the experiments. The lateral thermal drift rate was reduced to be less than 1 nm/min. The WSxM software package (Nanotech Electronica) was used for image rendering and data processing. (Horcas *et al*., 2007)

### 2.2.2 Two-dimensional force mapping

Two-dimensional (2D) frequency shift maps at the solid-liquid interfaces were acquired by collecting the frequency shift *vs.* Distance curves at 256 pixels allocated to a line segment on the surface. (Kimura *et al.*, 2010) The frequency shift of the cantilever was recorded while the tip was approached to the sample surface. When the frequency shift signal reached a predetermined threshold value, the tip was immediately retracted to its original position. (Kobayashi *et al.*, 2013) During this data acquisition, the cantilever peak-to-peak oscillation amplitude was reduced to 0.2 – 0.6 nm. Individual frequency shift *vs.* distance curves were converted to interaction force *vs.* distance curves to give 2D force maps. (Sader and Jarvis, 2004)

### 2.2.3 Calcite crystal

A calcite crystal (3 mm x 3 mm x 2 mm) was cleaved and fixed to the bottom of the open fluid cell so that the $(10\bar{1}4)$ face became parallel to the scanning plane. A 100-µl droplet of growth solution was loaded onto the calcite surface.

### 2.2.4 Organic additive: the synthetic polypeptide

The synthetic polypeptide DFDRPDPYDPYDRFD, which consisted of fifteen amino acid residues including six periodically interspaced aspartic acids was used as an organic additive (D: aspartic acid, F: phenylalanine, R: arginine, P: proline, Y: tyrosine). (Takagi and Miyashita, 2010) The water solubility was 1 mg/mL. The polypeptide was purchased from Hokkaido System Science Corporation Ltd. with a purity exceeding 90 %.

### 2.2.5 Preparation of growth solutions

The pure, additive-free supersaturated $CaCO_3$ solution was prepared by mixing 0.1 M $CaCl_2$, 0.1 M $NaHCO_3$ and 0.1 M NaCl solutions at room temperature. NaCl solution

was added in order to adjust the ionic strength of solution as 0.1 M in case magnesium ion-free or 0.2 M in the presence of magnesium ion. The supersaturation $\sigma$ is defined as:

$$\sigma \equiv \frac{\Delta\mu}{kT} = \ln\left(\frac{a_{Ca^{2+}} \cdot a_{CO_3^{2-}}}{K_{sp}}\right) \qquad (2\text{-}1)$$

where $\Delta\mu$ is the change in chemical potential per molecule, $k$ is Boltzmann constant, $T$ is the absolute temperature, and $a_{Ca^{2+}}$ and $a_{CO_3^{2-}}$ are the activities of calcium and carbonate ions, respectively. The supersaturation was adjusted to 0.8 using the solubility product $K_{sp\ of\ calcite}$ was $10^{-8.48}$ at 25 °C (Mucci and Morse, 1983).

The synthetic polypeptide (10 μg/mL) was added to the supersaturated $CaCO_3$ solution in a centrifuge tube and the mixture was stirred for 1 min using ultrasonic vibrations. A 0.1 M $MgCl_2$ solution was added to the mixture so that the resulting concentrations of calcium and magnesium ions equaled 0.01 and 0.05 M, respectively. The pH of each solution was adjusted to 8.1 ± 0.05 by adding a few drops of 0.5 M HCl and NaOH solutions before FM-AFM imaging.

## 2.3 Results

### 2.3.1 in Pure $CaCO_3$ solution

Figure 2-4a shows an atomic-resolution FM-AFM image of the $(10\bar{1}4)$ calcite surface in a $CaCO_3$ solution in the absence of additives. The calcite surface exhibited the spiral growth steps and 2D nucleation sites (images not shown). The atomic-resolution image was taken on a flat terrace of 2D islands over a scan area of 5 nm x 2 nm. AFM imaging has reportedly given two different patterns for the calcite $(10\bar{1}4)$ face depending on tip conditions: one lattice pattern for calcium atom locations and one characteristic zigzag pattern for oxygen atom locations. (Hillner *et al*., 1992; Rachlin *et al*., 1992; Ohnesorge and Binnig, 1993; Liang *et al.*, 1996; Stipp *et al.*, 1994; Rode *et al.*, 2009) The atomic-scale features shown in Figure 1a correspond to the zigzag pattern of the oxygen atoms.

Figure 2-4b shows a 2D frequency shift map acquired along the $[48\bar{1}]$ direction (Fig. 2-4) indicated by the dotted line in Figure 2-5a. The image was obtained in 3 s over a scan area of 5 nm in the lateral direction by 2 nm in the vertical direction. The observed contrast represented the frequency shift of the cantilever. The darkest area at the bottom of the 2D frequency shift map indicates the area without any data. The brightest area represents the area where the frequency shift was close to the predetermined threshold value. Note that the interface between the darkest and brightest areas roughly represents the surface topography of calcite. In this case, the convex and the valley positions show the location of oxygen atoms and calcium atoms, respectively.

Bright areas delimited by dotted circles originated from repulsive forces that arose when the tip was brought close to the calcite surface. Although the relationship between the hydration force and the density of the water molecules were not straightforward, these areas corresponded to locations where the density of water molecules was higher than in the bulk solution. Frequency shifts were quantitatively concerted to interaction forces exerted on the tip using Sader's method: (Sader and Jarvis, 2004)

$$F(z) = 2k \int_z^{\infty} \left(1 + \frac{a^{1/2}}{8\sqrt{\pi(t-z)}}\right) \Omega(t) - \frac{a^{3/2}}{\sqrt{2(t-z)}} \frac{d\Omega(t)}{dt}\, dt \qquad (2\text{-}2)$$

,where $k$ is the spring constant (40 N/m), $a$ is the amplitude of oscillation, $z$ is the distance of closest approach between tip and sample, and $\Omega(t)$ is the frequency shift, respectively. Positive and negative frequency shifts resulted from repulsive and attractive forces, respectively.

The site-specific force-distance curves for oxygen atoms and calcium atoms of calcite surface are shown in Figure 2-5c. Overall, each force-distance curve showed a peak indicated by the arrows in Figure 2-5c, suggesting that two hydration layers were formed in the $CaCO_3$ solution in the absence of additives.

### 2.3.2 with the synthetic polypeptide

An atomic-resolution FM-AFM image of the $(10\bar{1}4)$ calcite surface representing the zigzag pattern of the oxygen atoms was acquired in a $CaCO_3$ solution containing the synthetic polypeptide (Fig. 2-6a). In addition, the corresponding 2D frequency shift map was taken along the $[48\bar{1}]$ direction of the calcite crystal in 2 s over a scan area of 5 nm x 2 nm (Fig. 2-6b). This 2D hydration image was similar to the image obtained in the additive-free $CaCO_3$ solution. The closest water molecules were located between the oxygen atoms. The each site-specific force-distance curve showed a peak on the oxygen atoms and on the calcium atoms, respectively (Fig. 2-6c), indicating that the synthetic polypeptide did not affect the hydration structure of the calcite surface.

### 2.3.3 with magnesium ion

FM-AFM image of calcite representing the zigzag pattern of the oxygen atoms was obtained in a $CaCO_3$ solution containing magnesium ions (Fig. 2-7a). The corresponding 2D frequency shift map was taken in 3 s over a scan area of 5 nm x 2 nm (Fig. 2-7b). Bright areas marked by dotted circles in Figure 2-7b showed the closest packed water clusters. The site-specific force-distance curves showed two peaks each on the oxygen atoms and the calcium atoms, respectively (Fig. 2-7c), indicating four hydration layers formed in the presence of magnesium ions. The water molecules were

located on calcium atoms in the first and third layers and above the oxygen atoms in the second and forth layers. The repulsive force exerted on the tip weakened when its distance from the calcite surface increased. This result suggests that magnesium ions promote the hydration of calcite surfaces into multilayer.

### 2.3.4 with the synthetic polypeptide and magnesium ion

The 2D hydration structure of calcite in the presence of magnesium ions and the synthetic polypeptide was examined to determine the multiple effects of the additives. Figure 2-7a shows the FM-AFM lattice pattern of the calcium atoms of calcite surface taken in a $CaCO_3$ solution containing magnesium ion and the synthetic polypeptide. The 2D frequency shift map was acquired in 12 s over a scan area of 4 nm x 2nm on the terrace (Fig.2-8b). The closest packed water clusters marked by dotted circles were similar to those obtained in $CaCO_3$ solution containing magnesium ion. The closest water molecules were situated on the oxygen atoms. Overall, four hydration layers were recognized in the site-specific force-distance curves (Fig. 2-8c).

The closest packed patterns of water clusters were examined in $CaCO_3$ solutions containing 50, 100, and 300 μg/mL of the synthetic polypeptide. The 2D frequency shift maps and the force-distance curves acquired in the $CaCO_3$ solutions containing the synthetic polypeptide and magnesium ions are shown in Figs.2-9. This data indicates that calcite hydration does not depend on the synthetic polypeptide concentration.

## 2.4 Discussions

### 2.4.1 The effect of magnesium ion on hydration of calcite surface

The 2D hydration images showed that magnesium ions facilitated the formation of a multilayered hydration structure regardless of the presence of the synthetic polypeptide (Figs. 2-7b, 2-8b, and 2-9a-c). It has been estimated that magnesium ions incorporated in the calcite surface bind the closest water molecules rigidly, then outer hydration layers would be formed based on the rigid first hydration layer. (De Groot and Duyvis, 1966; Berner, 1966; Möller and Parekh, 1975; Reddy and Nancollas, 1976) However, measurements of the repulsive force, which is equivalent to the hydration force, showed that the hydration force of the first layer did not change regardless of the present of magnesium ions (Fig. 2-10). This result indicates that this hydration force does not influence the formation of the multilayered hydration structure. Although the mechanism governing this multilayered hydration is unknown, this data suggests that magnesium ions may contribute to the hydrogen bond among water molecules.

It is estimated that a thick hydration structure may hinder the ion capture by the

calcite surface and the ion diffusion on the terrace.

### 2.4.2 The effect of the synthetic polypeptide on hydration of calcite surface

Hydrophilic organic molecules have been proposed to capture water molecules and change the hydration structure of calcite surface by adsorption on the step fronts (Elhadj *et al.*, 2006a; Elhadj *et al.* 2006b) or the terrace (Maruyama *et al.*, 2009) of calcite. The hydrophilicity of the synthetic polypeptide was 61.2 kJ/mol according to the Hopp and Woods hydrophilicity scale, (Hopp and Woods, 1981) which mostly amounted to the same value as for the peptides used by Elhadj *et al*. (Elhadj *et al.*, 2006a) The addition of the synthetic polypeptide to the pure $CaCO_3$ solution did not change the hydration structure on the terrace, suggesting that organic molecules do not affect calcite even if these molecules are hydrophilic. Investigation on hydration structure of the step front is currently underway (see Appendix 1). After the visualization of the hydration of the step front, the effect of organic molecules at the step edge on the hydration would be revealed.

FM-AFM measurements also revealed that the addition of the synthetic polypeptide to the pure $CaCO_3$ solution did not change the hydration force. On the other hand, the repulsive force of the first and second layers increased twofold when the synthetic polypeptide and magnesium ion coexisted in the $CaCO_3$ solution compared to all other solutions (Fig. 2-10). When they were alone in the growth solution, magnesium ions and the synthetic polypeptides did not affect the hydration force. It indicates that the binding energy between the water molecules and the atoms of calcite surface increases due to the cooperative effects of the additives.

Considering the hydration force, which is suggested by repulsive force, the dehydration energy of the terrace in the $CaCO_3$ solution containing the synthetic polypeptide alone would be as well as that in the pure $CaCO_3$ solution. Therefore, it is estimated that the synthetic polypeptide would not affect the ion capture by the calcite surface and the surface diffusion on the terrace. On the other hand, when coexisting with magnesium ions, the synthetic polypeptides may contribute to interactions between water molecules and the atoms on calcite surface, making ion capture by the calcite surface and the surface diffusion more difficult than in the presence of magnesium ions alone. As a result, the calcite growth rate would decrease.

## 2.5 Summary

We showed the atomic-level change of the local distribution of the water molecules of calcite induced by magnesium ions and the synthetic polypeptide for the first time. FM-AFM imaging revealed that the four hydration layers consist of the closest packed water clusters at the vicinity of calcite surface in the presence of magnesium ions. These magnesium ions affected the distribution of water molecules but not the hydration force. Although hydrophilic organic molecules had previously been suggested to impact calcite hydration, the synthetic polypeptide had no effect on either the hydration structure or force of calcite terrace. This indicates that the hydrophilic organic molecules do not contribute to dehydration and surface diffusion of the ions on the calcite terrace. On the other hand, cooperative effects between the synthetic polypeptide and the magnesium ions made the hydration structure more rigid. It is predicted that the multilayered hydration structure and the interactions between calcite surface and water molecules may suppress calcite growth.

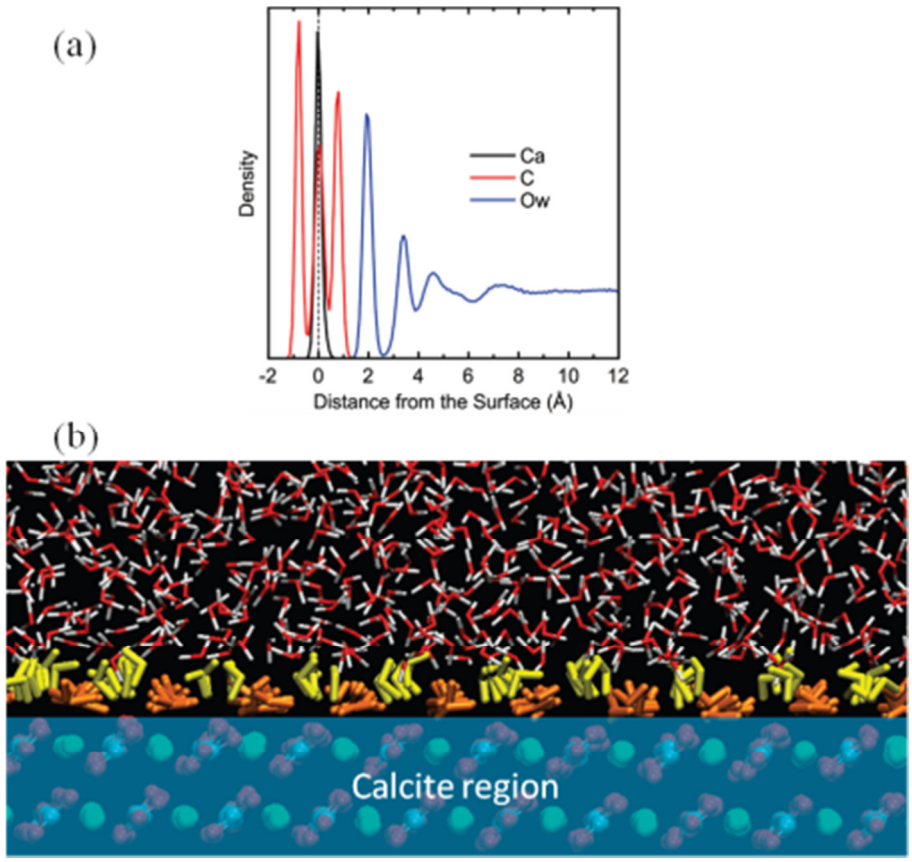


Fig. 2-1 Molecular dynamics simulation of water distribution of calcite surface (according to Raiteri *et al.*, 2010). (a) Density profiles water-calcite interface. (b) Water distribution at the vicinity of the $(10\bar{1}4)$ face of calcite.

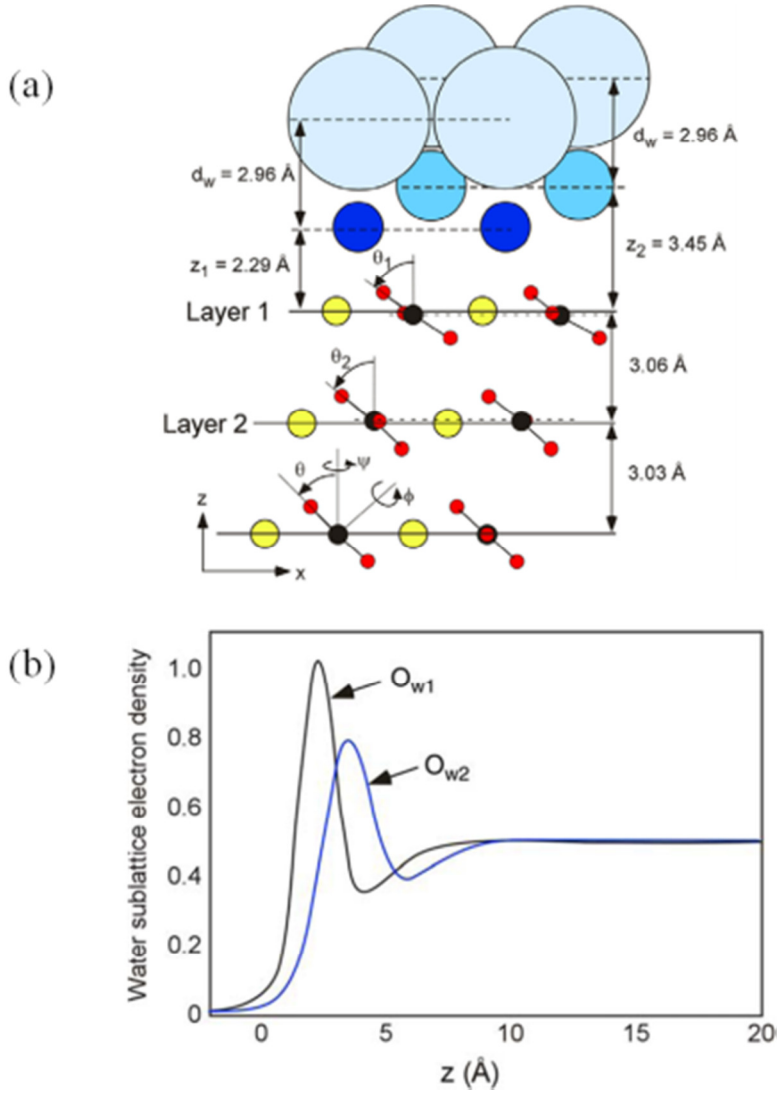


Fig. 2-2 surface-XRD measurement of hydration structure of water-calcite interface (Geissbühler *et al*., 2004). (a) Schematic of water distribution of calcite surface. (b) Laterally averaged density profile for the two water lattices.

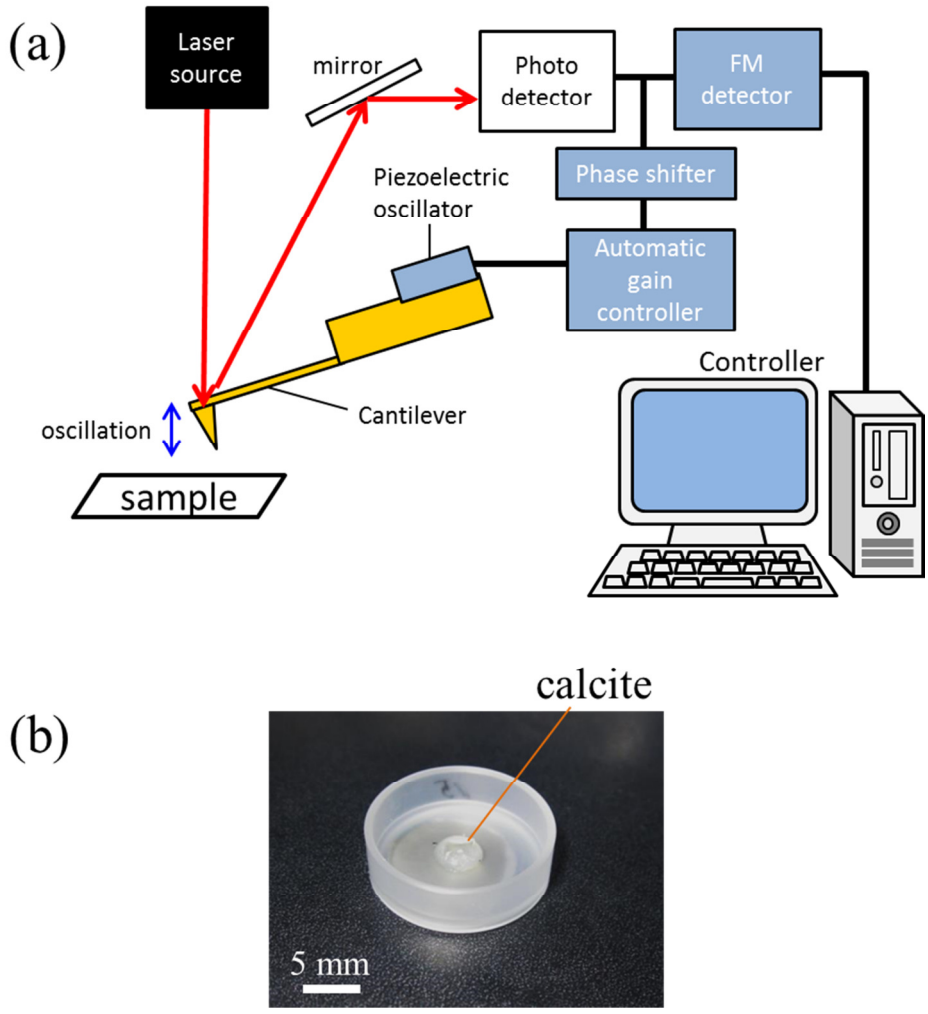


Fig. 2-3
(a) Photograph of observation system of FM-AFM. (b) Photograph of a calcite crystal glued at the bottom of sample holder for FM-AFM observation.

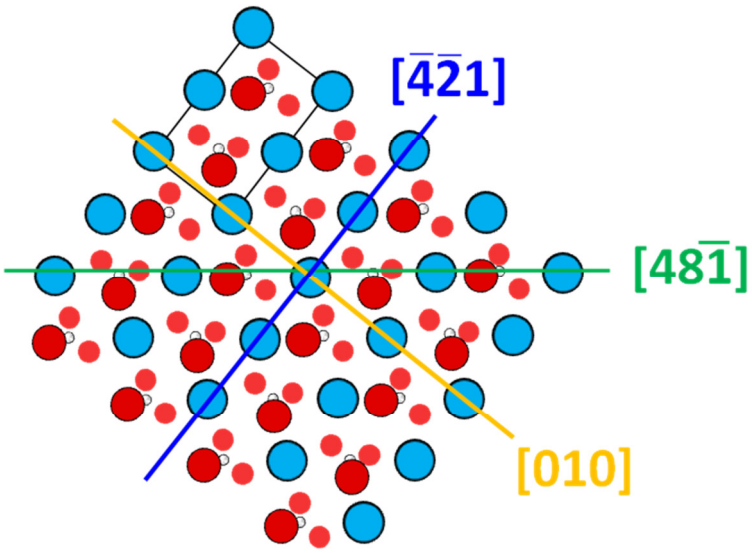


Fig.2-4

Schematic of the $(10\bar{1}4)$ face of calcite. Blue, red and white balls represent calcium, oxygen, and carbon atoms, respectively. Larger red balls locate above smaller red balls. The rectangular shows the surface unit cell.

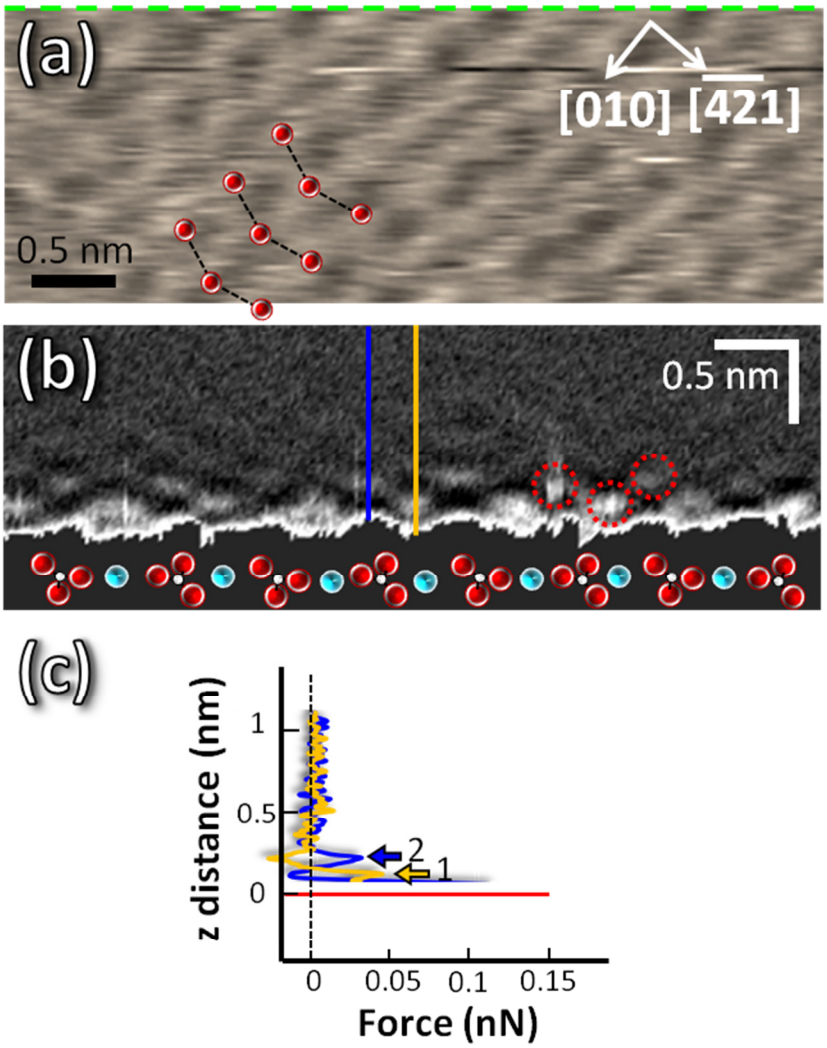


Fig.2-5

FM-AFM images and force-distance curves of calcite surface and solid-liquid interface in pure $CaCO_3$ solution. **(a)** Atomic-scale image of the calcite surface. The red balls represent oxygen atoms of the $(10\bar{1}4)$ face of calcite. **(b)** 2D frequency shift map taken along the $[48\bar{1}]$ direction of the calcite crystal (green dashed line, Fig.2-5a). The darkest area at the bottom of the image is the calcite crystal region. Blue, white, and red balls represent calcium, carbon, and oxygen atoms, respectively. Bright areas marked by red dashed circles correspond to water molecules. **(c)** Site specific force-distance curves measured along the blue and yellow lines shown in Fig. 2-5b. The red line indicates the position of the valley bottom in Fig. 2-5b. Peaks marked by arrows correspond to hydration layers.

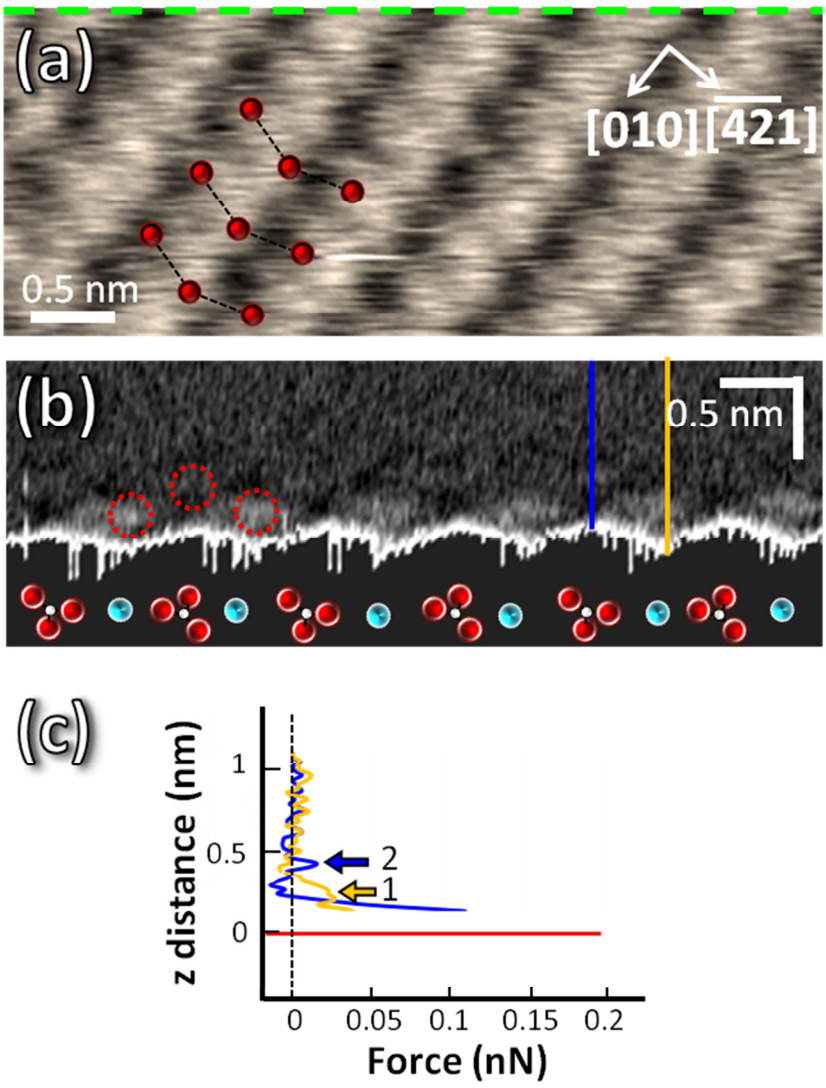


Fig.2-6

FM-AFM images and force-distance curves of the calcite surface and solid-liquid interface in a $CaCO_3$ solution containing the synthetic polypeptide. (a) Atomic-scale image of the calcite surface. The red balls represent oxygen atoms of the $(10\bar{1}4)$ face of calcite. (b) 2D frequency shift map taken along the [481] direction of the calcite crystal (green dashed line, Fig.2-6a). The darkest area at the bottom of the image is the calcite crystal region. Brighter areas marked by red dashed circles represent water molecules. Blue, white, and red balls correspond to calcium, carbon, and oxygen atoms, respectively. (c) Site specific force-distance curves measured along the blue and yellow lines shown in Fig. 2-6b. The red line indicates the position of the valley bottom in Fig. 2-6b. The peaks marked by arrows correspond to the hydration layers.

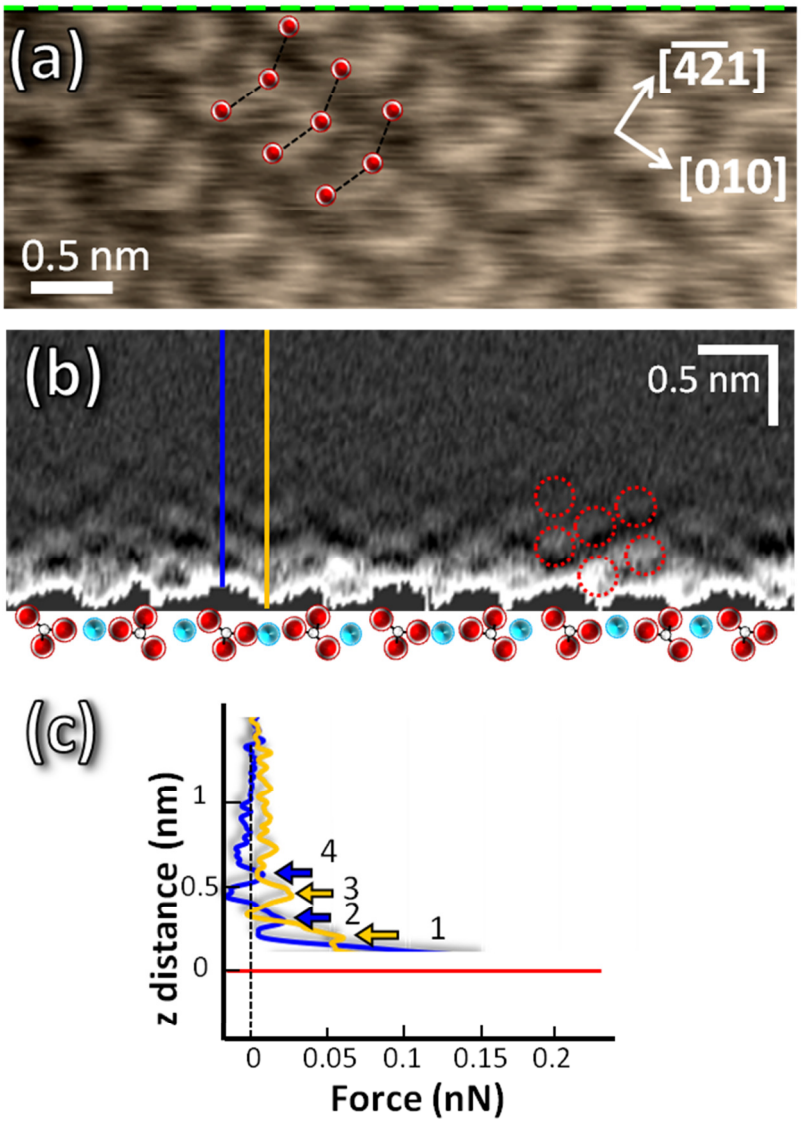


Fig.2-7

FM-AFM images and force-distance curves of the calcite surface and solid-liquid interface in a $CaCO_3$ solution containing magnesium ions. (a) Atomic-scale image of the calcite surface. The red balls represent oxygen atoms of the ($10\bar{1}4$) face of calcite. (b) 2D frequency shift map taken along the [481] direction of the calcite crystal (green dashed line, Fig. 2-7a). The darkest area at the bottom of the image is the calcite crystal region. Blue, white, and red balls represent calcium, carbon, and oxygen atoms, respectively. Brighter areas marked by red dashed circles correspond to water molecules. (c) Site specific force-distance curves measured along the blue and yellow lines shown in Fig. 2-7b. The red line indicates the position of the valley bottom shown in Fig. 2-7b. Peaks marked by arrows correspond to the hydration layers.

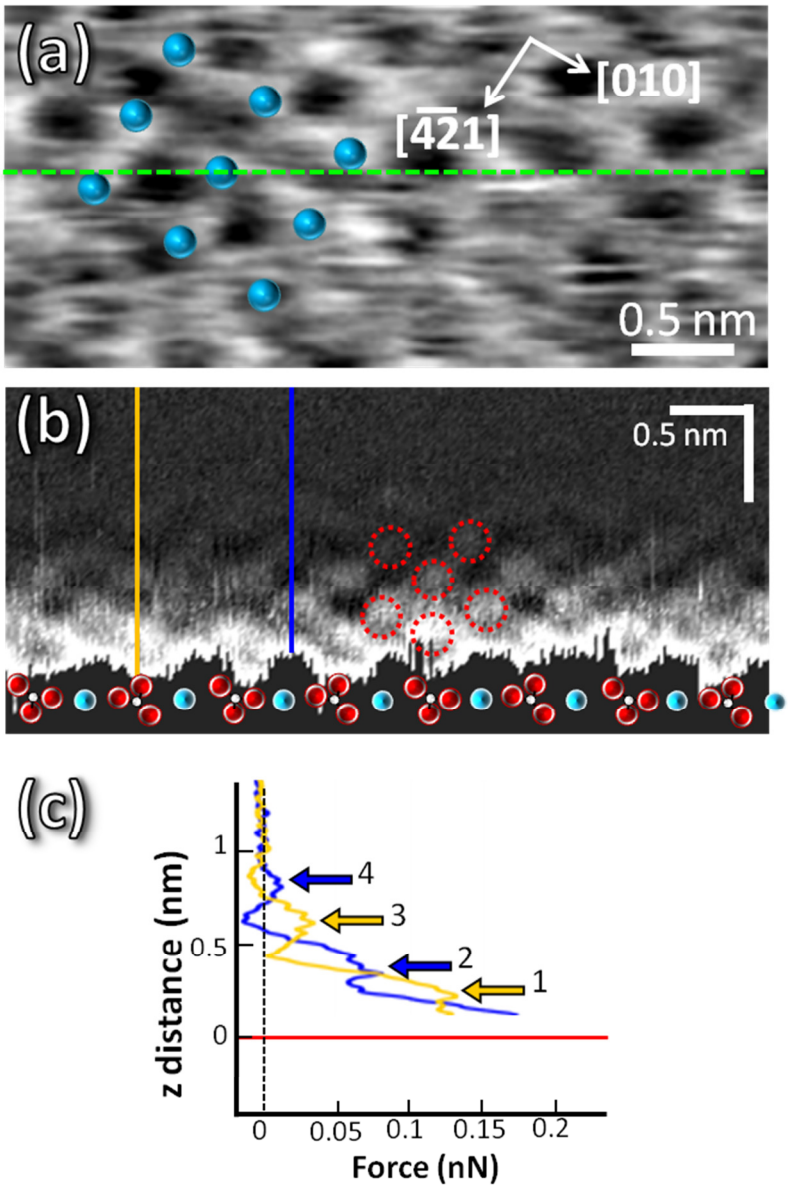


Fig. 2-8

FM-AFM images and force-distance curves of the calcite-solution interface in a $CaCO_3$ solution containing the synthetic polypeptide and magnesium ions. (a) Atomic-scale image of the ($10\bar{1}4$) face of the calcite surface. The blue balls represent calcium atoms of the calcite surface. (b) 2D frequency shift map taken along the [$48\bar{1}$] direction of the calcite crystal (green dashed line, Fig.2-8a). The darkest area at the bottom of the image is the calcite crystal region. Blue, white, and red balls represent calcium, carbon, and oxygen atoms, respectively. (c) Site specific force-distance curves measured along the blue and yellow lines shown in Fig. 2-8b. Peaks marked by arrows correspond to the hydration layers.

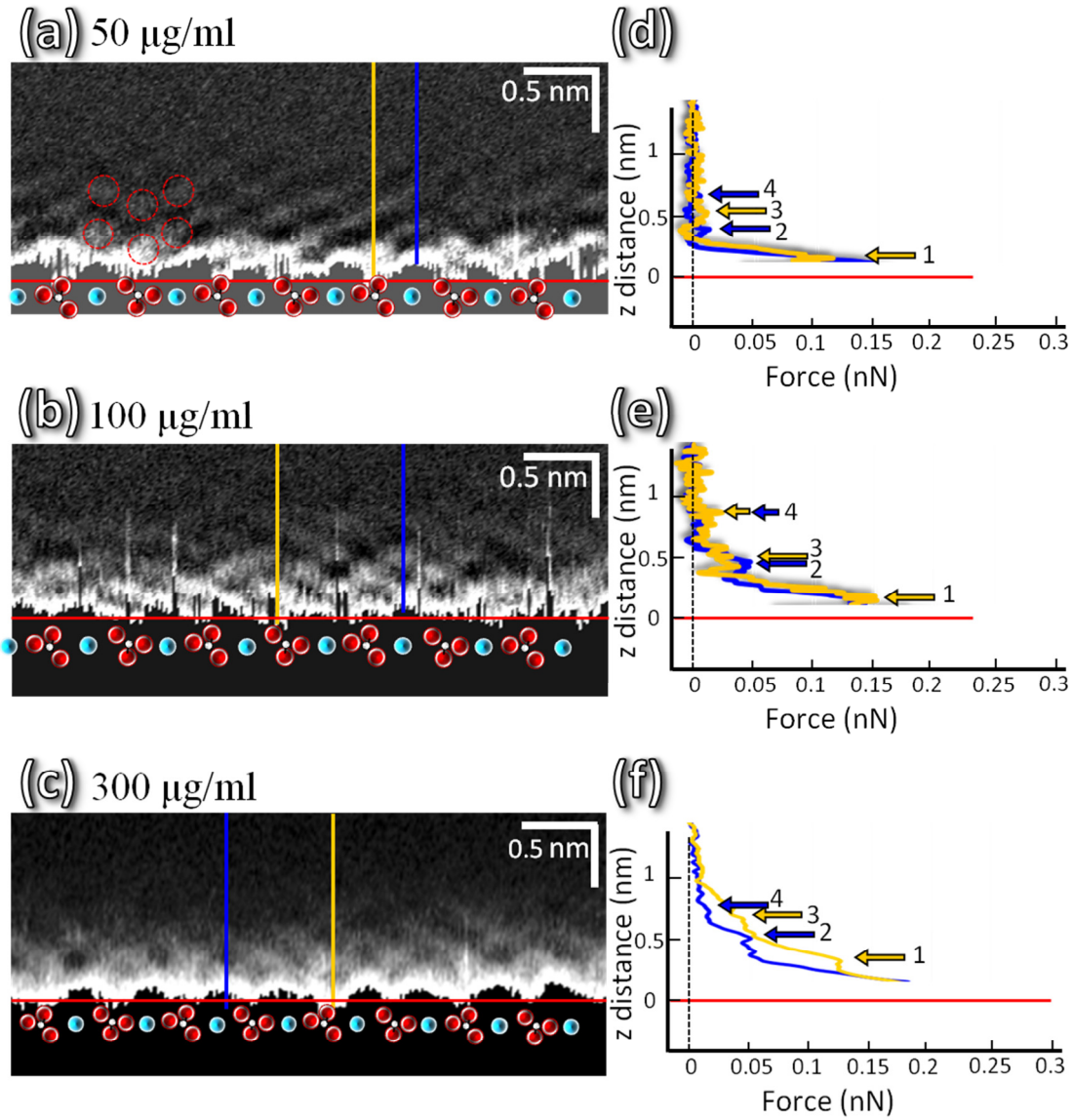


Fig. 2-9

FM-AFM images and force-distance curves of the calcite surface and solid-liquid interface in a $CaCO_3$ solution containing the synthetic polypeptide and magnesium ions. (a)-(c) 2D frequency shift map taken along the [48$\bar{1}$] direction of the calcite crystal in cases of 50, 100, 300 μg/ml the synthetic polypeptide, respectively. The darkest area at the bottom of the image is the calcite crystal region. Blue, white, and red balls represent calcium, carbon, and oxygen atoms, respectively. (d) – (f) Site specific force-distance curves measured along the blue and yellow lines shown in Figs. 2-9(a)-(c), respectively. Peaks marked by arrows correspond to the hydration layers.

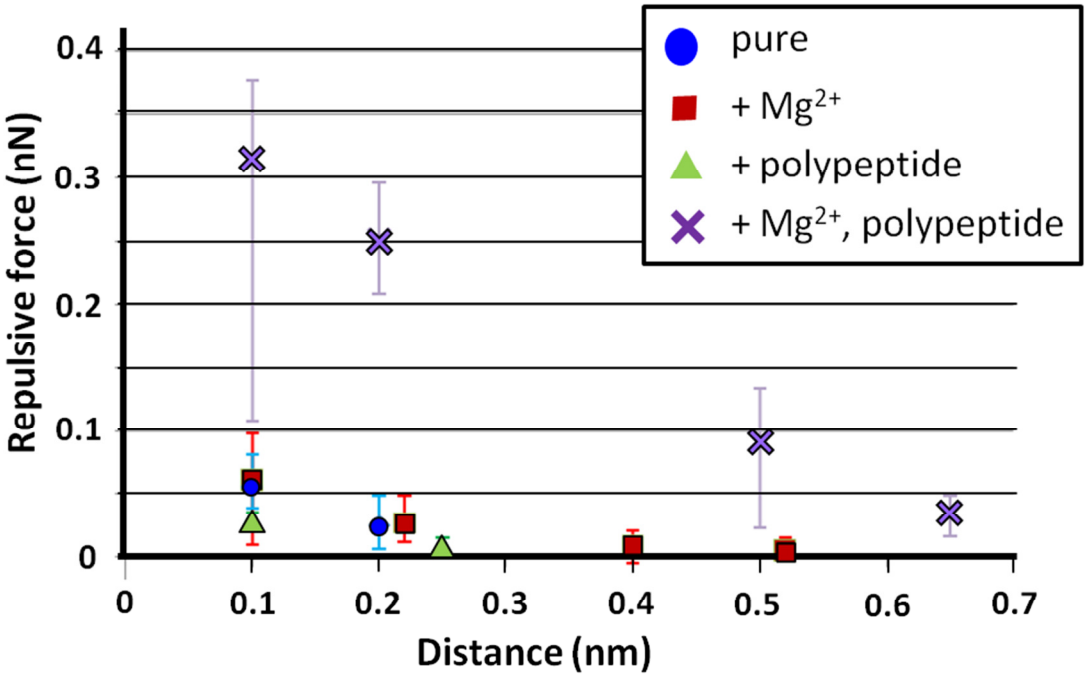


Fig. 2-10

Repulsive force exerted on the tip by each hydration layer. Force values were determined from the site-specific force-distance curves (Figs.2-5 – 2-8).

## *References in Chapter 2*


[1] Berner, R. A. *Science* **1966**, 153, 188-191.

[2] De Groot, K. and Duyvis, E. M. *Nature* **1966**, 212, 183-184.

[3] Elhadj, S.; De Yoreo, J. J.; Hoyer, J. R.; Dove, P. M. *Proc. Natl. Acad. Sci. U.S.A.* **2006**, 103, 19237-19242.

[4] Elhadj, S.; Salter, E. A.; Wierzbicki, A.; De Yoreo, J. J.; Han, N.; Dove, P. M. *Cryst. Growth Des*. **2006**, 6, 197-201.

[5] Fenter, P., and Sturchio, N. C., *Geochim. Cosmochim. Acta*, **2012**, 97, 58-69.

[6] Fenter, P., Kerisit, S., Raiteri, P., and Gale, J. D., *J. Phys. Chem.* C **2013**,117, 5028-5042.

[7] Fukuma, T.; Kimura, K.; Kobayashi, K.; Matsushige, K.; Yamada, H. *Rev. Sci. Instrum.* **2005**, 76(12), 126110.

[8] Fukuma, T.; Ueda, Y.; Yoshioka, S.; Asakawa, H. *Phys. Rev. Lett.* **2010**, 104, 016101.

[9] Geissbühler, P.; Fenter, P.; DiMasi, E.; Srajer, G.; Sorensen, L. B.; Sturchio, N.C.; *Surf. Sci.* **2004**, 573, 191-203.

[10] Hillner, P. E., Manne, S., Gratz, A. J., and Hansma, P. K. *Ultramicroscopy*, **1992**, 42, 1387-1393.

[11] Hopp, T. P.; Woods, K. R. *Proc. Natl. Acad. Sci. USA*, **1981**, 78, 3824-3828.

[12] Horcas, I.; Fernández, R.; Gómez-Rodríguez, J. M.; Colchero, J.; Gómez-Herrero, L. *Rev. Sci. Instrum.* **2007**, 78, 013705.

[13] Kimura, K.; Ido, S.; Oyabu, N.; Kobayashi, K.; Hirata, Y.; Imai, T.; Yamada, H. *J.Chem.Physic.* **2010**, 132, 194705.

[14] Kobayashi, K.; Oyabu, N.; Kimura, K.; Ido, S.; Suzuki, K.; Imai, T., Tagami, K., Tsukada, M.; Yamada, H. *J. Chem. Phys.* **2013**, 138, 184704.

[15] Liang, Y., Lea, A. S., Baer, D. R., and Engelhard, M. H. *Surf. Sci.* **1996**, 351(1 - 3) 172-182.

[16] Maruyama, M.; Tsukamoto, K.; Sazaki, G.; Nishimura, Y.; Vekilov, P. G. *Cryst. Growth Des*. **2009**, 9, 127-135.

[17] Möller, P. and Parekh, P. P. *Mar. Chem.* **1975**, 3, 63-77.

[18] Mucci, A.; Morse, J. W. *Geochim. Cosmochim. Acta*, **1983**, 47, 217-233.

[19] Ohnesorge, F., and Binnig, G. *Science* **1993**, 260, 1451-1456.

[20] Rachlin, A. L., Henderson, G. S., and Goh, M. C. *Am. Mineral.* **1992**, **77**, 904-910.

[21] Raiteri, P., Gale, J. D., Quigley, D., and Rodger, P. M. *J. Phys. Chem. C* **2010**, 114(13), 5997-6010.

[22] Reddy, M. M. and Nancollas, G. H., *J. Cryst. Growth*, **1976**, 35, 33-38.

[23] Reischl, B., Watkins, M., and Foster, A. S., *J. Chem. Theory Comput.* **2013**, 9, 600-608.

[24] Ricci, M., Spijker, P., Stellacci, F., Molinari, J. F., and Voïtchovsky, *Langmuir* **2013**, 29, 2207-2216.

[25] Rode, S.; Oyabu, N.; Kobayashi, K.; Yamada, H.; Kuehnle, A.; *Langmuir* **2009**, 25, 2850.

[26] Sader, J. E. and Jarvis, S. P. *Appl. Phys. Lett.* **2004**, 84, 1801-1803.

[27] Stipp, S. L. S., Eggleston, C. M., and Nielsen, B. S. *Geochim. Cosmochim. Acta.* **1994**, 58, 3023-3033.

[28] Takagi, R. and Miyashita, T., *Zoolog. Sci*., **2010**, 27(5), 416-426.

# *Chapter 3. The additive effects on growth rate of calcite*

## 3.1 Introduction

The importance of surface diffusion for solution growth has been found by the measurement of growth rate of sodium chlorate crystal (Bennema, 1967a, b). Dependence of growth rate on supersaturation of sodium chlorate crystal showed that surface diffusion of the solutes occurs even in solution growth. Thus, we can acquire information of solution properties and behavior of solutes, such as solubility, interfacial tension, adsorption of additives, and step energy, among others from growth rate.

Growth rate of calcite have been measured in the presence and absence of the additive by atomic force microscopy (Teng, *et al.*, 1999; Teng *et al.*, 2000; Davis *et al.*, 2000) and interferometric techniques (Meyer, 1984; Arvidson et al., 2003; Arvidson *et al*., 2006; Maruyama *et al*., 2009). The increase of solubility of calcite and the suppression of step propagation in the presence of additives has been confirmed by these previous studies. For example, Teng *et al*. measured the step velocity of calcite by step motion using contact mode AFM (Teng *et al.*, 1999). The dependence of growth rate and surface pattern of calcite on supersaturation was shown by Teng et al. (2000). Then, they found that the plot of step velocity versus supersaturation became non-linear at low supersaturation. That suggests the adsorption of impurities or low kink density of calcite steps (De Yoreo *et al*., 2009). On the other hand, growth rate measurement by interferometric technique showed that the plot of step velocity versus supersaturation kept linear even under low supersaturation (Maruyama et al., 2009). These results suggest that it is easier to observe the additive effect on adsorption of ions on calcite surface under lower super saturation than high super saturation. The phase shift interferometry enables us to measure ultraslow growth rate under low supersaturation without stirring of the solution by the tip of AFM measurement (detailed information of PSI will be shown in experimental section).

We validate the additive effect on the solution property and adsorption of ions on calcite steps by the measurement of growth rate of calcite by phase shift interferometry in order to clarify the effect of hydration on growth rate of calcite.

## 3.2 Experimental section

### 3.2.1 Phase shift interferometer

The white-beam phase shift interferometer (PSI) based on the Michelson-type interferometry has been achieved to measure ultraslow growth and dissolution rate in

the order of $10^{-5}$ nm/s (Onuma *et al*., 1988; Tsukamoto *et al*., 1992; Maruyama *et al.*, 2009; Van Driessche *et al*., 2011).

Fig.3-1 shows the schematic of the phase shift interferometry. A xenon lump was used as a source of non-coherent white light. The white light is employed to improve the lateral resolution comparing with the phase-shift interferograms of laser-based interferometer with speckles. The white light is filtered to green light with a wave length of 532 nm. And the light is converted to linear polarized light by a polarizer. The green light beam is separated to two optical paths toward the sample surface and the reference mirror, respectively by the beam splitter. The reflected beams from the sample surface and the mirror are joined in the beam splitter and are captured by CCD camera (Olympus, DP70). The depth resolution of the Michelson type interferometry is 200 nm calculated from following equation:

$$\Delta z = \lambda/2n \qquad \textbf{(3-1)}$$

where $\lambda$ is the wavelength of the light source, $n$ is the refractive index of the solution, 1.33 in our case. On the other hand, a phase shift image was obtained from three interferograms taken on three different phase positions at 0, $2\pi/3$ and $4\pi/3$ by the shifting of the reference mirror using a piezo-actuator (Fig.3-2). The three interferograms were captured every 30 s. In this case, the depth resolution of white-beam phase shift interferometer is better than 1 nm. The phase shift image was converted to an 8-bit grayscale image for analysis of growth rate.

### 3.2.2 Procedure of the measurement by PSI

Figure 3-3 shows the growth cell and the flow system of phase shift interferometric measurement. A cleaved calcite crystal (2 x 2 x 1 mm) was fixed on the titanium holder by silicone glue. In order to cancel the disturbance from stage vibration, we used ~10 μm gold foils as a reference of the calcite surface (Satoh *et al.*, 2007).

$CaCO_3$ supersaturated solution in the absence of the additive, in the presence of 0.05 M magnesium ion, $10^{-5}$ M the synthetic polypeptide, and 0.05 M magnesium ion and $10^{-5}$ M the synthetic polypeptide were prepared. Their conditions are in the same manner as Chapter 2. The solution was provided into the cell by a syringe pump at the flow rate of 40 μl/min. This value was determined to cancel the effect of volume diffusion of the ions. The PSI is placed in a clean room laboratory and the temperature was kept at 22 ± 0.2 °C. Before measurement, the ultrapure water (18 MΩ) was poured into the cell in order to clean the calcite surface. Some etch pits were formed on calcite

surface in water. In this study, we measured the growth rate at the dislocation center of the etch-pits and hillocks which were formed after supersaturated solution was poured.

### 3.2.3 Analysis of growth rate and step velocity

The time series variation of the height on a horizontal line of phase shift images is obtained after the compensation of the height by gold foils (Figs.3-4a, b). The change of the light intensity of an arbitrary point is converted to the height by the phase-shift algorithm as follows:

$$\Delta z = \lambda/2n \text{ x } I/255 \qquad \textbf{(3-2)}$$

where and $I$ is the intensity of a point of the crystal surface. Then, the time evolution of the height is plotted and the slope of height *vs* time corresponds to the growth rate (R) (Fig. 3-4c). Step velocity (V) was determined by the following equation.

$$V = \frac{R}{p} \qquad \textbf{(3-3)}$$

$p$ is slope of hillock and etch-pit. $p$ was measured from the cross section profile of hillock and etch pit directly (Fig. 3-4d).

## 3.3 Results

### 3.3.1 Determination of the equilibrium concentration

Fig.3-5 shows the dependence of the growth rate of calcite, R, on supersaturation, $\sigma$, in the presence and absence of the additives to determine the equilibrium concentration indicating the solubility of calcite. The supersaturation in Fig. 3-5 was calculated tentatively using $K_{sp} = 10^{-8.48}$ at 25 °C (Mucci and Morse, 1983).

The equilibrium concentration is not decided uniquely, because the calcite stops growing in certain range at low supersaturation. Therefore, we defined the equilibrium concentration as a point that calcite surface begins to dissolve ($R < 0$) in this work. As a result, the equilibrium condition was determined as $\sigma = 0.5$, $\sigma = 0.65$, and $\sigma = 0.65$ in the presence of magnesium ion, the synthetic polypeptide, and magnesium ion and the synthetic polypeptide, respectively. The equilibrium concentration of calcite increased in the presence of the additives. This is consistent with the results of previous studies (Yoshino and Kagi, 2008; Davis *et al.*, 2000; Maruyama *et al.*, 2009).

### 3.3.2 Comparison of growth rate and step velocity of calcite

Fig.3-6 shows the dependence of the calcite growth rate, R, on supersaturation. The

supersaturation reflected the solubility shift determined in 3.3.1. The R *vs* $\sigma$ curves were parallel to the curve of pure $CaCO_3$ solution in the presence of magnesium ion and the synthetic polypeptide alone (Fig.3-6a, b). On the other hand, the growth rate increased in the presence of magnesium ion and the synthetic polypeptide comparing with in the absence of the additives (Figs.3-6 c). Note that three-dimensional nucleation of calcium carbonate crystal was occurred in the presence of magnesium ion and the synthetic polypeptide at $\sigma$ = 0.65 just after the mixing of mother solutions.

Both slopes of acute steps and obtuse steps increased in the presence of magnesium ion comparing with that of the additive-free solution (Fig.3-7a, b). The increase of slope indicates decrease of the step spacing and increase of the step density. In the presence of the synthetic polypeptide alone, the slope of both steps increased at higher supersaturation (Fig, 3-7c, d). On the other hand, the slope of acute steps decreased and the slope of obtuse steps had no change in the coexistence of magnesium ion and the synthetic polypeptide (Fig. 3-7e, f).

Step velocity of acute and obtuse steps of calcite determined from growth rate and slope of hillocks and etch-pits are shown in Figure 3-8. The step velocity of both acute and obtuse steps decreased in the presence of magnesium ion and the synthetic polypeptide alone comparing with that of the additive-free solution (Figs. 3-8a-d). On the other hand, in the coexistence of magnesium ion and the synthetic polypeptide, the step velocity of acute and obtuse step increased (Fig. 3-8 e, f).

## 3.4 Discussions

### 3.4.1 The additive effect on nucleation rate of calcite

Our measurement showed that the growth rate had no change in the presence of magnesium ion and the synthetic polypeptide alone, although growth rate should decrease with decreasing of step velocity. It can be cause of increase of nucleation rate. It has been confirmed that spiral growth was changed to two-dimensional nucleation by the addition of magnesium ion and the synthetic polypeptide even in lower supersaturation than the additive-free solution by differential interference contrast microscopy and the contact mode atomic force microscopy (Fig. 3-9) (Araki, undergraduate thesis, 2008; Davis *et al*., 2004; Stephenson *et al.*, 2011). Furthermore, step edges of calcite seem to be rough in the additive solutions in the phase shift images (Fig. 3-10). It is suggested that 2D islands were formed on the terraces of spiral hillocks (Liu *et al*., 1997). The 2D nucleation between the spiral steps has been observed by Maiwa *et al.* (1998) on Barium nitrate crystal. In addition, in the case of coexistence of magnesium ion and the synthetic polypeptide, three-dimensional nucleation occurred. It

indicates that the nucleation rate more increased in the coexistence of magnesium ion and the synthetic polypeptide than that of the other additive solutions. It is suggested by the acceleration of growth rate of calcite as shown in Fig. 3-6c.

### 3-4-2. The additive effect on adsorption of ions on calcite surface

The step velocity of calcite decreased in the presence of magnesium ion and the synthetic polypeptide alone. The decrease of step velocity indicates that the adsorption of ions on step front is suppressed. Considering the change of slope hillocks and etch-pits of calcite, step spacing is smaller in the presence of magnesium ion and the synthetic polypeptide than that of pure solution. The decrease of adsorption of ion on step fronts seems to be due to the decrease of step spacing. Note that although volume diffusion of ions also affects adsorption of the ion on step edge, the effect of volume diffusion was canceled by solution flow (Maruyama *et al*., 2009). According to the surface diffusion model (Burton *et al*., 1951), the ions which adsorbed on crystal surface diffuse on terrace between steps until the ions are captured at the kinks. If the step spacing was enough larger than the characteristic surface diffusion length, the ions would be captured to the closer step (Fig. 3-11a). However, if the step spacing was small, the ions would be scrambled by the adjacent steps because the catchment zone of the two steps overlaps (Fig. 3-11b). As a result, the step velocity would decrease. Considering this model, it is estimated that the decrease of step velocity in the presence of magnesium ion and the synthetic polypeptide alone is because of the scramble to get the ion by adjacent steps.

The growth rate, the step velocity and the slope were almost the same between in the presence of magnesium ion and the synthetic polypeptide alone. Therefore, it is considered that the resistance for adsorption of ions on the step front of calcite is the same between in the presence of magnesium ion and the synthetic polypeptide alone. On the other hand, the step velocity of calcite was accelerated in the coexistence of magnesium ion and the synthetic polypeptide, although the slope of hillocks and etch-pits is almost the same as the other additive solutions. It indicates that the adsorption of ion at the step front is accelerated in the coexistence of magnesium ion and the synthetic polypeptide. That is a noteworthy combined effect of magnesium ion and the synthetic polypeptide on kinetics.

## 3.5 Summary

We found the additive effects on calcite growth by the measurement of calcite growth rate as follows:

(1) Nucleation rate and adsorption of the ions on step fronts are accelerated by the combined effect of magnesium ion and the synthetic polypeptide

(2) Adsorption of the ions on calcite step was suppressed by scramble to get the ion by steps in the presence of magnesium ion and the synthetic polypeptide alone.

(3) The effect on the resistance for adsorption of ions on the step front is the same in the presence of magnesium ion and the synthetic polypeptide alone.

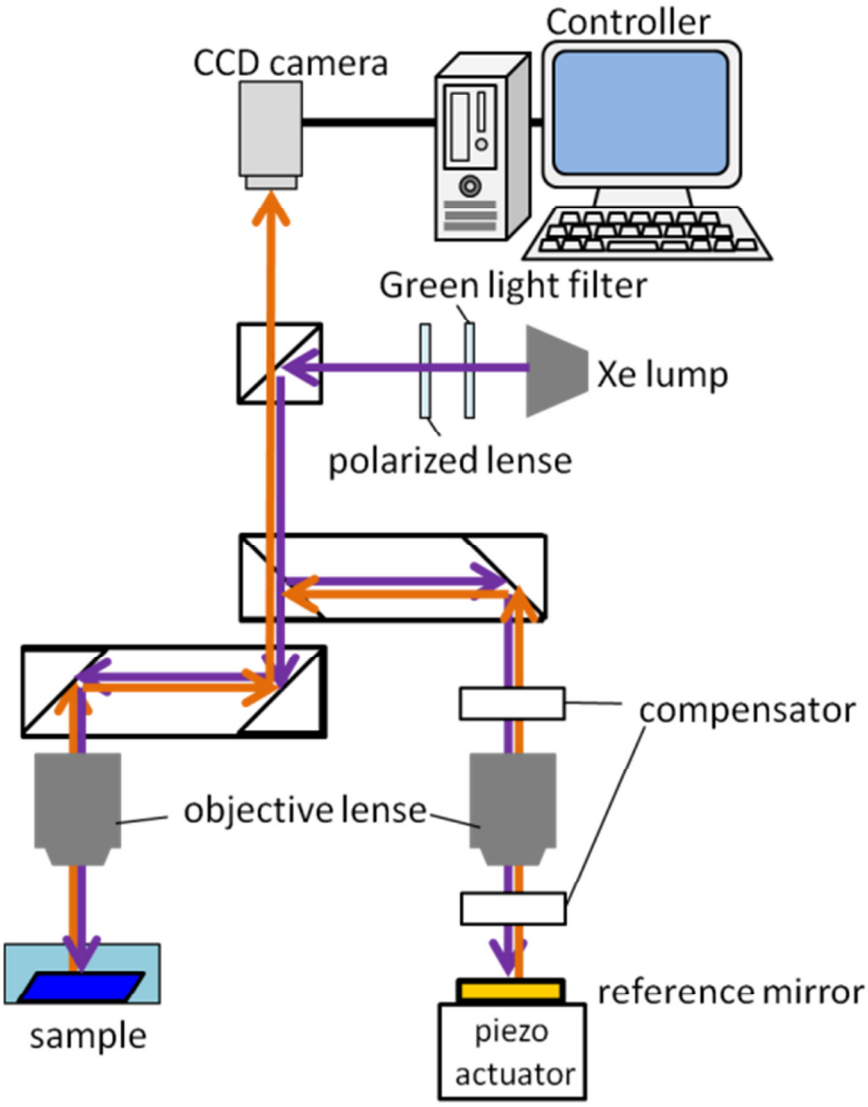


Fig.3-1

Schematic image of observation system of white-beam phase shift interferometry. Arrows represent optical paths.

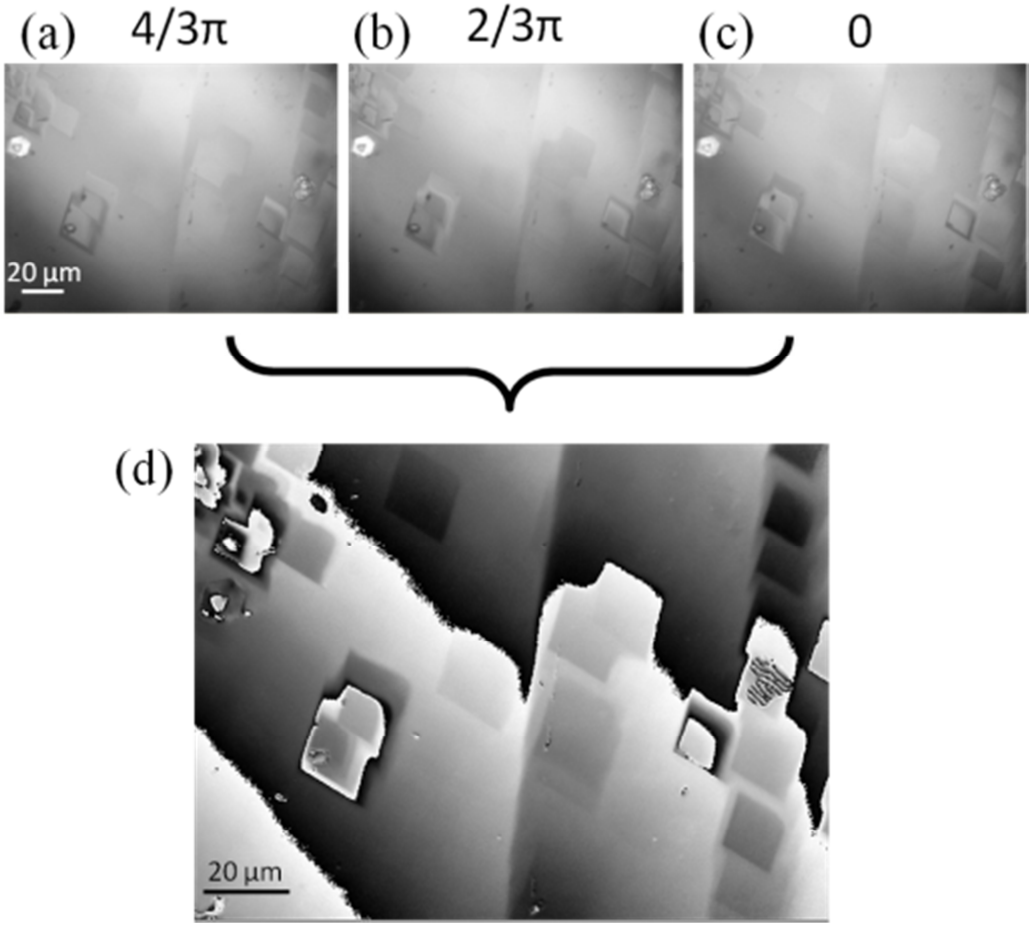


Fig.3-2
(a) – (c) Conventional interferograms of calcite surface taken at three different phase positions. (d) A phase shift image calculated from the three conventional interferograms.

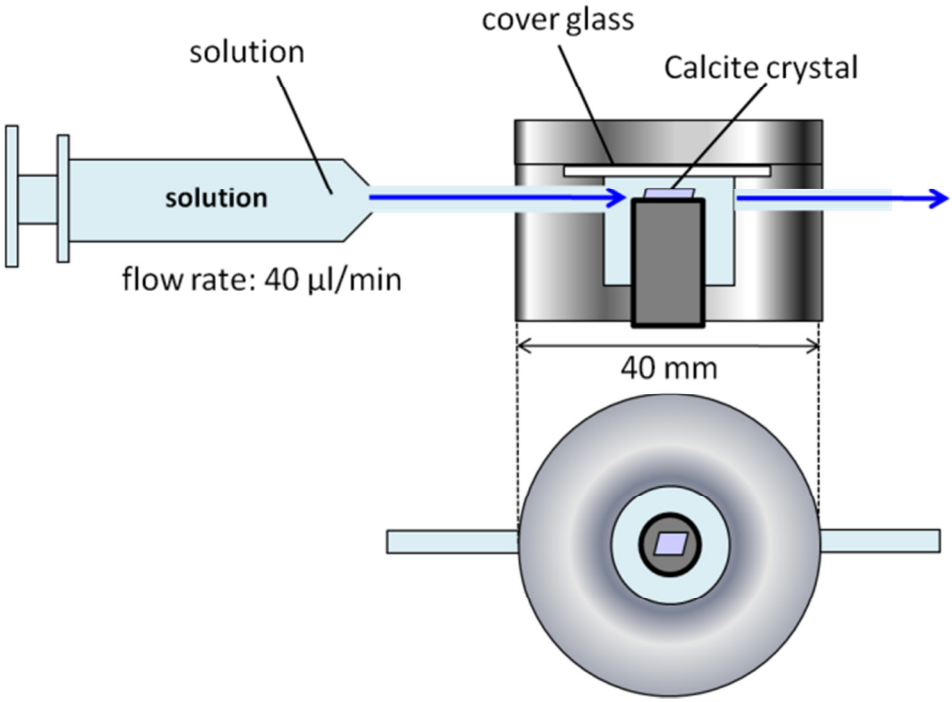


Fig.3-3
Schematic of the flow system of growth cell of the measurement of phase shift interferometry.

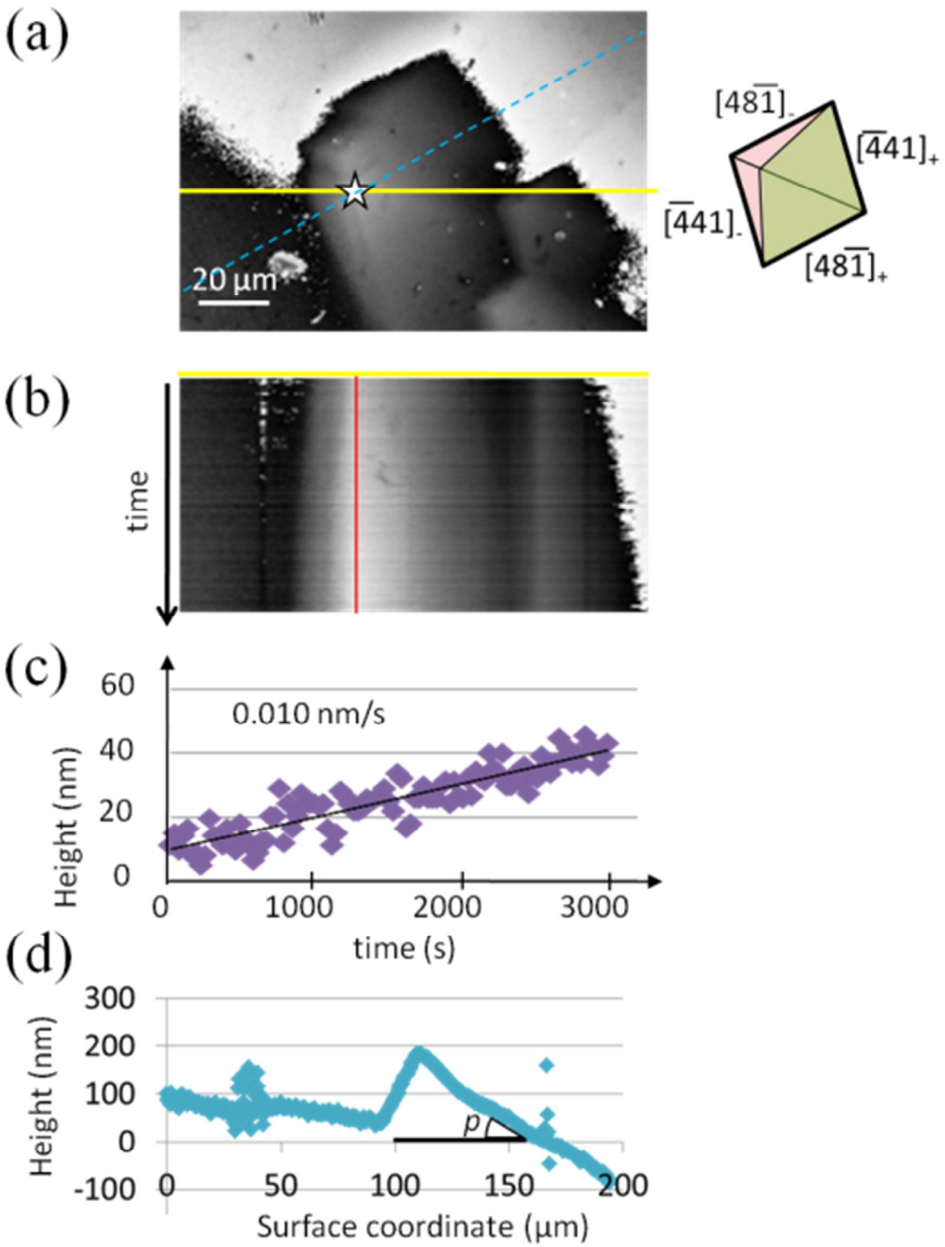


Fig.3-4

(a) A phase shift image of calcite surface. (b) time series variation of the contrast taken along yellow line of Fig.3-3a. (c) The time evolution of the height measured along red line of Fig.3-3b. (d) The cross-section profile of calcite hillock taken on dashed line of Fig.3-3a.

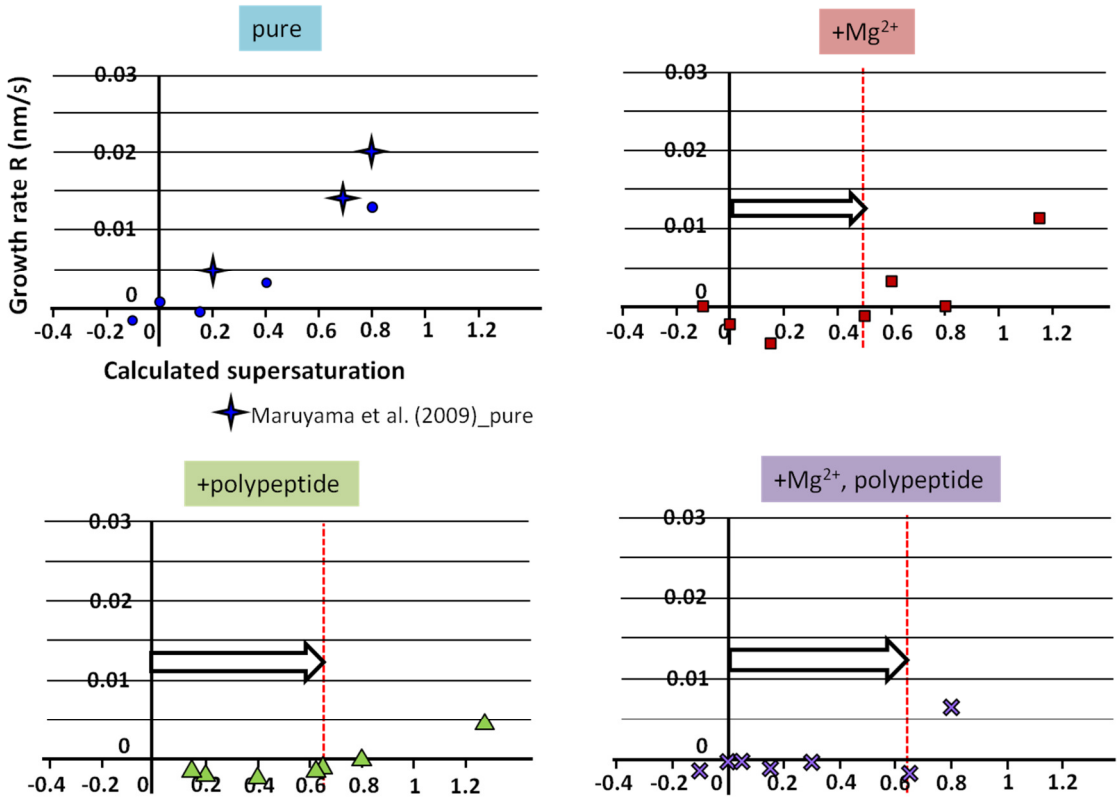


Fig.3-5

The plots of growth rate versus calculated supersaturation. Red dashed lines indicate the equilibrium concentration. The data of Maruyama *et al.* (2009) measured by PSI in pure $CaCO_3$ solution was plotted for comparison.

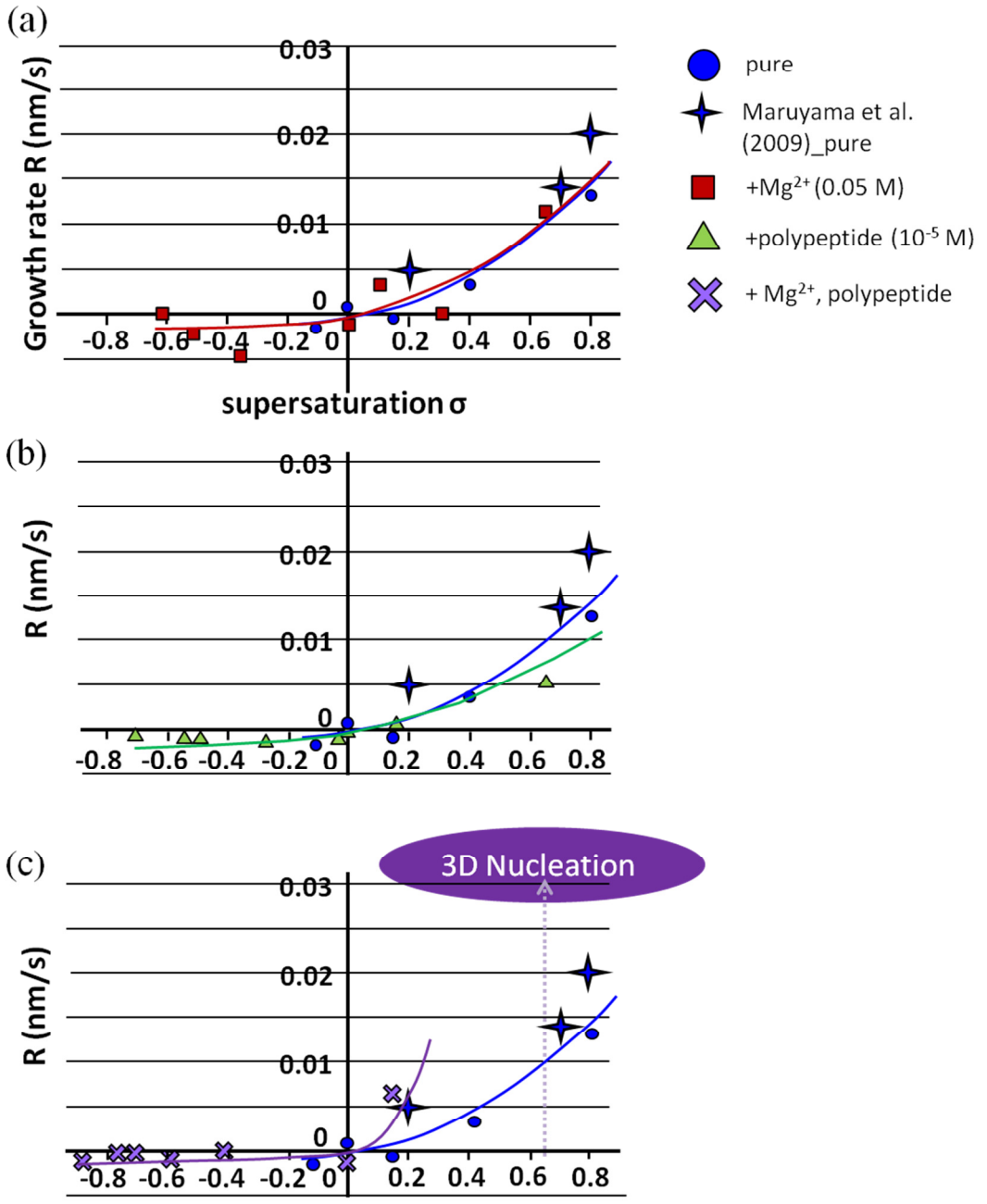


Fig.3-6

Additive effect on growth rate versus supersaturation. The data of Maruyama *et al.* (2009) measured by PSI in pure $CaCO_3$ solution was plotted for comparison.

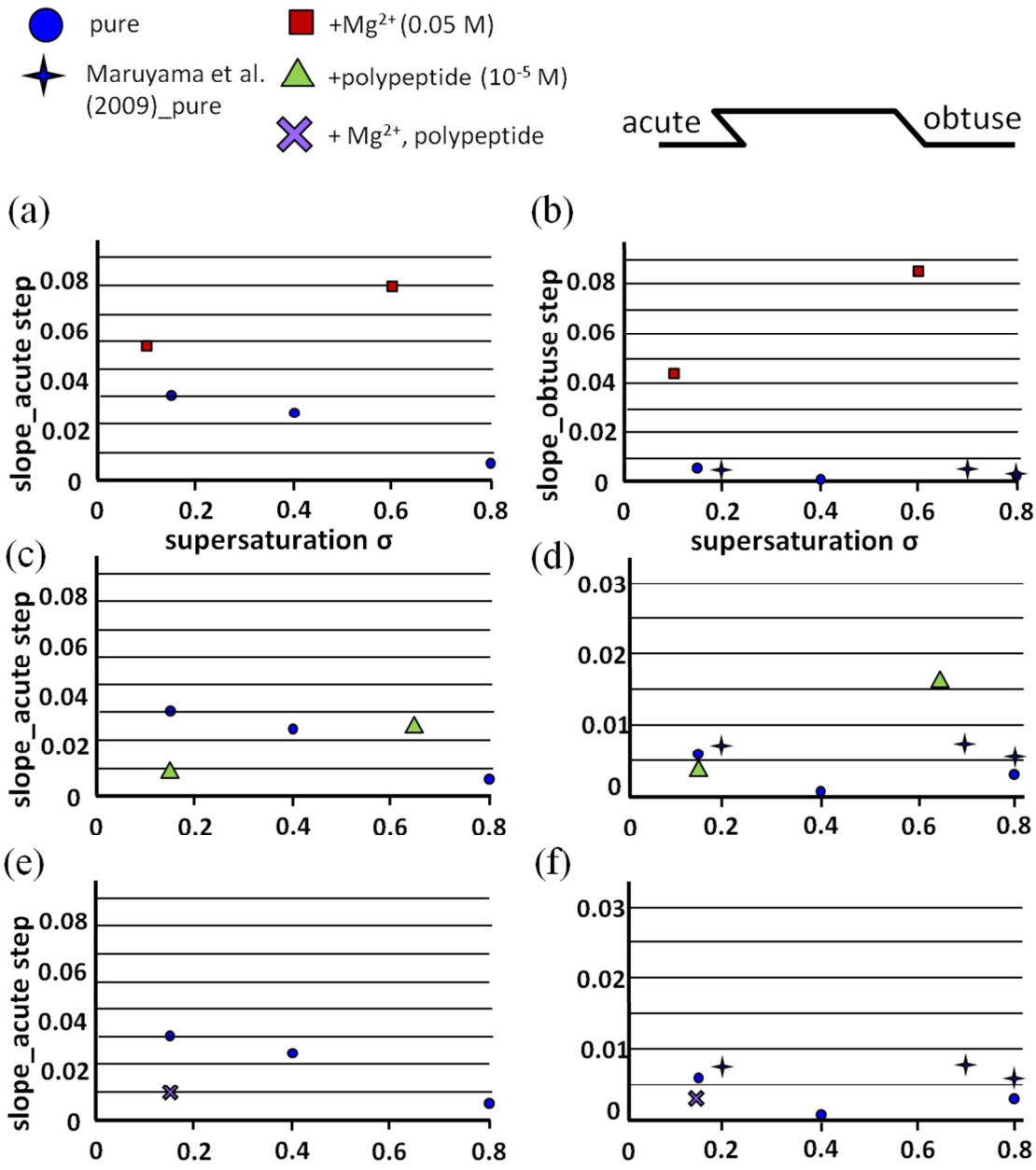


Fig.3-7 Additive effect on the slope of hillocks and etch-pits. Maruyama *et al*. (2009) measured by PSI in pure $CaCO_3$ solution was plotted for comparison.

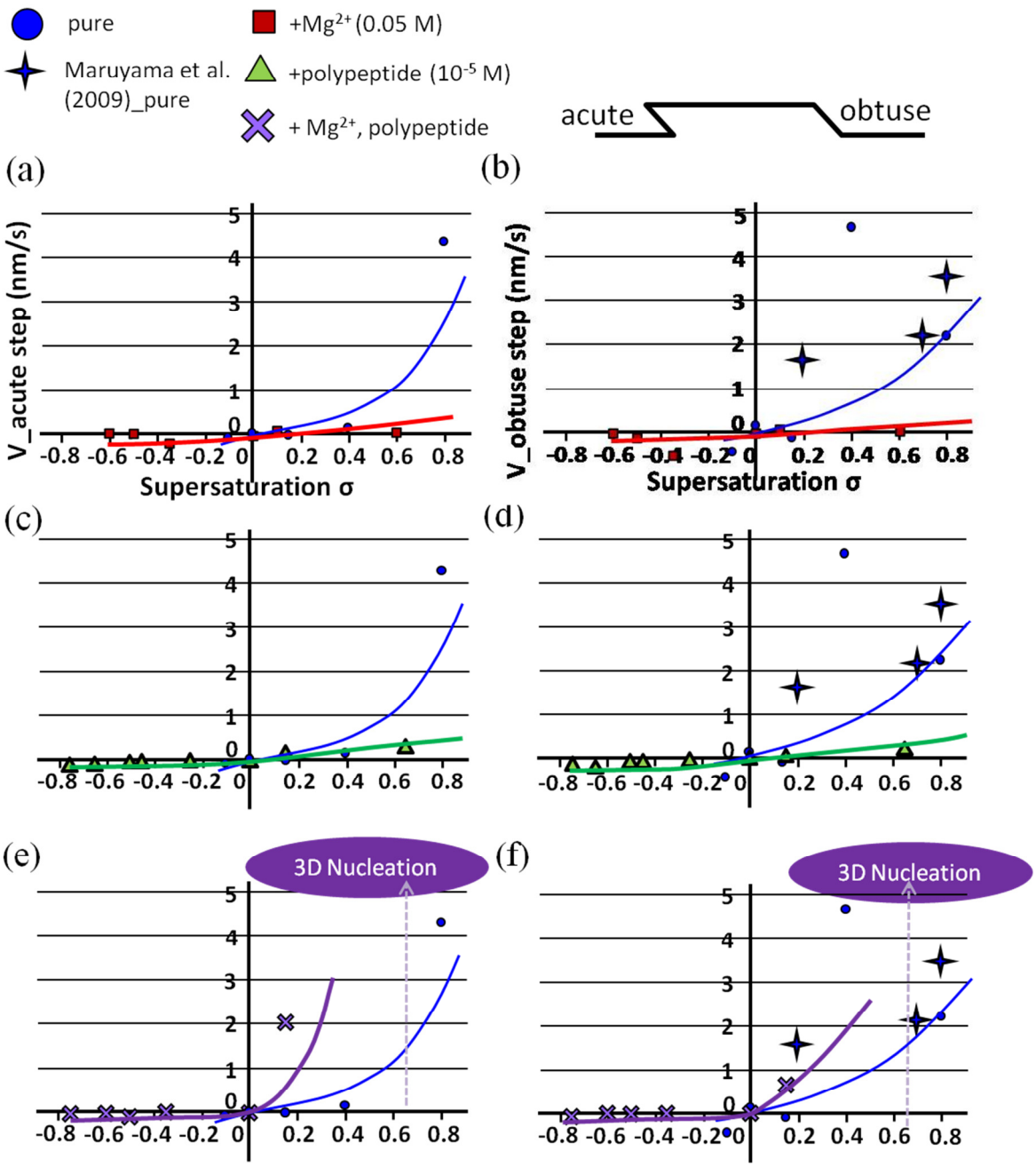


Fig.3-8

Additive effect on the step velocity of obtuse and acute steps of calcite. Maruyama *et al.* (2009) measured by PSI in pure $CaCO_3$ solution was plotted for comparison.

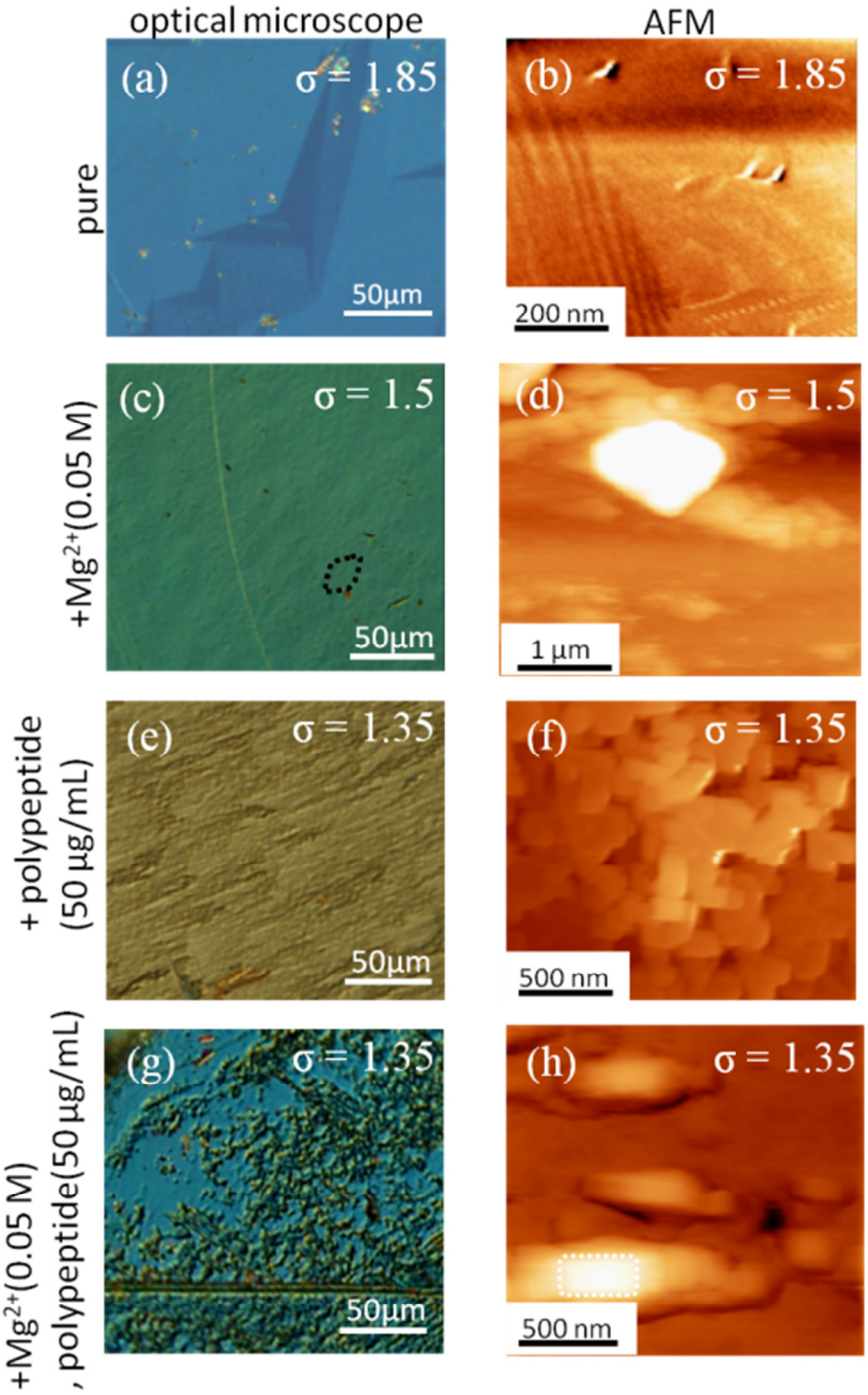


Fig.3-9

Additive effect on surface pattern of calcite (Araki, undergraduate thesis, 2008).

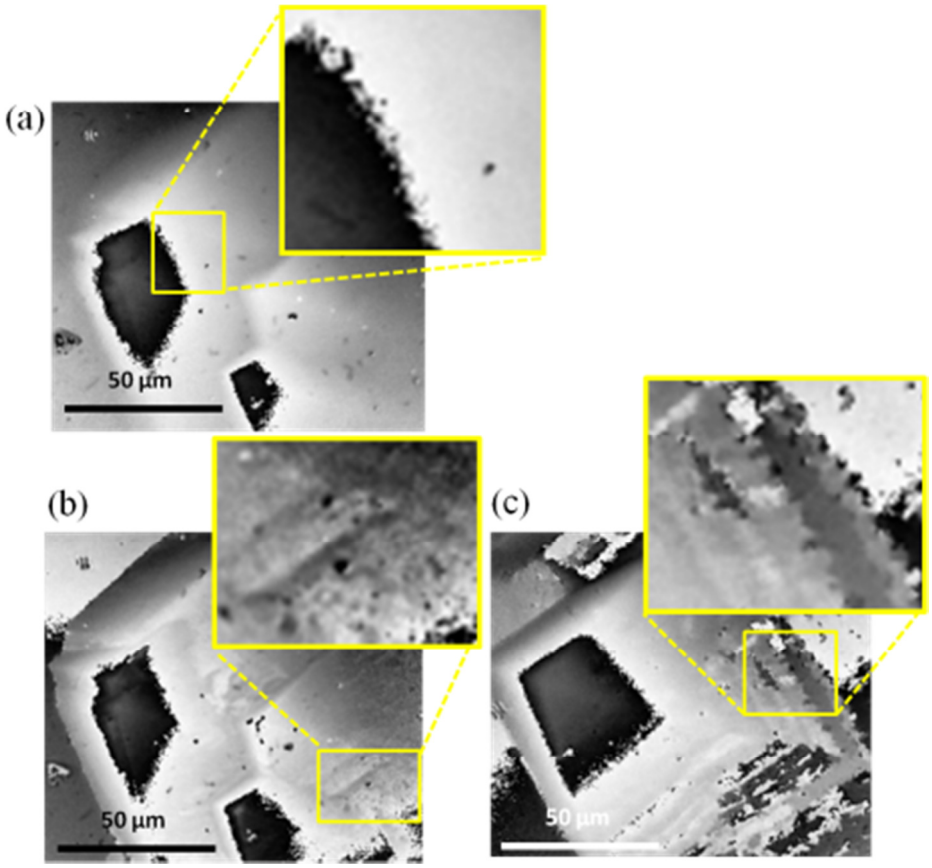


Fig.3-10

Phase shift images of calcite hillock (a) in the absence of the additive , (b) in the presence of the synthetic polypeptide alone, and (c) magnesium ion and the synthetic polypeptide, respectively.

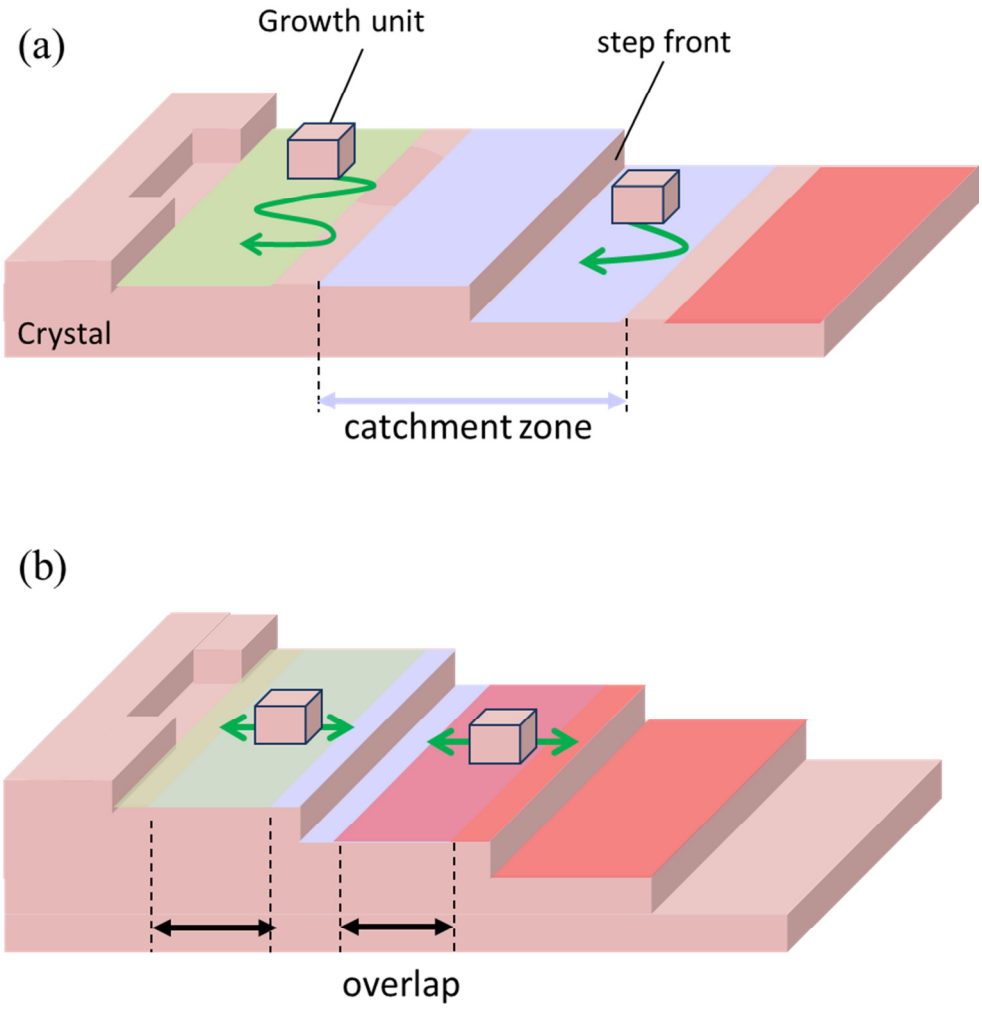


Fig.3-11

A schematic of adsorption of ion on steps. (a) surface diffusion on wide terrace. (b) overlap of catchment zone.

## *References in Chapter 3*


[1] Araki, Y., *undergraduate thesis, Tohoku University*, **2008**.

[2] Arvidson, R. S., Ertan, I. E., Amonette, J. E., Luttge, A. *Geochim. Cosmochim. Acta*, **2003**, 67, 1623-1634.

[3] Arvidson, R. S., Collier, M., Davis, K. J., Vinson, M. D., Amonette, J. E., Luttge, A. *Geochim. Cosmochim. Acta*, **2006**, 70, 583-594.

[4] Burton, W. K., Cabrera, N., Frank, F. C. *Phil. Trans. Roy. Soc. London Ser.* **1951**, A243, 299-360.

[5] Davis, K. J.; Dove, P. M.; De Yoreo, J. J. *Science* **2000**, 290, 1134-1137.

[6] Davis, K. J., Dove, P. M., Wasylenki, L. E., De Yoreo, J. J. *Amer. Mineral.* **2004**, 89, 714-720.

[7] De Yoreo, J. J., Zepeda-Ruiz, L. A., Friddle, R. W., Qiu, S. R., Wasylenki, L. E., Chernov,A. A., Gilmer, H., Dove, P. M. *Cryst. Growth Des*. **2009**, 9, 5135-5144.

[8] Liu, X. Y., Maiwa, K., Tsukamoto, K., J. Chem. Phys. **1997**, 106, 1870.

[9] Maiwa, K., Plomp, M., van Enckevort, W. J. P., Bennema, P. *J. Cryst. Growth* **1998**, 186, 214-223.

[10] Maruyama, M.; Tsukamoto, K.; Sazaki, G.; Nishimura, Y.; Vekilov, P. G. *Cryst. Growth Des*. **2009**, 9, 127-135.

[11] Meyer, H. J., *J. Cryst. Growth* **1984**, 66, 639-646.

[12] Mucci, A., and Morse, J. W. *Geochim. Cosmochim. Acta*, **1983**, 47, 217-233.

[13] Onuma, K., Tsukamoto, K., Sunagawa, I., *J. Cryst. Growth* **1988**, 89, 177.

[14] Satoh, H., Nishimura, Y., Tsukamoto, K., Ueda, A., Kato, K., Ueta, S. *Am. Mineral.* **2007**, 92, 503-509.

[15] Stephenson , A. E., Hunter, J. L., Han, N., De Yoreo, J. J., Dove, P. M., *Geochim. Cosmochim. Acta*, **2011**, 75, 4340-4350.

[16] Teng, H. H., Dove, P. M., De Yoreo, J. J., *Geochim. Cosmochim. Acta*, **1999**, 63, 2507-2512.

[17] Teng, H. H., Dove, P. M., De Yoreo, J. J., *Geochim. Cosmochim. Acta*, **2000**, 64, 2255-2266.

[18] Tsukamoto, K. *Faraday Discuss.* **1993**, 95, 183-189.

[19] Van Driessche, A. E. S., García-Ruíz, J. M., Tsukamoto, K., Patiño-Lopez, L. D., Sato, H. *PNAS* **2011**, 108, 15721-15726.

[20] Yoshino, T., and Kagi, H. *Chemistry Lett.* **2008**, 37, 508-509.

## *Chapter 4. The effect of hydration on calcite growth*

### 4.1 The effect of hydration on interfacial tension between calcite surface and solution

Effects of the additive on the hydration structure, growth rate, and solution properties are presented in Table.2. The nucleation rate of calcite increases in additive solutions. From the data presented in Chapter 3, it is evident that the nucleation rate in a solution containing both the magnesium ion and the synthetic polypeptide is higher than that in the other solutions. Considering them, first, we discuss the effect of the additive on the interfacial tension via the change in hydration structure.

Nucleation rate depends on the free energy of formation of nucleus as follows:

$$\Delta G^* = \frac{16\pi\gamma^3 v^2}{3\Delta\mu^2} \qquad (4\text{-}1)$$

where $\gamma$ is interfacial energy, $v$ is moral volume of growth unit, and $\Delta\mu$ is the change in chemical potential per molecule. This equation shows that the nucleation rate is determined by interfacial tension. Therefore, the increase of nucleation rate in additive solution indicates the decrease of interfacial tension between calcite surface and the solution. The nucleation rate increased when the hydration became multilayered in the presence of magnesium ions alone, although it has been reported that homogeneous nucleation of calcite is suppressed in the presence of magnesium ion, likely due to an increase in interfacial tension (Bischoff, 1968; Söhnel and Mullin, 1982). Our observation suggests that the energy gap between the calcite surface and the solution may be eased by the lattice-like structure adapted by the water molecules. In that case, the interfacial tension decreases due to the multilayered hydration structure in the presence of magnesium ions. As a result, it is proposed that the nucleation rate increases.

On the other hand, the nucleation rate increased in the presence of the synthetic polypeptide alone, although the hydration structure had no change. In this case, it is considered that the interfacial tension decreased by the adsorption of the synthetic polypeptide on calcite surface. The adsorption of organic molecules on calcite is known to reduce the interfacial tension and induce heterogeneous nucleation (Williams, 1984; Manoli *et al*., 2002). It has been observed the synthetic polypeptides are weakly adsorbed on the surface of calcite and only for a short duration (Araki, master's thesis, 2010). It has been demonstrated that organic molecules exert a significant influence on the surface pattern, in particular, the morphology of hillocks even if the time of

adsorption is short (Maruyama, doctoral thesis, 2008). Therefore, it is suggested that the increase of the nucleation rate is due to the temporary adsorption of the synthetic polypeptide.

The nucleation rate especially increased in the coexistence of magnesium ions and the synthetic polypeptides. This suggests that the interfacial tension between calcite and the solution is lesser when the two additives are simultaneously present in the $CaCO_3$ solution than when either of the additives is present individually. The change of hydration structure was remarkable in that solution. It suggests that the multilayered and rigid hydration structure leads to a reduction in the interfacial tension. Additionally, the adsorption of the synthetic polypeptide also helps to reduce interfacial tension of calcite surface. As a result, the remarkable increase of nucleation rate was induced. The strengthening of hydration and the acceleration of nucleation in calcite growth is a noteworthy combined effect of magnesium ion and the synthetic polypeptide.

In addition, the change of interfacial tension is also shown in the solubility shift. The relation between interfacial tension and solubility has been reported by Nielsen and Söhnel (1971), who describe the solubility of calcite as a function of the experimentally determined values of interfacial tension (Fig.4-1). Considering the relation of interfacial tension and the solubility, the solubility shift can be ascribed to the decrease in interfacial tension due to the formation of the multilayered hydration structure in the presence of magnesium ion. In the case of the synthetic polypeptides, it is considered that the solubility shift is caused by the lattice strain in the surface by the adsorbed polypeptide. When the calcite is grown in the presence of the synthetic polypeptide, the lattice strain is evident from the change in morphology from rhombic hillock to rectangular 2D island (Fig. 3-9) (Araki, undergraduate thesis, 2008).

Interfacial tension is the factor that regulates the polymorphic attributes of calcium carbonate (Navrotsky, 2004). Therefore, it is suggested that the additives influence polymorphism by regulating the interfacial tension via the change of hydration structure.

## 4.2 The effect of hydration on adsorption of ions on calcite surface

Next, we discuss the influence of additives on adsorption of the ions on calcite surface via the change of hydration structure. In Chapter 2, we predicted that in the presence of the polypeptide alone, the growth rate of calcite does not change since the hydration structure at the surface is not different from that in pure solution. Intriguingly, as evident from the results in Chapter 3, the step velocity of calcite decreases with the sole addition of the synthetic polypeptide due to small step spacing, not due to pinning

effect (Fig.4-2). Therefore, we conclude that the adsorption of ions on step fronts is suppressed regardless of the hydration structure. On the other hand, the hydration of calcite surface is rigid when the magnesium ion and the synthetic polypeptide coexist and the step velocity is accelerated, indicating the increase of adsorption of ions on calcite surface. These results suggest that the adsorption of ions on calcite surface does not depend on the hydration structure. Although it is necessary to observe the effect of additives on hydration structure at the step front in order to reveal the dependence of adsorption of ions on the step front on hydration, our results strongly suggest that growth rate does not depend on the dehydration process. This observation is in contrast with the previous studies that claim that dehydration is a rate-determining process in solution growth (Bennema, 1967a, b; Vekilov *et al*., 1992a,b).

.

Table 2. Summary of the additive effects on properties of crystal growth

| additive | Hydration structure | Surface pattern | Nucleation rate | Growth rate | Step velocity | | slope | | Solubility |
|---|---|---|---|---|---|---|---|---|---|
| pure | 2 layers | Spiral growth and 2D nucleation | | | | | | | |
| $Mg^{2+}$ | Multilayered (4 layers) | Spiral growth and 2D nucleation | + | = | **Obtuse** | - | **Obtuse** | + | + |
| | | | | | **Acute** | - | **Acute** | + | |
| Poly-peptide | No change (2 layers) | 2D nucleation | + | = | **Obtuse** | - | **Obtuse** | + | + |
| | | | | | **Acute** | - | **Acute** | + | |
| $Mg^{2+}$+ Poly-peptide | Multilayered + rigid (4 layers) | 2D nucleation and 3D nucleation | +++ | + | **Obtuse** | + | **Obtuse** | = | + |
| | | | | | **Acute** | + | **Acute** | - | |

+: increase, -: decrease, =: no change

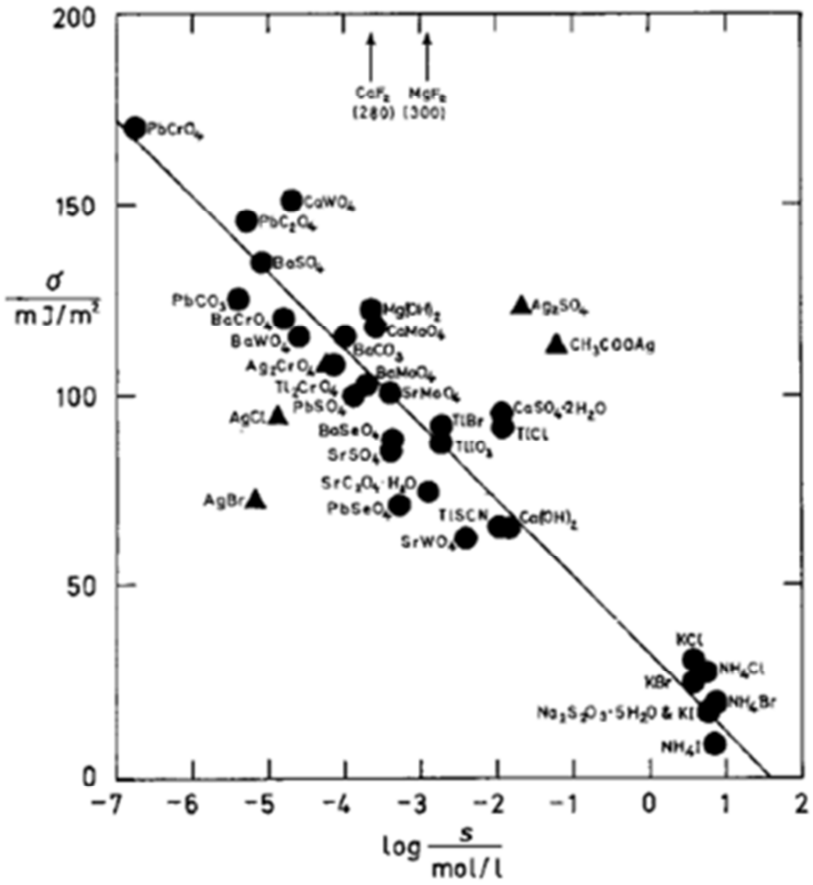


Fig.4-1

Plot depicting the relationship between interfacial tension and logarithm of solubility (Nielsen and Söhnel, 1971).

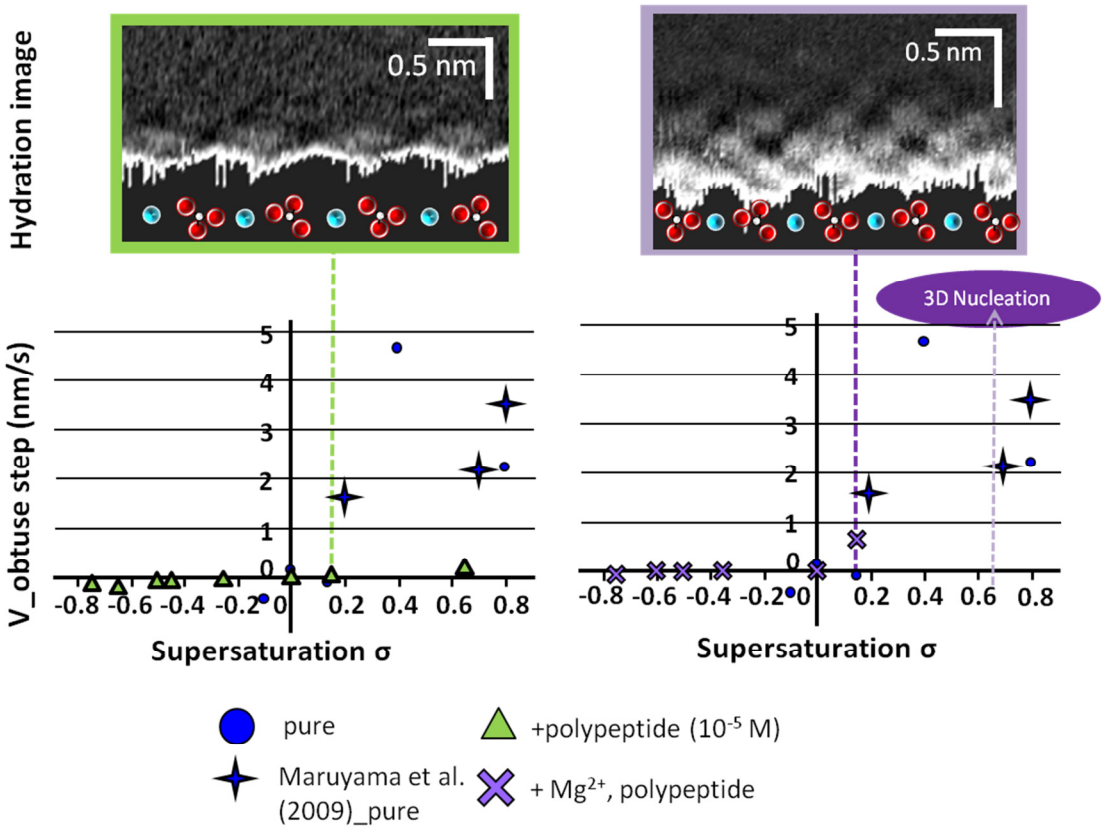


Fig.4-2 Comparison of hydration image and step velocity of calcite.

## *References in chapter 4*


[1] Araki, Y., *undergraduate thesis, Tohoku University*, **2008**

[2] Araki, Y., *master's thesis, Tohoku University,* **2010**.

[3] Bennema, P., *J. Cryst. Growth* **1967**, 1, 278-286.

[4] Bennema, P., *J. Cryst. Growth* **1967**, 1, 287-292.

[5] Bischoff, J. L. *J. Geophys. Res.* **1968**, 73, 3315-3322.

[6] Manoli, F., Kanakis, J., Malkaj, P., Dalas, E. *J. Cryst. Growth* **2002**, 236, 363-370.

[7] Maruyama, M., *doctoral thesis, Tohoku University,* **2008**.

[8] Navrotsky, A. *PNAS* **2004**, 101, 12096-12101.

[9] Nielsen, A. E., and Söhnel, O. *J. Cryst. Growth* **1971**, 11, 233-242.

[10] Söhnel, O., and Mullin, J. W. *J. Cryst. Growth* **1982**, 60, 239-250.

[11] Vekilov, P. G., Kuznetsov, Y. G., Chernov, A. A. *J. Cryst. Growth* **1992**, 121, 44-52.

[12] Vekilov, P. G., Kuznetsov, Y. G., Chernov, A. A. *J. Cryst. Growth* **1992**, 121, 643-655.

[13] Williams, R. J. P. *Phil. Trans. R. Soc. Lond. B* **1984**, 304, 411-424.

## *Conclusions*

We reveal for the first time the effects of additives on the local hydration structure on the surface of calcite at atomic-level by FM-AFM. The visualization of the hydration structure and evaluation in the context of growth rates lead to the following observations:

(1) The synthetic polypeptide, even that with high hydrophilicity, does not affect hydration at the surface of calcite.
(2) Combination of magnesium ions and the synthetic polypeptides provides a rigid hydration structure at the surface of calcite.
(3) Magnesium ions and the synthetic polypeptides influence hydration and the surface pattern of calcite, respectively.
(4) Structured water distribution eases the energy gap between the calcite surface and solution. As a result, the interfacial tension between the calcite surface and solution decreases.
(5) Magnesium ions and the synthetic polypeptide act in unison to accelerate nucleation via changes in hydration structure.
(6) Hydration contributes to interfacial energy of calcite‐solution interface, but not for the adsorption of ions.

We provide experimental evidence to show that additives affect the interfacial tension by altering hydration structure; however, there is hardly any change in the adsorption of ions on calcite surface due to the hydration structure. We also experimentally demonstrate that dehydration is not a rate-determining process, an observation that is contrary to the currently prevailing theory. Although the observation of hydration of step front is necessary to discuss the effect of hydration on adsorption of ions in detail, we claim that this observation is possible by utilizing FM-AFM.

We believe that our results contribute to the development of methods that can regulate the polymorphism of calcium carbonate. Our results provide a deeper understanding into the mechanism that regulates surface tension—a parameter with an influence on polymorphic types.

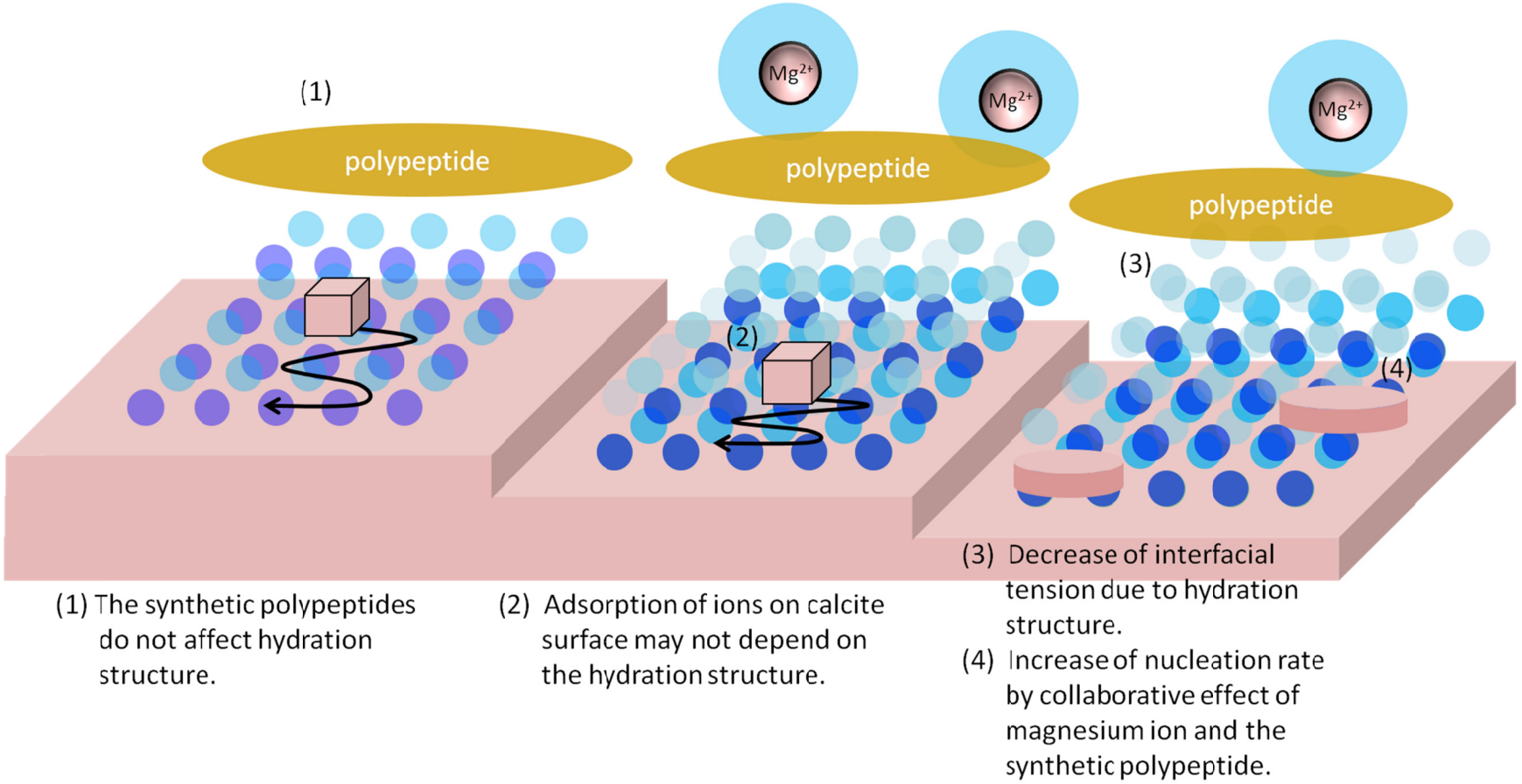


Fig. 5-1 Schematic image of the influence of additives on hydration and growth rate of calcite surface.

# *Appendix*

## *A1. Observation of hydration on step front of calcite*

In order to discuss the relation of hydration and adsorption of the ions on calcite steps in detail, the observation of hydration structure at the step front is necessary. The observation of the step front is the biggest advantage of the measurement using FM-AFM. We aim to reveal the difference of hydration between at the step front and on the terrace of calcite.

### Experimental section

Detail fundamental of FM-AFM is shown in experimental section of Chapter 2. The two dimensional force mapping on step fronts was carried out in $CaCO_3$ supersaturated solution in the absence of the additive. The supersaturated solution of $CaCO_3$ in the absence of the additive was prepared in the same manner as Chapter 2. The solution in the observation cell was left for 20 hours so as to be equilibrium concentration, because it was difficult to observe advancing step front in scanning. The solution was covered by the oil to prevent evaporation of water (Fig.A1-1). The concentration of calcium carbonate gradually decreased with calcite growth in the closed cell for 20 hours.

### Results and discussions

The 2D frequency shift maps were obtained above three steps of 2D islands as shown in Fig.A1-2. The step motion was almost stopped. Fig.A1-3a shows the topography of the steps of calcite surface. The cross-section profile of the steps is shown in Fig.A1-3b. The profile indicates they are monomolecular steps. Fig.A1-3c shows a 2D frequency shift map taken in 7 s. over a scan area of 10 x 2 nm on the calcite steps. The darkest area in the bottom of 2D frequency shift map indicates calcite region. The brightest area just above the darkest area represents the area in which the frequency shift was close to the predetermined threshold value. Hydration layer was indicated by the brighter area. The positions of each step edge were different between Fig.A1-3b and c because of the time lag of imaging. The site specific force - distance curves taken on the terrace and the step front are shown in Figs.A1-3d and e. Two peaks were detected on the terrace, on the other hand, no peaks was detected on the step front. The number of hydration layers on the terrace is consistent with the result of chapter 2. Both two peaks were detected on the one force-distance curve, although the hydrated water molecules distribute like the closest packed pattern as shown in Chapter 2 (Fig.

2-5). It is considered that the hydrated water molecules in two hydration layers seemed to overlap, because the scanning area is larger than that of Fig. 2-5. 2D force mapping of step fronts suggests that although the terrace was covered with hydration layer, there is no hydrated water molecule above the step front.

If the step front does not hydrate, the ions highly likely to be transported to step front directly by volume diffusion. It supports our conclusion which the hydration may not affect the absorption of the ion. The observation of local hydration structure around the step edges will enable us to understand the effect of the hydration on kinetics of calcite growth in detail.

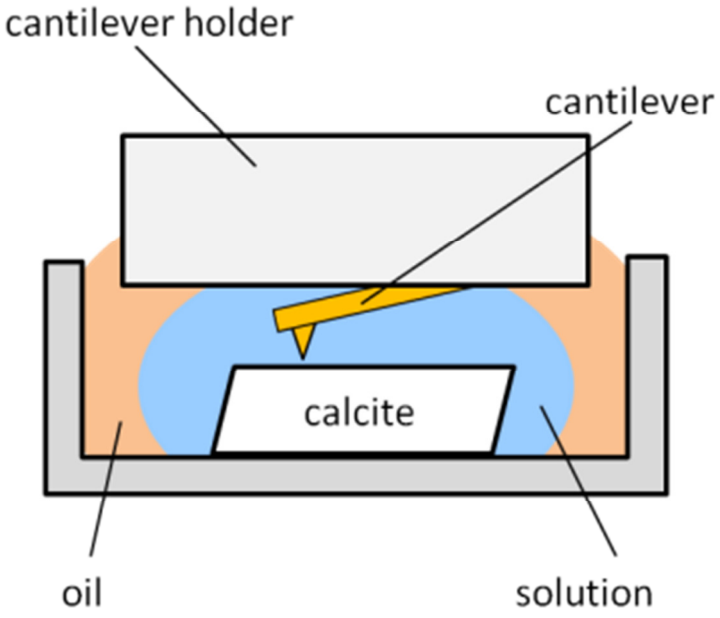


Fig.A1-1A schematic of cross-section of the observation cell.

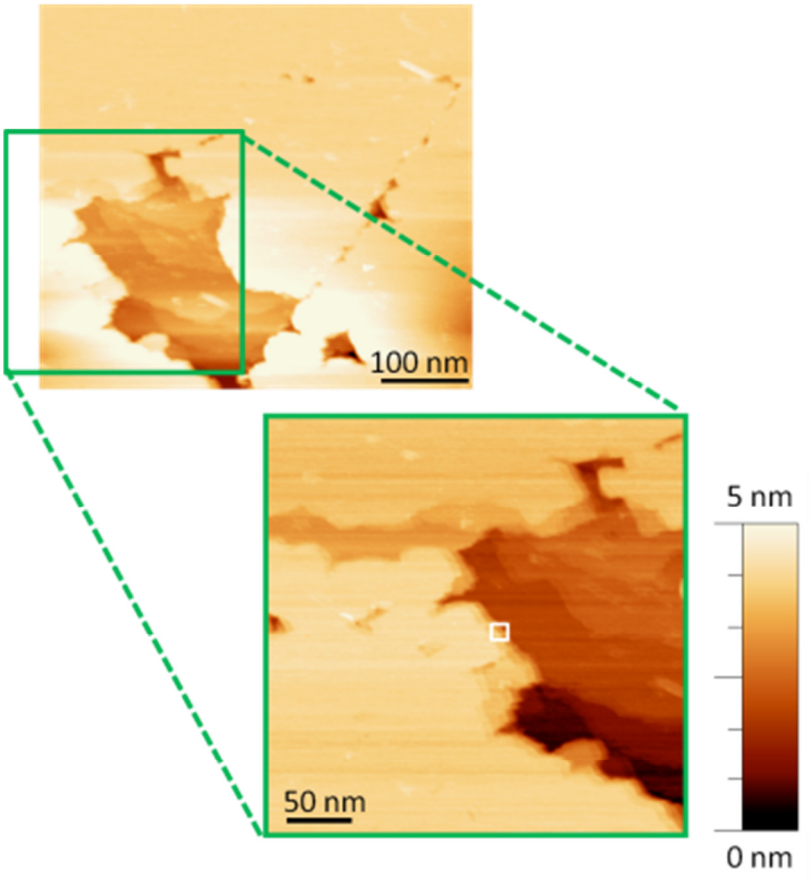


Fig.A1-2

Topographic image of 2D nucleation site of calcite surface taken in pure $CaCO_3$ solution. 2D force map was obtained in the white box in this image. The scale of height is shown at the right of the image.

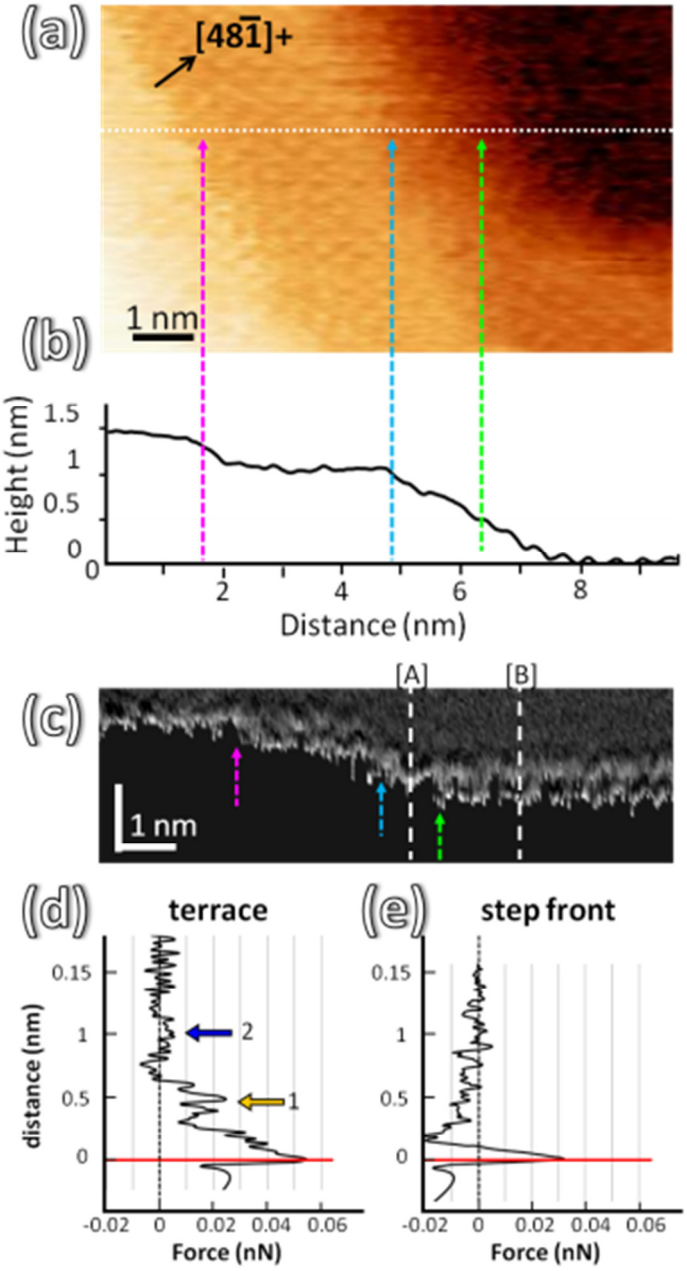


Fig.A1-3

(a) Topographic image of monomolecular steps of calcite surface taken in pure $CaCO_3$ solution. The contrasts of the image correspond to the difference of height. (b) The cross-section profile of monomolecular steps on white dotted line in Fig.A1-3a. Pink, blue and green allows indicate each step edge. (c) A 2D frequency shift map on the molecular steps taken on the white dotted line in (a). (d) site specific force－distance curves taken on white dashed line of [A] terrace and [B] step front in Fig. A1-3c, respectively.

## *A2. 3D Force mapping on calcite surface in pure $CaCO_3$ solution*

We need to estimate the density of hydration on calcite surface in order to reveal the effect of hydration on the capture of ions on calcite surface. Therefore, it is expected to visualize the three-dimensional (3D) distribution of hydrated water molecules. We tried to obtain the 3D hydration image on calcite surface.

**Experimental section**

3D hydration image was obtained by 3D force mapping. The 3D hydration image is pictured by collecting of several 2D frequency shift maps (see Chapter 2) taken at constant interval by FM-AFM (Fukuma *et al*., 2007; Kobayashi *et al.*, 2013) (Fig.A2-1). A 2D frequency shift map was taken in 4 nm in x-direction by 2 nm in z-direction on the terrace of the 2D island in 12 s. Total 18 images of 2D frequency shift map were collected at the interval of 0.15 nm for y-direction. Then, we obtained a 3D force mapping image in 4 nm in x-direction by 3 nm in y-direction.

The 3D force mapping was performed in the supersaturated $CaCO_3$ solution containing 0.05 M magnesium ion and 10 μg/ml the synthetic polypeptide. The preparation of the solution was in the same manner in Chapter 2.

**Results and discussions**

Fig.A2-2 shows the horizontal images of four hydration layers which were constructed by 3D force mapping. Brighter areas in the images indicate the position of high density of water molecules. The structure which consisted of water clusters was kept until fourth hydration layer located at 0.75 nm above calcite surface [Figs.A2-2 (c) - (f)]. It was confirmed that the horizontal hydration structure of each layer reflects the calcite surface structure, although the lateral thermal drift seems to affect the imaging. Especially the lattice spacing for $[\bar{4}2\bar{1}]$ direction was consistent (Fig.10).

The hydration structure of calcite surface in water has been estimated by molecular dynamics (MD) simulation (Raiteri *et al.*, 2010; Reischl *et al.* 2012). Comparing our images with the result of MD simulation,

Although the resolution of 3D mapping is not enough to compare the distribution of hydrated water molecules in detail with the simulation, the easing of the hydration structure when distance of hydration layers from the calcite surface increased was observed. The resolution of 3D force mapping depends on the interval of 2D frequency shift images. In order to obtain detail information of 3D distribution of hydrated water

molecules, the control of the lateral thermal drift is required.

3D hydration image would show the difference of the density of hydration layers on calcite in the absence and presence of the synthetic polypeptide. It will contribute to determine the resistance for the absorption of the ions on calcite surface directly.

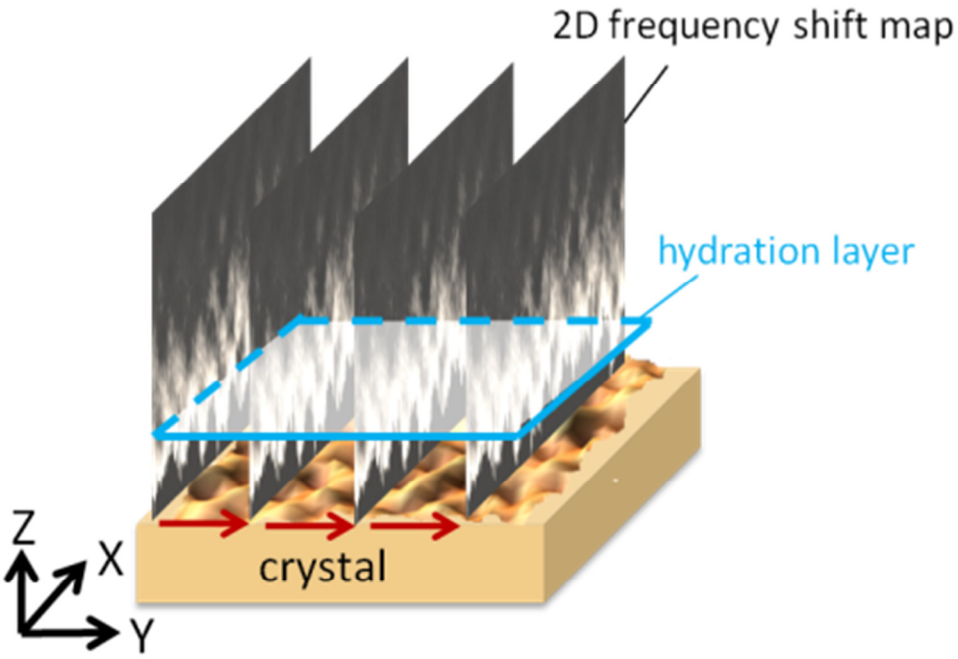


Fig.A2-1 A schematic of 3D force mapping by FM-AFM.

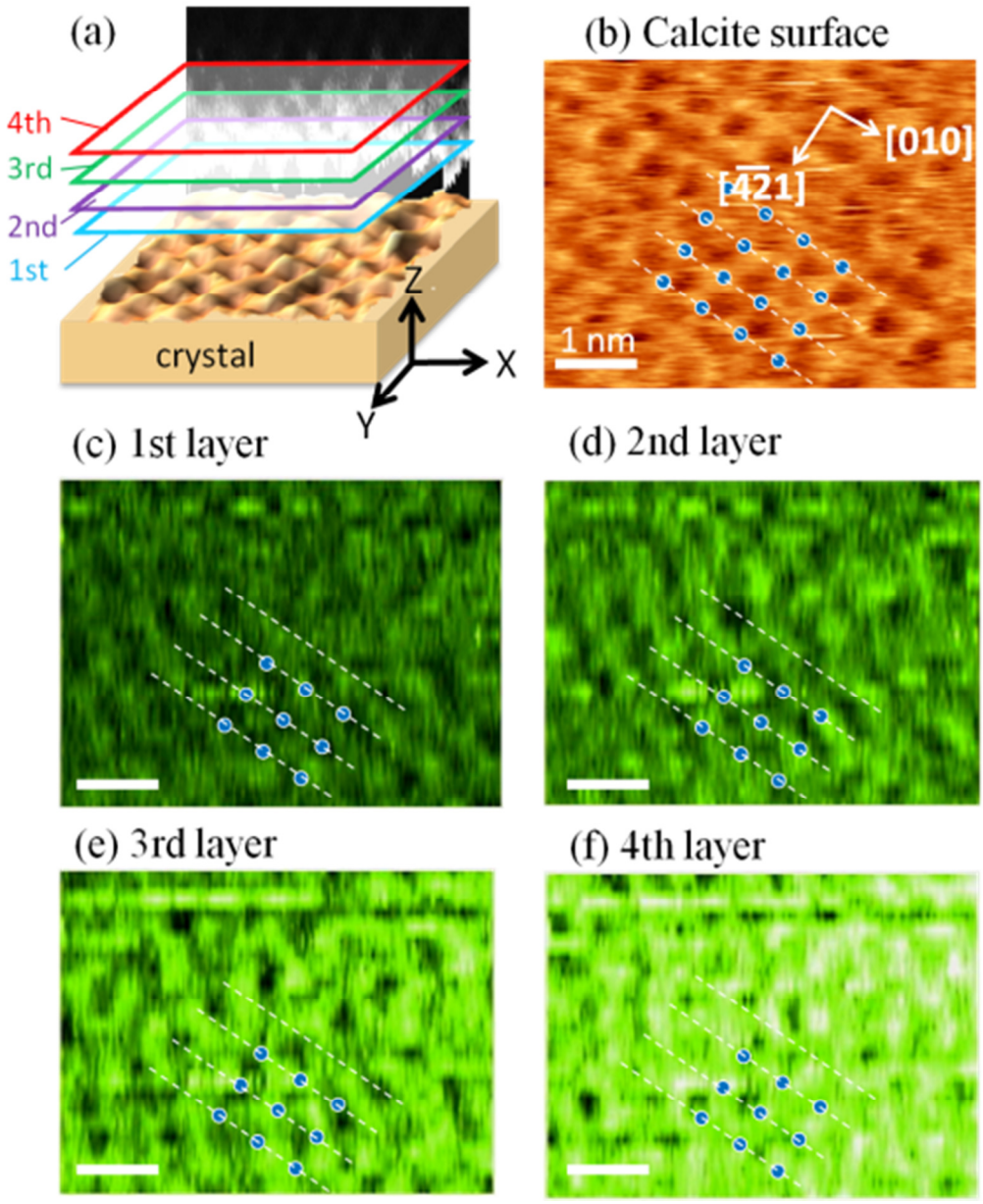


Fig.A2-2

3D force mapping of the interface calcite and $CaCO_3$ solution in the presence of 10 μg/ml the synthetic polypeptide. (a) Schematic image of 3D construction of hydration image. (b) Topographic image of calcite surface. (c) – (f) constructed lateral pattern of hydration in first, second, third, forth layer, respectively. White dashed lines indicate the lattice spacing of [4̄21] direction of calcite.

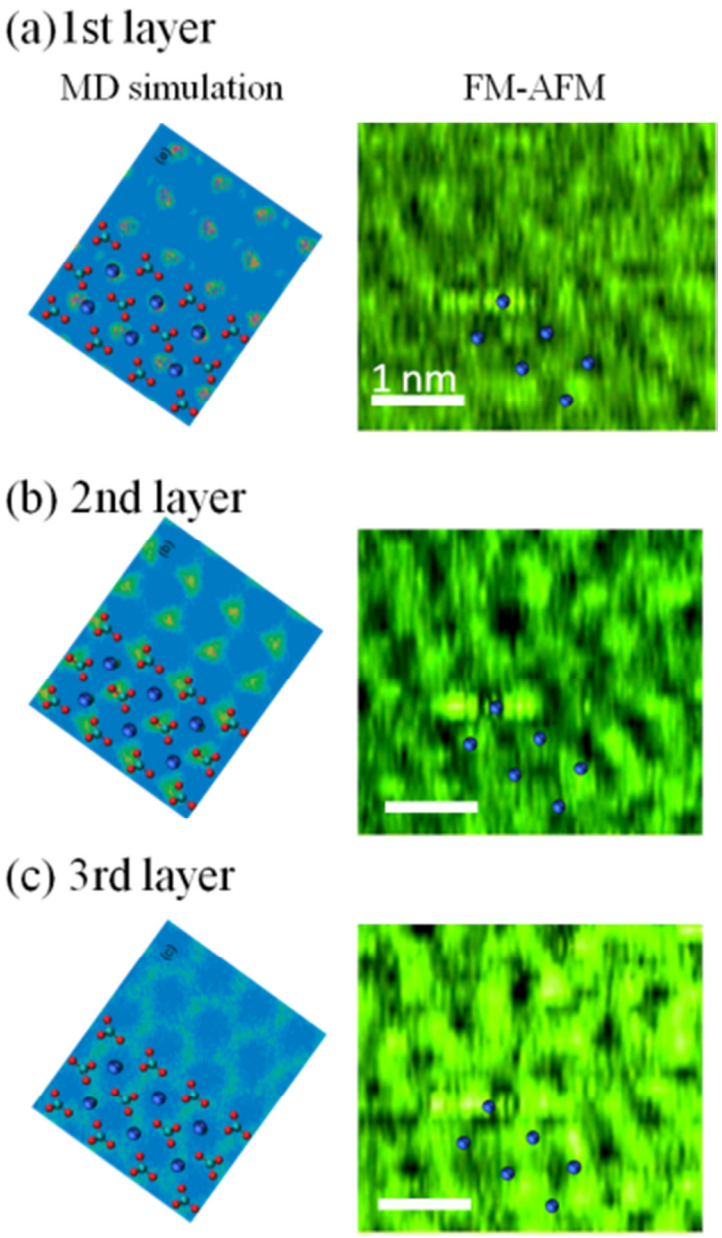


Fig.A2-3

Comparison of the image of MD simulation (from Raiteri *et al*., 2009) and FM-AFM. Green areas indicate the position of hydrated water molecules. Blue balls represent the calcium atoms on the calcite $(10\bar{1}4)$ surface.

## *References in Appendix*

[1] Fukuma, T.; Higgins, M. J.; Javis, S. P. BiophysJ. **2007**, 92, 3603-3609.

[2] Kobayashi, K.; Oyabu, N.; Kimura, K.; Ido, S.; Suzuki, K.; Imai, T., Tagami, K., Tsukada, M.; Yamada, H. *J. Chem. Phys.* **2013**, 138, 184704.

[3] Raiteri, P., Gale, J. D., Quigley, D., and Rodger, P. M. *J. Phys. Chem. C* **2010**, 114(13), 5997-6010.

[4] Reischl, B., Watkins, M., and Foster, A. S., *J. Chem. Theory Comput.* **2013**, 9, 600-608.

# 参考論文


1. 炭酸カルシウム結晶表面の液中原子分解能イメージング
**荒木優希**, 塚本勝男, 大藪範昭, 小林圭, 山田啓文.
*NanotechJapan Bulletin* (2011) vol.4, No.1.

2. Atomic Imaging of Aragonite (001) Surface in Water by FM-AFM
**Yuki Araki**, Katsuo Tsukamoto, Noriaki Oyabu, Kei Kobayashi, Hirofumi Yamada.
*Jpn. J. Appl. Phys.* (2012) **51**, 08KB09.

NanotechJapan Bulletin

特集 フォーカス26

フォーカス 26 ＜第１８回＞：成果事例クローズアップ（京都・先端ナノテク総合支援ネットワーク）

# 炭酸カルシウム結晶表面の液中原子分解能イメージング

東北大学　荒木優希，塚本勝男
京都大学　大藪範昭，小林圭，山田啓文


（左から）　東北大学　荒木優希，塚本勝男


（左から）　京都大学　大藪範昭，小林圭，山田啓文

## １．はじめに

骨や貝殻などの生物における重要な硬組織は無機鉱物（バイオミネラル）から構成される．このバイオミネラルは，後述する生体鉱物形成作用（バイオミネラリゼーション）によって作られるが，そのメカニズムについては依然不明な点が多い．東北大学では，常温・常圧環境にもかかわらず，高圧相で安定となる炭酸カルシウム結晶を作り出す，この貝の結晶成長メカニズムを明らかにすることを目的として研究を進めていたが，この研究では溶液中における成長結晶表面の構造変化を捉えることが必要不可欠となる．こうした中，先進の周波数変調方式原子間力顕微鏡（FM-AFM）技術に基づき，京都大学・山田グループが開発した，液中環境で高分解能表面観察が可能な AFM プローブシステムを，京都・先端ナノテク総合支援ネットワークを通じて，利用できることを塚本，荒木らは知り，共同利用支援を受けるに至った．上記 FM-AFM 装置を用いることで，溶液中での炭酸カルシウムの結晶成長過程を原子レベルで観察することに成功した．

## ２．身近に存在する「結晶」

「結晶」と聴いて，まず何を思い浮かべるだろうか．石英結晶，雪の結晶，塩の結晶･･･自然界は，さまざまな「結晶」であふれている．しかし，結晶がわれわれの生活に密接に関わっていることは意外に知られていない．先に挙げたものの他にも，チョコレートやバターなどの油脂，胆石などの体内に形成する結石，骨や歯なども結晶から成っている．これらの結晶がどのように形成・成長するのか，温度や圧力，添加物の効果でどのように物性が変わるのか，という結晶成長メカニズムの解明は食品，医療，工業など様々な分野で重要な課題である．

## ３．生体による鉱物形成作用 ーバイオミネラリゼーションー

一般に結晶の成長メカニズムは，結晶が形成する環境，添加物など，様々なファクターによって異なる．その中でも，生体が関与する結晶化作用は「バイオミネラリゼーション」と呼ばれている．バイオミネラリゼーションという言葉は世間に浸透していないが，われわれの歯や骨の形成もバイオミネラリゼーションによるもので，非常に身近な現象であることがわかる．数あるバイオミネラリゼーションの中で，本研究の対象は貝殻のバイオミネラリゼーションである．これも存外知られていない事実であるが，貝殻も結晶から構成されている．多くの海洋生物の殻の主成分は炭酸カルシウム結晶（$CaCO_3$）で，貝の場合には外套膜から分泌される特殊なタンパク質と炭酸カルシウム結晶との相互作用によって，結晶の形態，組織が制御されている [1]．特に，アワビやアコヤガイといった暖かい海に生息する二枚貝では，地表環境では起こり得ない現象が見られることが古くから知られている．常温・常圧下では，炭酸カルシウム結晶の安定相である

＊ 問い合わせ：
京都・先端ナノテク総合支援ネットワーク
京都大学
〒 615-8530　京都市西京区京都大学桂　インテックセンター 205
京都・先端ナノテク総合支援ネットワーク事務室
電話：075-383-2139
E-mail：nano-net@nsn.kyoto-u.ac.jp

カルサイトが一般的に見られ，有孔虫やウニの殻はカルサイトから構成されている．これに対し，アワビなどの殻には，高圧相であるアラゴナイトがカルサイトと共存している．アラゴナイトが常温常圧下で安定に存在するメカニズムは明らかになっていないが，これまでの先行研究によって，貝が分泌するタンパク質が重要な役割を果たしていることが明らかとなっている [2][3]．さらに，近年の分析技術の発達により，アスパラギン酸を始めとする酸性アミノ酸の配列が重要であることまでわかってきた [4]．では，炭酸カルシウム結晶とそれらのアミノ酸の配列がどのように作用してアラゴナイトは形成されるのだろうか？

## 4．結晶成長その場観察の重要性

結晶の形成メカニズムを明らかにするために多くの手法が存在するが，結晶の形成過程の「その場」観察は，起こっている現象を忠実に理解するために重要である．これまでにも，種々のタンパク質を添加した系でのその場観察実験が行われている [5][6]．それらの実験では，貝殻の形成を模擬して，複数のタンパク質から成る有機物膜やカルサイト結晶を基板として，その表面に結晶を成長させている．その際，結晶表面観察には原子間力顕微鏡（AFM）が頻繁に用いられている．AFM は，観察環境や試料を選ばない高分解能観察装置である．しかし，一般的に用いられているコンタクトモードやタッピングモードでは，真の原子分解能を引き出すのは非常に難しい．したがって，原理的には原子レベルの観察が可能であるものの，結晶表面に生じる成長丘の形態や，成長ステップの形状の観察が主な用途となっている．これまでの実験では，アラゴナイトが形成する瞬間は捉えられていない．アラゴナイト形成の観察において問題となるのが，どのようにして「結晶成長その場観察」と「結晶相の同定」を同時に行うかということである．その場観察中に結晶相の同定ができなければ，基板上にアラゴナイトがいつ形成したのかを確認することができない．結晶相同定の一般的な手法である分光法や XRD などは，主に大気中で有効な方法である．また，基板表面に形成した原子一層分のアラゴナイトを検知することはできない．

そこで，本研究で着目したのは，カルサイトとアラゴナイトの結晶構造の違いである．もし，溶液中で結晶表面を原子分解能で観察することができれば，結晶表面の原子配列の変化から結晶相を同定することができる．また，アラゴナイトが形成する瞬間を原子レベルでみることができ，タンパク質がどのように結晶構造を変化させているかを直に見ることができるはずである．このアイデアを持ちつつ，溶液中で結晶表面を原子レベルで観察できる装置はあるか，と考えていたところで出会ったのが，京都大学工学研究科において開発された周波数変調方式原子間力顕微鏡（FM-AFM）である．FM-AFM は，探針を試料表面に接触しないように走査させ，結晶表面原子と探針の相互作用によって変化するカンチレバーの周波数の微小変化を検知し，表面形状を観察することができる．通常，溶液中ではカンチレバーの動きが溶液の抵抗を受けてしまうため，Q 値が低下して原子分解能を引き出すことが難しくなる．しかし，カンチレバーの変位検出系の低ノイズ化，微小振幅 FM 検出が実現したことにより，溶液中において真の原子分解能を有することが確認されている [7]．

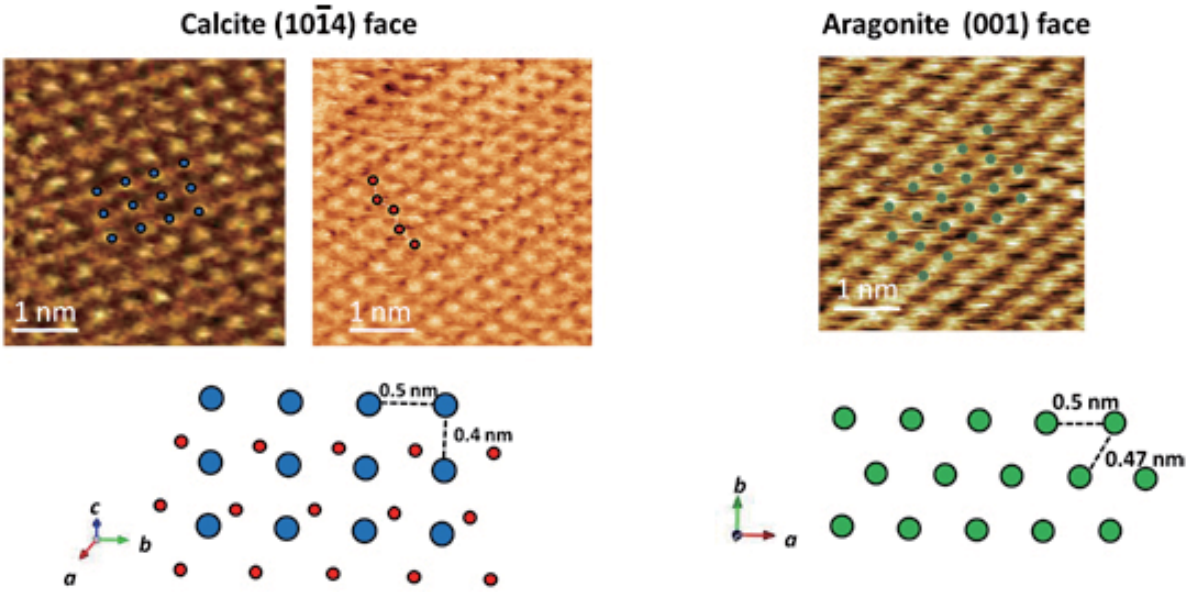


図 1　カルサイト (10$\bar{1}$4) 面，アラゴナイト (001) 面の原子配列（上）と原子配列のモデル図（下）．
青はカルサイトのカルシウム原子，赤は酸素原子を，緑はアラゴナイトのカルシウム原子を表している．

## 5．FM-AFM によるカルサイト，アラゴナイト表面の原子分解能観察

本研究では，数ミリ大のカルサイト結晶を基板として，その表面の原子配列の変化を観察することが目的である．したがって，まずは超純水中でカルサイトとアラゴナイトそれぞれの単結晶表面の観察を行い，原子配列の違いが明瞭に見られるかを確認した．基板として用いるカルサイト劈開面の観察は，既に本装置を用いた観察結果が報告されているが [8]，本観察でもカルシウムのパターンと酸素原子のパターンが特徴的に見られた（**図 1** 左）．一方，AFM に限らず，アラゴナイト表面の観察は光学顕微鏡でもほとんど行われていない．FM-AFM を用いてアラゴナイト単結晶の表面観察を行ったところ，明瞭なカルシウムの配列が観察された（**図 1** 右）．これらの観察結果から，原子分解能観察でカルサイトとアラゴナイトを明瞭に区別できることを確認した上で，次のような実験を行った．

## 6．アラゴナイト形成過程の原子レベルその場観察

成長溶液に添加する有機物としては，合成ポリペプチドを用いた．この合成ポリペプチドは，アコヤガイに含まれるタンパク質のアミノ酸配列を模擬したもので，アラゴナイトの形成を促すことが確認されている [4]．合成ポリペプチドを添加した炭酸カルシウム過飽和溶液をカルサイト基板上に数 10μl 滴下し，その原子配列の変化をその場観察した．溶液を基板上に滴下してから約 90 分後に，表面の原子配列に変化が見られた（**図 2**）．それまで表面に見られたカルサイト表面の酸素原子のパターンの画面上半分が異なるパターンになっている．さらにその直後の走査では，画面全体がこのパターンに完全に変化した．新しく現れたこのパターンを解析してみると，アラゴナイト表面のカルシウムのパターンと合致し，アラゴナイト形成の瞬間を観察していることが明らかとなった．すなわち，カルサイトからアラゴナイトへの相転移が起こるという，アラゴナイト形成メカニズムの新たな可能性を示唆する結果が得られた．この結果の詳細については，近く専門誌にて報告する予定である．

FM-AFM を結晶成長観察に適用したことによって，アラゴナイト形成メカニズムを原子レベルで理解することが可能となった．今後も形成過程の観察から，ポリペプチドがどのようにアラゴナイトを形成させているのかを明らかにしたい．特に，相転移が起こる際に結晶構造がどのように，どこから変化しているのかを捉えることが課題である．

## 7．おわりに

FM-AFM の共同利用により，結晶成長過程の原子レベルその場観察という，世界に先駆けた大きな成果を挙げることができた．この結果は，アラゴナイト形成メカニズムの解明に向けて，新たな視点を与えるものであると確信している．

本研究を通して，観察装置や分析技術の開発がさまざまな分野の発達につながっていることを強く実感している．技術の向上によって数多くの観察・分析装置が発展し続けているが，これらの装置は他の分野と広く関わることで新たな用途を見出される．他分野との関わりを積極的にもたらすという点で，京都・先端ナノテク総合支援ネットワークは非常に重要な存在であると感じている．FM-AFM が最新鋭の結晶表面観察装置として，様々な分野で活躍していくであろうことは想像に難くないが，それを推進するためにも学際的研究を目指していきたい．

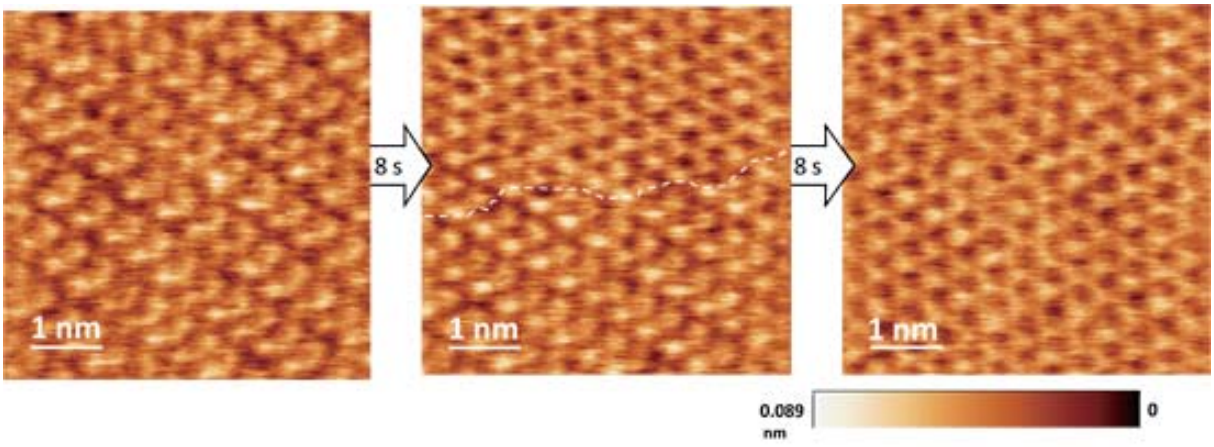


図 2　合成ポリペプチド，マグネシウムを添加した成長溶液中でのカルサイト基板表面の原子配列の変化．
このときの一回のスキャンにかかった時間は約 8 秒．

## 参考文献

[1] 渡辺哲光 " バイオミネラリゼーション - 生物が鉱物を作ることの不思議 -", 東海大学出版会 (1997)
[2] A. M. Belcher, X. H. Wu, R. J. Christensen, P. K. Hansma, G. D. Stucky and D. E. Moese, Nature, 381, 56-58 (1996).
[3] F. Nudelman, E. Shimon, E. Klein, M. Rousseau, X. Bourrat, E. Lopes, L. Addadi and S. Weiner, J. Struct. Biol., 162, 290-300 (1996).
[4] R. Takagi and T. Miyashita, Zoolog. Sci., 27, 416-426 (2010).
[5] D. A. Walters, B. L. Smith, A. L. Belcher, G. T. Paloczi, G. D. Stucky, D. E. Morse and P. K. Hansma, Biophys. J., 72, 1425-1433 (1997)
[6] J. B. Thompson, G. T. Paloczi, J. H. Kindt, M. Michenfelder, B. L. Smith, G. Stucky, D. E. Morse and P. K. Hansma, Biophys. J., 79, 3307-3312 (2000).
[7] T, Fukuma, M. Kimura, K. Kobayashi, K. Matsushige and H. Yamada, Rev. Sci. Instrum. 76, 053704 (2004).
[8] S. Rode, N. Oyabu, K. Kobayashi, H. Yamada and A. Kuhnle, Langmuir, 25(5), 2850-2853 (2009)

（東北大学理学研究科　荒木優希）

*Reprinted from*

JAPANESE JOURNAL OF
APPLIED
PHYSICS

**REGULAR PAPER**

# Atomic-Resolution Imaging of Aragonite (001) Surface in Water by Frequency Modulation Atomic Force Microscopy

Yuki Araki, Katsuo Tsukamoto, Noriaki Oyabu, Kei Kobayashi, and Hirofumi Yamada

Jpn. J. Appl. Phys. **51** (2012) 08KB09

Japanese Journal of Applied Physics **51** (2012) 08KB09 **REGULAR PAPER**
http://dx.doi.org/**10.1143/JJAP.51.08KB09**

# Atomic-Resolution Imaging of Aragonite (001) Surface in Water by Frequency Modulation Atomic Force Microscopy

Yuki Araki*, Katsuo Tsukamoto, Noriaki Oyabu[1], Kei Kobayashi[2], and Hirofumi Yamada[1]

*Graduate School of Science, Tohoku University, Sendai 980-8578, Japan*
[1]*Department of Electric Science and Engineering, Kyoto University, Kyoto 615-8510, Japan*
[2]*Office of Society-Academia Collaboration for Innovation, Kyoto University, Kyoto 615-8520, Japan*

Received January 18, 2012; revised March 27, 2012; accepted May 7, 2012; published online August 20, 2012

Aragonite is a high-pressure phase of calcium carbonate crystals. However, aragonite is formed under normal pressure with the help of biomineralization. Although it is important to observe growth features to understand the growth mechanism of the aragonite surface, only a few research groups have succeeded in observing the growth steps. In this study, we performed observation of the (001) face of a natural aragonite crystal surface at the atomic scale by the newly developed frequency modulation atomic force microscopy (FM-AFM). On the (001) face of aragonite, several growth islands with flat terraces were observed. We have succeeded in obtaining atomic-resolution images of the pseudo-hexagonal arrangement of calcium ions on the terraces. We also obtained atomic-resolution images on the calcite ($10\bar{1}4$) face by FM-AFM, which highlights the difference in the surface atomic arrangements of the two polymorphs was clearly visualized.


## 1. Introduction

Calcite and aragonite are polymorphs of calcium carbonate crystal ($CaCO_3$) which is an abundant mineral on the earth. Calcite is a trigonal crystal that belongs to $R\bar{3}c$ space group, and is the most stable phase at normal temperature and pressure. On the other hand, aragonite is an orthorhombic crystal whose space group is *Pmcn* (Fig. 1). Aragonite is a metastable phase under normal pressure.[1–3] However, aragonite is widely distributed as a component of the shell of marine organisms[4,5] and it is favorably grown from calcium carbonate solution with metallic ions, such as magnesium ions.[2] In particular, it is well known that both calcite and aragonite are formed as molluscan shells. The mechanism of control polymorph is focused on in the biomimetic field to develop a novel material with a high strength, such as sea shells.[6] However, the growth mechanisms of aragonite are not fully understood, and even the surface structures of aragonite have not been characterized until now except for only a few reports on the observations of the aragonite surface.[7,8] On the other hand, the surface of calcite has been observed by many researchers well,[9–15] and recently the atomically-resolved images of calcite cleavage surface has been obtained by newly developed frequency modulation atomic force microscopy (FM-AFM) in liquid.[16] Atomically-resolved AFM images allow us to understand the atomic phenomena in crystal growth. It is highly expected to perform the FM-AFM observation on aragonite. In this study, we employed FM-AFM for the observation of aragonite surface in water and successfully observed the (001) face of aragonite with an atomic resolution. The atomically-resolved images of the ($10\bar{1}4$) face of calcite were also obtained, which showed clearly different patterns reflecting their surface atom arrangements.

## 2. Experimental Section

Experiments were conducted using a recently developed high-resolution and low-thermal-drift FM-AFM working in liquid based on a commercial AFM (Shimadzu SPM-9600) with a home-built controller.[17] We used highly doped n-Si cantilevers with gold coatings (Nanosensors PPP-NCHAuD)

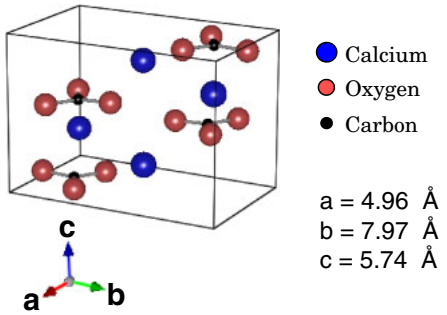


**Fig. 1.** (Color online) Unit cell of aragonite.[2] This image is drawn by VICS.[29]

whose nominal eigenfrequency was 160 kHz, a spring constant was about 40 N/m, and $Q$-factor was 8.79 in Milli-Q ultrapure water (Millipore). The cantilever oscillation amplitude was kept constant at 0.394 nm. A very sufficiently low lateral thermal drift rate of typically less than 1 nm/min in liquid was achieved by an accurate temperature control of the FM-AFM environment at $294 \pm 0.15$ K for 10 h by a commercial incubator (Mitsubishi Electric Engineering CN-40A).

The sample was a natural aragonite crystal produced in Morocco [Fig. 2(a)]. The purchased aragonite crystal was divergent and was formed by pseudo-hexagonal cyclic twin crystals. Although aragonite is orthorhombic, a pseudo-hexagonal shape is often formed in nature as a cyclic twin with three individuals on the (110) face.[2]

The surface of the aragonite (001) face was rough at the optical level [Fig. 2(b)]. An aragonite pseudo-hexagonal prism was cut on the (001) face from the purchased crystal. The diameter of the (001) face of the sample was about 2 mm. A natural single crystal of calcite produced in Mexico was also cleaved on the ($10\bar{1}4$) face. The diameter of the ($10\bar{1}4$) face was about 3 mm.

Then, the crystals were glued at the bottom of open fluid cells by epoxy adhesive so that the (001) face of aragonite and the ($10\bar{1}4$) face of calcite were parallel to the bottom [Fig. 2(c)]. The calcite cleavage surface was observed in order to compare the atomically-resolved image with the

*E-mail address: b1sd6001@s.tohoku.ac.jp

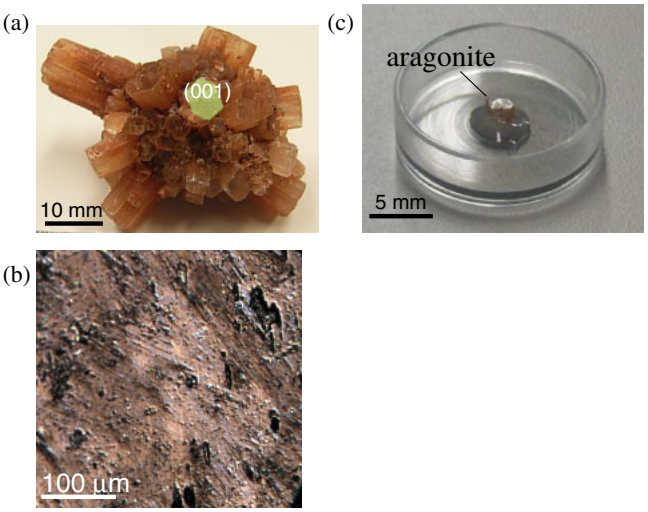


**Fig. 2.** (Color online) (a) Photograph of a natural aragonite crystal. A (001) facet on a prismatic part was indicated in the photograph. (b) Differential interference contrast microscopy image of the aragonite (001) face. (c) Photograph of a prismatic aragonite crystal glued at the bottom of sample holder for FM-AFM observation.

(001) face of aragonite. After the crystals were glued on the cells, a 100 μl droplet of ultrapure water was then placed on the (001) face of aragonite and on the $(10\bar{1}4)$ face of calcite using a pipet. We show only raw data except for a plane subtraction by WSxM (Nanotec).[18)]

## 3. Results and Discussion

First, we observed the surface of the aragonite (001) face in the area of $40 \times 40\,\mathrm{nm}^2$. The surface was covered with several polygonal islands with flat terraces of the area $10 \times 10\,\mathrm{nm}^2$. The shape of the islands was assumed to correspond to the pseudo-hexagonal shape of the crystal [Figs. 3(a) and 3(b)]. When the scan area was reduced to $10 \times 10\,\mathrm{nm}^2$, the periodic lattice patterns corresponding to the macroscopic shape were observed at the edges of the islands, as shown in Fig. 3(c).

When the scan area was reduced to $5 \times 5\,\mathrm{nm}^2$ on the flat terrace of an island, an atomically-resolved image was obtained, as shown in Fig. 4(a). Bright dots show the positions of atoms. The arrangement image shows a pseudo-hexagonal pattern which suggests the surface atoms are ordered periodically along the $[\bar{1}30]$, [130], and [100] directions, as shown in Fig. 4. A fast Fourier-transformed image clearly showed six bright spots, as shown in Fig. 4(b). This symmetry corresponds to the arrangement of calcium ions on the aragonite (001) face. Note that the atomically-resolved images consecutively taken by scanning upward and downward showed almost no differences, suggesting that the lateral thermal drift was negligible during the scan. The interatomic distances of calcium ions along the [100] and [010] directions in Fig. 4(a) were about 0.46 and 0.80 nm, respectively. These values correspond to the unit cell of aragonite whose dimensions are 0.496 and 0.796 nm in the [100] and [010] directions, respectively.

A schematic of the aragonite crystal seen from the [010] direction [Fig. 5(a)] shows that the layer of the calcium ions on the (001) face is located between two parallel layers of

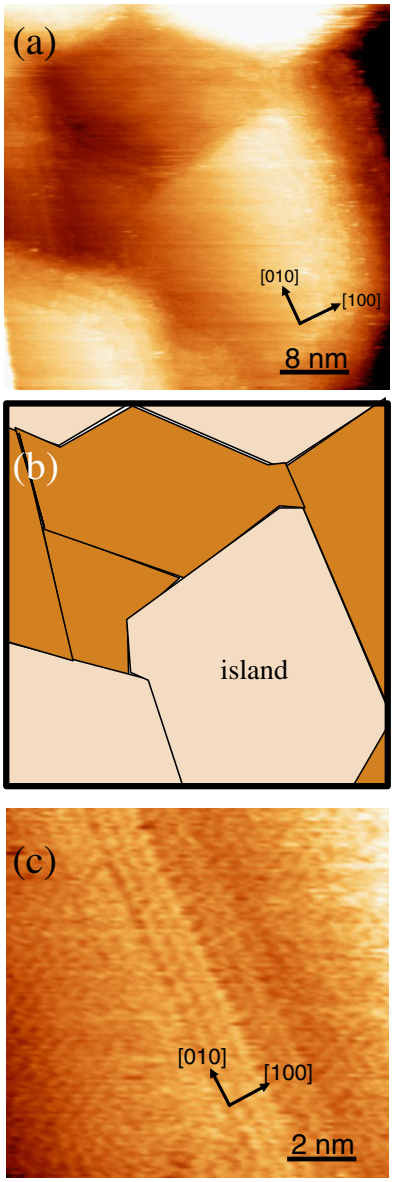


**Fig. 3.** (Color online) (a) Surface image of aragonite (001) face in $40 \times 40\,\mathrm{nm}^2$ and (b) schematic picture of the islands of (a). Light and dark colors indicate upper and lower islands, respectively. (c) Magnified image of the edge of an island. The bright line in (c) shows the lattice pattern corresponding to the lines of calcium.

carbonate ion layers [Fig. 5(a)]. The carbonate ions are arranged triangularly with the lattice constant of the unit cell in the same plane. The arrangement of the carbonate ions in the lower layer is the same as that in the upper one, but the lower carbonate ions do not overlap with those in the upper one, as shown in Fig. 5(b). Although carbonate ions should be located above the calcium layer, in this series of FM-AFM observations, we only observed pseudo-hexagonal atomic features corresponding to the arrangement of the calcium ions on the aragonite (001) face. A possible reason why only the arrangement of the calcium ions was observed is that the outmost layer is favorably terminated with the calcium ion layer.[19,20)] A previously reported contact-mode AFM observation on the aragonite (001) face in air after dissolution in water showed a stripe pattern of the calcium ion rows, which also suggests the surface termination with

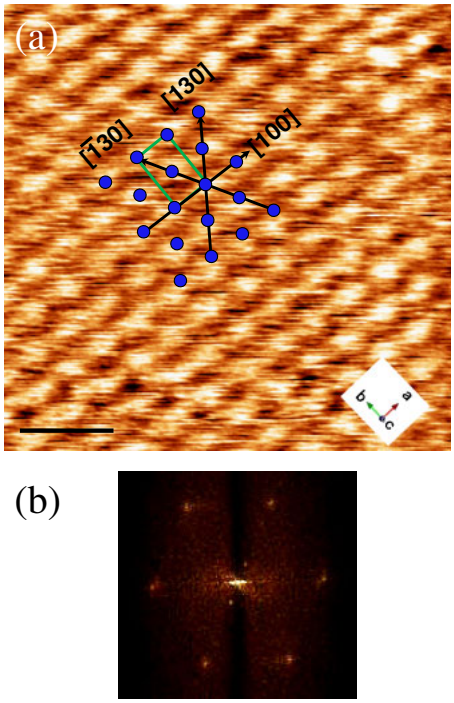


**Fig. 4.** (Color online) (a) Atomic image of aragonite (001) face and (b) the Fourier-transformed image of (a). Circles on the image show the arrangement of calcium atoms on the aragonite (001) face. The rectangle indicates the surface unit cell. The scale bar is 1 nm.

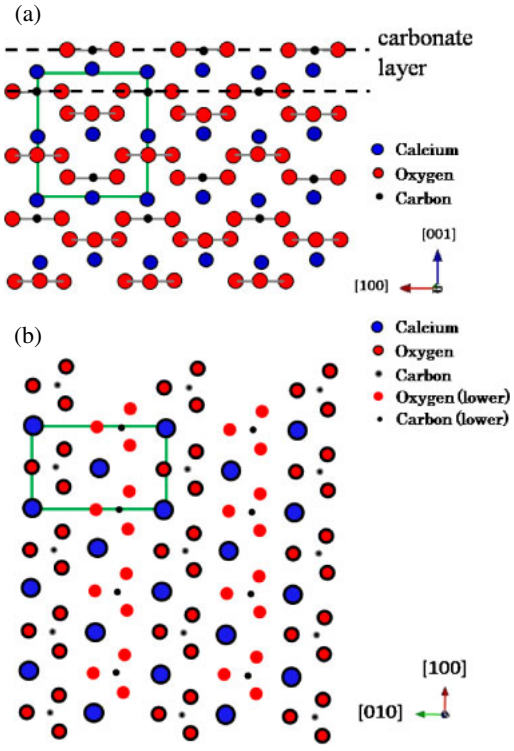


**Fig. 5.** (Color online) (a) Schematic of aragonite crystal seen from [010] direction. Dashed lines in (a) indicate carbonate layers. The calcium layer is located between two carbonate layers. (b) Top view of aragonite (001) face. The rectangles in (a) and (b) show surface unit cells.

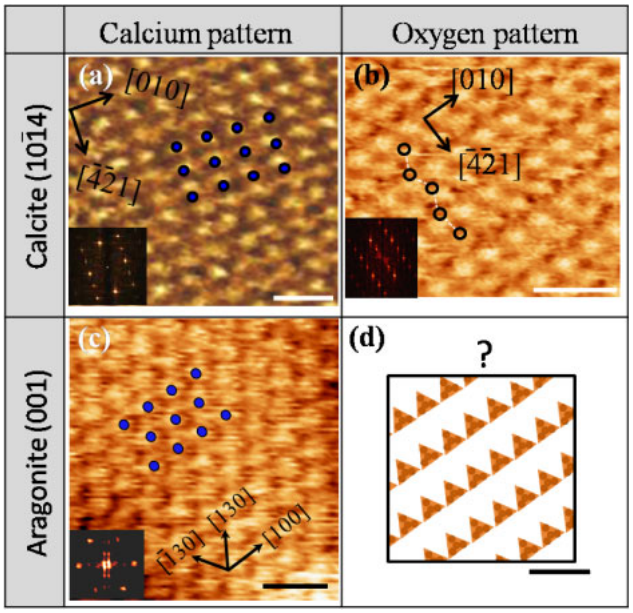


**Fig. 6.** (Color online) Comparison of atomically-resolved and Fourier-transformed images of calcite cleavage (10$\bar{1}$4) and aragonite (001) faces. On the calcite cleavage plane, (a) a latticed calcium layer and (b) a zigzag oxygen pattern are observed. On the other hand, (c) the calcium layer was only observed on the (001) face of aragonite. Although oxygen atoms on the aragonite (001) face are not observed, the patterns from (a) to (c) are considered different, as shown in (d) the predicted image of oxygen atoms on the aragonite (001) face. These patterns can also be identified on the basis of the Fourier-transformed images. The scale bar is 1 nm. Filled and open circles indicate calcium and oxygen atoms, respectively, in (a) to (c). Triangles in (d) show $CO_3$ ions of the topmost layer on the aragonite (001) face.

the calcium ions.[7] We also observed atomically-resolved FM-AFM images on the (10$\bar{1}$4) face of the calcite crystal, and they are compared in Fig. 6. As shown in the upper row of Fig. 6, we observed two types of contrasts, which were the rectangular unit cell pattern [Fig. 6(a)] and the characteristic zigzag pattern [Fig. 6(b)]. Several observations of the calcite cleavage surface in liquid have been performed by contact-mode AFM[9–11,13–15,21] and FM-AFM.[16] These studies also showed that the calcite (10$\bar{1}$4) face shows various patterns. By the comparison with these images, Figs. 6(a) and 6(b) can be attributed to those showing the arrangements of the calcium ions and the oxygen atoms of the carbonate ions, respectively. In the case of the calcite (10$\bar{1}$4) surface, both the calcium and oxygen atoms of carbonate ions are located within the same plane. Many theoretical studies suggest that these variations in contrasts are caused by the termination of tips.[22–26] The pseudo-hexagonal pattern observed on the aragonite (001) face in this study was clearly different from any of those patterns obtained on the calcite surface.

If the oxygen atoms of the carbonate ions of the aragonite (001) face would be observed, the atomic observed pattern would be as that shown in Fig. 6(d). However, as mentioned above, we have never observed such a rectangular unit cell pattern on aragonite, probably because the aragonite (001) surface in water is terminated with the calcium ion layer.

It should be noted that it is possible that atomically-resolved contrasts, such as those observed here by FM-AFM, are caused by the structured hydration layers on the surface, and that they do not directly reflect the arrangements of the surface ions. To clarify the imaging mechanisms, hydration

structure measurements by FM-AFM[27] and theoretical studies on the hydration structures on the calcium carbonate crystals[28] are currently under way.

## 4. Conclusions

We have performed FM-AFM observation on the (001) face of a natural aragonite crystal to successfully find that the grown surface is covered with flat islands. On these islands, we have, for the first time, obtained the atomic-resolution AFM images with a pseudo-hexagonal pattern, which can definitely be differentiated from the patterns observed on the calcite surface. The pseudo-hexagonal pattern corresponds to the atomic arrangement of the calcium ions, which strongly suggests that the aragonite (001) surface is stably terminated with the calcium ion layer.

## Acknowledgments

This work was supported by Kyoto-Advanced Nanotechnology Network with regard to the use of FM-AFM. Particular thanks are due to Matsushige Laboratory, Kyoto University, for technical support. Financial support was obtained through Grants-in-Aid for Challenging Exploratory Research for K.T. and for the Research Fellow of the Japan Society for the Promotion of Science for Y.A.

1) W. Johannes and D. Puhan: Contrib. Mineral. Petrol. **31** (1971) 28.
2) W. A. Deer, R. A. Howie, and J. Zussman: *An Introduction to the Rock Forming Minerals* (Prentice Hall, Upper Saddle River, NJ, 1992) 2nd ed., p. 654.
3) S. A. T. Redfern, E. Salje, and A. Navrotsky: Contrib. Mineral. Petrol. **101** (1989) 479.
4) S. Mann: *Biomineralization* (Oxford University Press, Oxford, U.K., 2001) 6.
5) W. S. Fyfe and J. L. Bischoff: Soc. Econ. Paleontol. Mineral. Spec. Publ. **13** (1965) 3.
6) G. Mayer and M. Sarikaya: Exp. Mech. **42** (2002) 395.
7) H. Shindo and M. Kwak: Phys. Chem. Chem. Phys. **7** (2005) 691.
8) R. Giles, S. Manne, S. Mann, D. E. Morse, G. D. Stucky, and P. K. Hansma: Biol. Bull. **188** (1995) 8.
9) P. E. Hillner, S. Manne, A. J. Gratz, and P. K. Hansma: Ultramicroscopy **42–44** (1992) 1387.
10) A. L. Rachlin, G. S. Henderson, and M. C. Goh: Am. Mineral. **77** (1992) 904.
11) F. Ohnesorge and G. Binnig: Science **260** (1993) 1451.
12) G. Raina, R. W. Gauldie, S. K. Sharma, and C. E. Helsley: *Atomic Force Microscopy/Scanning Tunneling Microscopy* (Plenum Press, New York, 1994) 195.
13) Y. Liang, A. S. Lea, D. R. Baer, and M. H. Engelhard: Surf. Sci. **351** (1996) 172.
14) S. L. S. Stipp, C. M. Eggleston, and B. S. Nielsen: Geochim. Cosmochim. Acta **58** (1994) 3023.
15) J. J. De Yoreo, L. A. Zepeda-Ruiz, R. W. Friddle, S. R. Qiu, L. E. Wasylenki, A. A. Chernov, G. H. Gilmer, and P. M. Dove: Cryst. Growth Des. **9** (2009) 5135.
16) S. Rode, N. Oyabu, K. Kobayashi, H. Yamada, and A. Kühnle: Langmuir **25** (2009) 2850.
17) T. Fukuma, M. Kimura, K. Kobayashi, K. Matsushige, and H. Yamada: Rev. Sci. Instrum. **76** (2005) 053704.
18) I. Horcas, R. Fernández, J. M. Gómez-Rodríguez, J. Colchero, and J. Gómez-Herrero: Rev. Sci. Instrum. **78** (2007) 013705.
19) P. Fenter, P. Geissbühler, E. DiMasi, G. Srajer, L. B. Sorensen, and N. C. Sturchio: Geochim. Cosmochim. Acta **64** (2000) 1221.
20) N. H. de Leeuw and S. C. Parker: J. Phys. Chem. B **102** (1998) 2914.
21) J. B. Thompson, G. T. Paloczi, J. H. Kindt, M. Michenfelder, B. L. Smith, G. Stucky, D. E. Morse, and P. K. Hansma: Biophys. J. **79** (2000) 3307.
22) A. S. Foster, C. Barth, A. L. Shluger, and M. Reichling: Phys. Rev. Lett. **86** (2001) 2373.
23) J. V. Lauritsen, A. S. Foster, G. H. Olesen, M. C. Christensen, A. Kuhnle, S. Helveg, J. R. Rostrup-Nielsen, B. S. Clausen, M. Reichling, and F. Besenbacher: Nanotechnology **17** (2006) 3436.
24) M. Watkins and A. L. Shluger: Phys. Rev. Lett. **105** (2010) 196101.
25) M. Watkins, M. L. Berkowitz, and A. L. Shluger: Phys. Chem. Chem. Phys. **13** (2011) 12584.
26) M. Harada and M. Tsukada: Phys. Rev. B **82** (2010) 035414.
27) K. Kimura, S. Ido, N. Oyabu, K. Kobayashi, Y. Hirata, T. Imai, and H. Yamada: J. Chem. Phys. **132** (2010) 194705.
28) P. Raiteri, J. D. Gale, D. Quigley, and P. M. Rodger: J. Phys. Chem. C **114** (2010) 5997.
29) K. Momma and F. Izumi: Comm. Crystallogr. Comput. IUCr Newsl. **7** (2006) 106.